Local Calibration of the MEPDG Using Test Track Data

by

Xiaolong Guo

A thesis submitted to the Graduate Faculty of
Auburn University
in partial fulfillment of the
requirements for the Degree of
Master of Science

Auburn, Alabama
December 14, 2013

Keywords: MEPDG, Local Calibration, Transfer Function, Input Level 1

Approved by

David H. Timm, Chair, Professor of Civil Engineering
Rod E. Turochy, Associate Professor of Civil Engineering
Randy West, Director of National Center of Asphalt Technology

ABSTRACT

The Mechanistic-empirical Pavement Design Guide (MEPDG), now known as AASHTOWare Pavement ME Design, is a state-of-art mechanistic-empirical design method. It has been adopted by the American Association of State Highway and Transportation Officials (AASHTO) as the new standard for pavement design in the U.S. However, the MEPDG was calibrated to various types of pavements located across the country representing diverse design conditions. Since the default transfer functions were nationally-calibrated, the performance prediction for local projects sometimes may not correlate well with the local performance measurements. The National Center for Asphalt Technology (NCAT), equipped with a full-scale accelerated Test Track, supported the evaluation and local calibration of the nationally-calibrated models. The study results showed the nationally-calibrated fatigue cracking model and the IRI model matched the measured values in the 2003 research cycle, and no better coefficients were found to improve the model predictions. However, applying the same fatigue coefficients to the 2006 research cycle resulted in poor correlations to measured performance and no significant improvement to fatigue cracking prediction was found. The nationally-calibrated rutting model over-predicted rut depths, but the accuracy of the rutting model was significantly improved by local calibration. The research methods and findings may be useful for the transportation agencies to perform local calibration studies.

ACKNOWLEDGMENTS

I would like to sincerely acknowledge my academic advisor Dr. David Timm for his professional guidance on my graduate study. His patience, inspiration, and rigorousness motivated me to reach deeper and be more involved in the research of civil engineering. I not only learned a wealth of knowledge and skills, but also shaped research perspectives based on his expertise of pavement design and asphalt technology. I truly appreciate his understanding of my program progress. It is his critical advice that strengthens my confidence to insist on the study until a completion of this program.

I am truly grateful to Dr. Rod Turochy for his endeavor to support my study, and also thank his family for bringing me in community activities. I also would like to thank Dr. Randy West for taking time from his busy schedule to review my work and participate as one of my committee members.

I am thankful to Dr. Raymond Powell, Dr. Mary Robbins, and Dr. Fabricio Leiva-Villacorta for their assistance in conducting experiments. I would like to thank Derong Mai, Xiao Zhao, Jingwen Li, and Boyao Zhao, as well as other students of the civil engineering program here for their kind help with my work and my life. I also would like to acknowledge Miller Writing Center at Auburn University library for supporting the writing development. I appreciate the professional suggestions to my thesis writing from their tutors, especially Courtney Hewitt.

Finally, I would like to thank my parents, my relatives and friends in China for their selfless care and encouragement during my study.

TABLE OF CONTENTS

LIST OF FIGURES

LIST OF TABLES

CHAPTER 1

INTRODUCTION

BACKGROUND

Overview of Pavement Design

Pavement design is critical to successful road construction. It provides a workable plan to specify the pavement section before it is built. The effectiveness of pavement design usually determines whether an application can serve for a long time with good quality at an affordable cost for owners. A good quality pavement means durable support, skid resistance, and energy conservation for road users. However, engineers are inevitably faced with a variety of design challenges when considering traffic, the environment, or subgrade soils with local characteristics. For a highway agency, pavement design relies on material specifications, pavement design policies, and construction practice. Obviously, it is never easy to achieve a pavement design that fulfills the requirements above. In this case, pavement design procedures or guides are needed for providing a paradigm of generating appropriate designs. The common procedures account for these main design factors such as traffic, materials, the environment, and performance predictions.

Main design factors

Traffic

Pavements are designed to sustain recurring loadings of vehicles. Vehicles impose weight at the interface between tires and pavement, as a result, the stress is distributed into the pavement structure, attenuating from the top to the bottom. The heavier the vehicle is, the greater the stresses. It is a rule of thumb that doubled axle weight will increase induced damage by 16 times (*Equivalent Single Axle Load*, 2007). With repetitive vehicle loadings, the pavement endures a tremendous amount of cycles of deforming and rebounding. If the allowable volume of traffic

loading is reached, the pavement will experience a loss of serviceability and become distressed. From the standpoint of pavement design, the repetitive vehicle loadings in a period of time should be related to how much damage they impose. Therefore, traffic is decomposed into a number of axle groups based on configurations and weights, and the induced damage of each axle group is estimated. In this way, the total damage of traffic during a period of time can be determined by an accumulation of damage of these axle groups. To design a new pavement, designers need to derive future traffic predictions based on the current trend. However, traffic may fluctuate due to unexpected situations, such as rapid economic activity or population growth, and this should be within the concern of pavement design.

Materials

Materials physically comprise a layered pavement structure, containing surface, base, and subgrade. The properties of the materials reflect the capacity of the pavement to withstand damage. For example, a subgrade with high strength can prevent compressive or shear stress failure under heavy loads. Open-graded asphalt courses allow rainwater to drain through the pavement surface, reducing the amount of splash and spray on highways. The adoption of good quality material helps pavements to last longer, but it may greatly increase project costs. Therefore, engineers sometimes choose economical materials with local availability.

Environment

It is common sense that civil engineering structures must function within the environment where it is built. The material properties of structures are significantly affected by environmental variations. This principle can be applied to pavements. The viscoelastic properties of asphalt are affected significantly by pavement temperature changes and loading frequency. Furthermore, the asphalt binder will be oxidized if exposed in air and the asphalt mixture will become stiffer and

brittle. Therefore, the material property changes due to environment should be considered in the pavement design process.

Performance

Pavements are affected by a combination of traffic loading and environmental effects. As a result, the performance degrades over time. Engineers need an efficient way to define the performance of pavement so that they know whether an in-service pavement is still in good condition. From the view of pavement design, a clear definition of performance can prepare engineers to set their design goal. In fact, the pavement performance is defined from the experience, but in different ways at project and network levels. At a project level, performance is defined by distress, loss of serviceability index, and skid resistance. On a network level, it is defined by overall condition of the network and even policy and economics (Lytton, 1987). Generally, serviceability, defined as the current ability of a pavement to serve the traffic, is taken as an overall indicator to represent the pavement performance.

Approaches to Pavement Design

Approaches to pavement design are required to provide a link between the inputs of a design scenario (i.e., traffic, environment, materials, and tolerable degradation of pavement) with an output design (i.e., material type and layer thickness). The approaches currently available can be generally divided into two categories: empirical methods and mechanistic-empirical (M-E) methods.

Empirical method

Empirical methods correlate important variables based on experiments or experience. The important variables account for design factors in a measurable or quantitative way. Empirical methods were an effective method for early engineering practice; however, because it is

statistics-based or experience-based, the applicability of the model would be limited by the range of the experimental data or experience. For example, the 1993 AASHTO (American Association of State Highway and Transportation Officials) method is an empirical approach. The empirical relationship between important variables and a thickness-related "structural number" is described by design equations aimed to determine pavement thickness. This method is built on the limited conditions and materials present in the 1950s, so it is not widely applicable to other conditions or current pavement materials.

Advantages

Through many trial-and-errors, the empirical approach can build upon what is already observed, and respond more appropriately to real world design scenarios. It does not need cogent theoretical derivation to prove the reasonableness of empirical relationships.

Disadvantages

The validity of the empirical approach is usually limited by the dataset on which the approach was based. The dataset inherently specifies the value range of the important variables or considers a limited set of contributing variables. Thus, the extreme condition, for instance, in which a variable falls out of the pre-defined value range or the neglected variable that may have a big impact, is not accounted for. Additionally, a fairly solid empirical model takes a long time to build and needs calibration before use.

Mechanistic-empirical method

In contrast with the empirical methodology, mechanistic-empirical methods integrate mechanistic analysis of pavement structures into a design procedure. Mechanistic analysis can determine the response of pavement layers (i.e., strain, stress, or deflections) and these responses

are highly related with the propagation of various pavement distresses. The relationship between them can be statistically defined by empirical regression equations called transfer functions.

Advantages

Mechanistic-empirical methods contain broader variable sets to characterize design inputs more realistically, so they has ability to account for new materials, advanced traffic technology, and changes of environmental conditions. Thus, designers are able to compose pavement designs for a wide variety of local areas and conditions. Additionally, the M-E method is able to predict various distresses by sophisticated algorithms and enables engineers to set a failure criterion for each of them.

Disadvantages

Along with advanced design concepts, a large number of inputs will require designers much time to collect the design input information. Since many agencies are still using old AASHTO methods, they will need to upgrade technical capabilities and to provide training for implementation of the mechanistic-empirical methods. It is also important that the M-E method requires local calibration to ensure its effectiveness.

Development of Empirical Method

The development of the AASHTO empirical method dates back to a first application of the Highway Research Board (HRB) soil classification in estimating the subbase and total pavement thickness. An method with a strength test was first used by the California Highway Department in 1929 (Porter, 1950). The thickness of pavement was related to the California Bearing Ratio (CBR), which defines the penetration resistance of a subgrade soil relative to a standard crushed rock. In the 1960s, AASHTO initiated to develop design equations and nomographs for both flexible and rigid pavements, primarily based on the regression of the data

from the AASHO (American Association of State Highway Officials) Road Test. These empirical methods had been adopted until the appearance of M-E method (Huang, 1993).

AASHO road test and AASHTO methods

In the late 1950s, AASHO conceived a grand plan of building real-world testing facilities to examine the performance of pavement structures of known thickness under moving loads of known magnitude and frequency. A long list of pooled-funding sponsors spent $27 million (1960 dollars) to complete the construction of 6 loops of two-lane pavements, with half asphalt and half concrete. The road test provided the foundation for analytical evaluation of pavement response, load equivalencies, climate effects, and much more. The precious performance information greatly helped to build the regression equations for AASHTO design methods. The initial version was completed in 1961 relating loss in serviceability, traffic, and pavement thickness and it was revised in 1972 by introducing the consideration of foundation, material, and environmental conditions. Then, the next version released in 1986 improved the characterization of the subgrade and unbound materials, considered drainage effects, and incorporated a reliability factor. The latest update was released in 1993 and had some additions for pavement rehabilitation designs.

The AASHTO methods have gained popularity through relatively straightforward procedures; however, the design equations reflect a single traffic volume, single environmental condition, and limited design variables described in the late 1950s. Studies have shown that despite adjustments made over the years to the design equation in attempts to expand its suitability to different climate regions and materials, the design of flexible pavements still lacks accuracy in performance predictions and compatibility to include different materials and their complex behavior (Schwartz, 2007). The performance indicator PSI (Present Serviceability

Index) cannot address today's need in the situation that road designers and managers require more accurate evaluation of pavement performance regarding distresses and overall smoothness.

Development of Mechanistic-Empirical Methods

Brief introduction

It was noted that Kerkhoven and Dormon in 1953 first suggested using vertical compressive strain on the surface of subgrade as a critical indicator of permanent deformation (Huang, 1993). In 1960, Saal and Pell recommended the use of horizontal tensile strain at the bottom of asphalt layer as a critical predictor of fatigue cracking (Huang, 1993). Afterwards, the use of these concepts was first presented for pavement design in the US by Dormon and Metcalf in 1965. These two criteria have been adopted by Shell Petroleum International (Claussen et al, 1977) and the Asphalt Institute (Shook et al., 1982) in their proposed mechanistic-empirical methods.

The concepts and principles of M-E design were extensively discussed in details in the National Cooperative Highway Research Program (NCHRP) 1-26 project – "Calibrated Mechanistic Structural Analysis Procedures for Pavements." In this project, the available M-E design at that time was assessed, evaluated, and applied on a nationwide level, and researchers recognized that the M-E method represents one step forward from empirical methods. In the 1990s, several M-E design approaches by computer software were developed, including MnPAVE adopted by Minnesota Department of Transportation, the 2002 AASHTO Mechanistic-Empirical Pavement Design Guide (MEPDG), EverSeries by Washington Department of Transportation, and Michigan Flexible Pavement Design System (MFPDS) by Michigan State.

M-E design framework

The basic outline of M-E design includes calculating the pavement response under the impact of traffic by mechanistic models and applying transfer functions to predict number of loads to failure. Miner's hypothesis (Miner, 1945) was integrated afterwards as an incremental approach to calculate the cumulative damage in the pavement life. The approach allows the summation of fatigue or rutting damage by axle loads of varying magnitudes under varying environmental conditions.

As Figure 1.1 shows, the pavement structure specifies the material and thickness of layers, which constitutes the basic elements for mechanistic analysis. Environmental conditions impact the properties of materials by temperature, precipitation, wind speed, and so on. Traffic applies vehicle loading to induce pavement response depending on axle types and magnitudes. In order to predict long-term performance, the transfer functions are used to link dynamic pavement response with allowable repetitions of loads. It is also worthy to note that the magnitude of loading significantly affects mechanistic properties of stress-sensitive materials, such as resilient modulus of unbound materials. Further, for one of the strain levels, the damage is quantified as the ratio of actual repetitions of loads to allowable repetitions of loads. Thus, the total damage in pavement life is a summation of damage ratios for all levels of strain. If the total damage is greater than 1, the pavement is "under-designed", so it is necessary to modify the original pavement design, such as increasing the thickness of layers or adopting more durable materials. The modification of pavement design should be re-evaluated, and this iterative procedure is processed until the damage ratio is less than 1. Otherwise, if the total damage is much lesser than 1, which indicates pavement is "over-designed", it is necessary to propose a less conservative design by reducing the thickness of layers or choosing poorer quality materials.

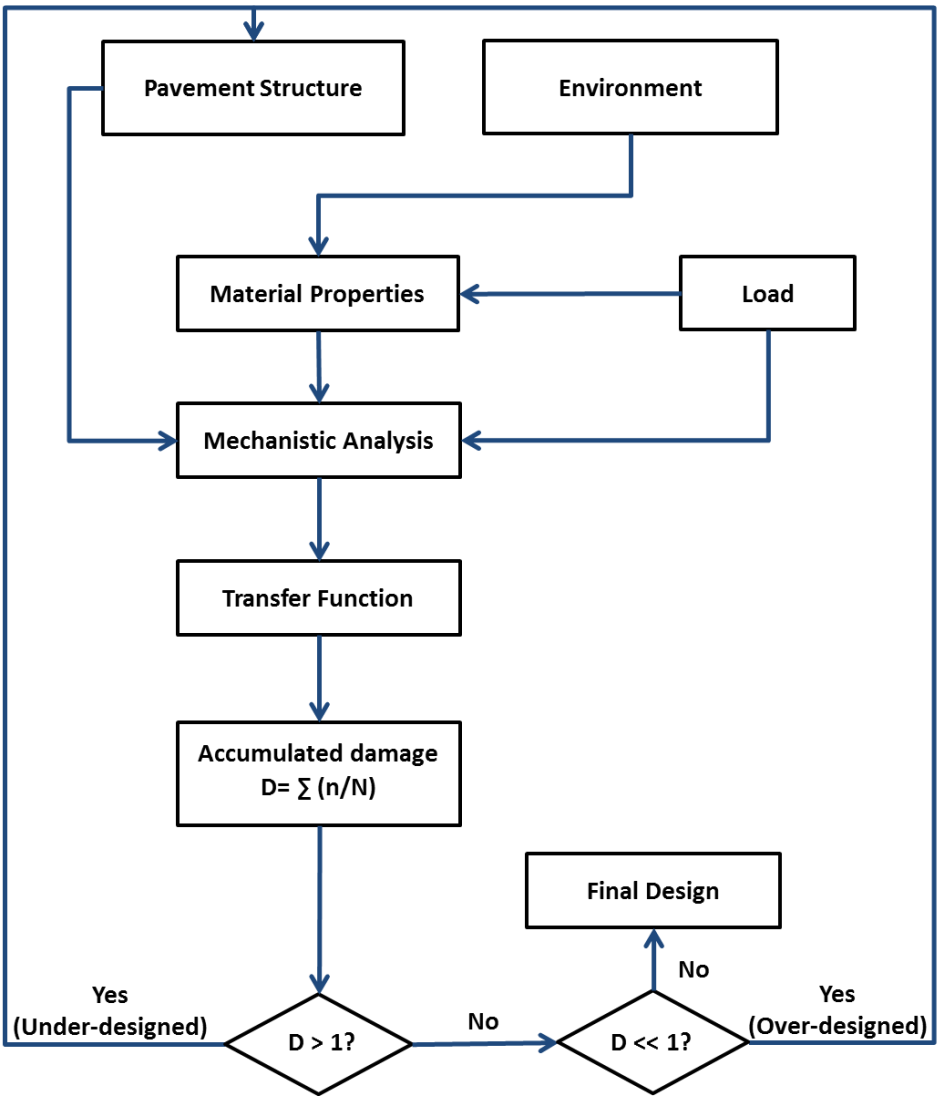

Figure 1.1 Scheme of the M-E design

MEPDG

Background

At the time when the 1986 AASHTO method was adopted, the benefits of mechanistically-based pavement design were clearly recognized and it had become apparent for transportation agencies that there was a great need for an advanced design method that accounts for modern traffic, current materials, and diverse climates. Subsequently, the Washington State Department of Transportation (DOT), North Carolina DOT, and Minnesota DOT developed their

mechanistic-empirical procedures. The National Cooperative Highway Research Program (NCHRP) 1-26 project provided the basic framework for most of efforts attempted by state DOTs (Schwartz, 2007). To embrace the widely-accepted transition from empirical to mechanistic-empirical design methods, the AASHTO Joint Task Force on Pavements, in cooperation with NCHRP and FHWA (Federal Highway Administration), invited a group of top pavement engineers in the U.S. to a workshop on "pavement design" in March, 1996 in Irvine, California. They were identifying means to develop the AASHTO mechanistic-empirical design procedure by 2002. Based on the conclusion and recommendation of the workshop, the NCHRP 1-37A project, named "Development of 2002 Guide for New and Rehabilitated Pavement: Phase II", was awarded to the ERES Consultants division of Applied Research Associates Inc. in Feb, 1998 for software generation. The version 0.7 of software was first released in 2004, named "Mechanistic-Empirical Pavement Design Guide (MEPDG)".

Adoption and implementation

In order to facilitate MEPDG implementation among highway agencies, a list of NCHRP projects was carried out after the first release to deal with issues regarding traffic data, independent review, user manual, local calibration, technical assistance, models for predicting HMA overlay reflective cracking, models for predicting top-down cracking, sensitivity analysis, and so on (Qiang Li et al, 2011). Many of these have been completed and adopted as supportive strategies and implementation guides for application of the new software. The version 1.0 of MEPDG was issued in 2007 under the NCHRP 1-40D project, and then it was taken as the Interim Pavement Design Guide by AASHTO in 2008. By 2009, 80 percent of states in the U.S. had implementation plans for the MEPDG ("MEPDG Overview & National Perspective", January 2009). The latest version of MEPDG is called "AASHTOWare Pavement ME Design".

It is the next generation of AASHTO pavement design software with many improvements and is a production-ready tool to support day-to-day operations for engineers.

To take an example of MEPDG implementation, the Indiana DOT began their program on January 1st, 2009. They initiated a steering committee, in cooperation with design engineers, FHWA, pavement associations, and contractor associations to discuss details and issues in practice. The Indiana DOT also provided support for engineers and consultants to facilitate the use of the MEPDG software. Most of designers and consultants gained familiarity with the new design procedure within six months. From January to December 2009, the Indiana DOT designed more than 100 pavement sections by using the MEPDG. The thickness of most concrete pavements on the Interstate and U.S highway systems was reduced by 2 inches compared with using the AASHTO 1993 method; a less prominent reduction applied to pavements on state routes. For 11 HMA projects of US highway and state route, the average thickness reduction was 2 inches and the savings were estimated to be $3,637,000 (TR News, Nov-Dec 2010).

Need of MEPDG Local Calibration

For the M-E design methods, the transfer functions link the bridge the mechanistic and empirical analyses, but the NCHRP 1-26 report concluded this to be the weak link in M-E design. Studies conducted in Washington State (Li et al, 2009), North Carolina (Muthadi and Kim, 2008), and Minnesota (Hoegh et al, 2010) suggested that transfer functions in MEPDG produce predictions that contained significant bias or variance. Indeed, the accuracy of the transfer functions needs to be improved so the field verification and local calibration are strongly recommended before it is used locally. To satisfy the need of implementing MEPDG for southeastern states, especially Alabama, local calibration is needed.

OBJECTIVE

The main objective of this research was to evaluate the validity of the nationally-calibrated transfer functions built in the MEPDG version 1.1 which were developed based on the Long Term Pavement Performance (LTPP) program database. The second objective was to calibrate these transfer functions to the local conditions at the NCAT Test Track.

SCOPE

NCAT Test Track

The NCAT Test Track (Figure 1.2), a 1.7-mile oval accelerated pavement testing track located in Opelika, Alabama, was used in this research. The outside lane of track was divided into forty-six test sections, each 200 feet long, and sponsored on three-year cycles. During each cycle, NCAT operates a truck fleet to apply 10 million Equivalent Standard Axle Loads (ESALs) and collects field performance data on a continuous basis. In this study, eight sections from the 2003 cycle were simulated in the MEPDG to evaluate nationally-calibrated models and subsequently to adjust the transfer functions for the Test Track. Eleven sections from the 2006 cycle were utilized to validate results of the local calibration.

Figure 1.2 NCAT Test Track

Evaluation and Calibration Process

The process of evaluation was to first characterize traffic, material properties and environmental conditions at the NCAT Test Track and generate inputs for the MEPDG. The next step was to run the software and to compare the predicted performance from the MEPDG with observed performance on the Test Track. If the differences were small, it means the MEPDG performed very well for the Test Track conditions. Otherwise, poor predictions were obtained which means the MEPDG needs to be locally calibrated. The calibration was an iterative process that required varying the calibration coefficients in the transfer functions to calibrate the MEPDG predictions to the observed values.

ORGANIZATION OF THESIS

Chapter 2 will further provide a background literature review about traditional design methods, the MEPDG, and local calibration efforts conducted by some states. Chapter 3 covers an explanation of the datasets involved in the study such as the NCAT facilities, traffic operation, climate file generation, and data collection methods. Next, the methodology of validation and local calibration is described in Chapter 4. A method of programming for running the MEPDG automatically is introduced in Chapter 5. This method greatly reduces labor intensity involved in running the software. Chapter 6 presents the results of calibration and validation. Finally, the conclusions and recommendations are presented in Chapter 7.

CHAPTER 2

LITERATURE REVIEW

INTRODUCTION

This chapter provides a general overview of pavement concepts, including pavement types, distresses, and design factors. Traditional design methods and the MEPDG are investigated to describe the evolution of pavement design and understand the purpose and significance of this study. Furthermore, MEPDG local calibration efforts by Washington State, North Carolina, Ohio and Minnesota were researched to guide the conduction of this study.

PAVEMENT DESIGN OVERVIEW

Pavement Types

Pavement is usually classified into two categories based on surface materials, flexible and rigid. The flexible pavement is selected as the first choice in the U.S., which is determined by state highway agencies based on policy, economics, or both. In regard to service life, flexible pavement requires maintenance or rehabilitation every 10 to 15 years, while rigid pavement can last for 20 to 40 years. However, owing to high cost of rehabilitation, rigid pavement is narrowly adopted in urban and high traffic areas.

Flexible pavement

Flexible pavement is surfaced with the mixture of mineral aggregate and asphalt. Mineral aggregate, as the major component, accounts for 92 to 96 percent by volume and it provides pavement surfaces with qualities related to hardness, texture, and resistance to stripping. As a binding medium, asphalt becomes a viscous liquid at higher temperatures but turns to a solid at ambient air temperatures. Due to the effect of asphalt, the pavement will bend or deflect when traffic loads are applied without breaking; thus it is “flexible”. A flexible

pavement structure is normally composed of flexible surface courses and several layers of base materials which can accommodate and distribute this "flexing" over a larger area, downward to the subgrade.

Rigid pavement

Rigid pavement, also called portland cement concrete (PCC), is composed of aggregate, portland cement, and water. The aggregate accounts for 70 to 80 percent of portland cement concrete by volume and it can be either coarse aggregate (i.e., crushed stone and gravel) or fine aggregate (i.e., sand). The portland cement is the chief binding agent in rigid pavements. Once mixed with water, they harden into a solid mass. Because of high stiffness, rigid pavement tends to distribute the load over a relatively wide area of subgrade. The concrete slab itself provides most of a rigid pavement's structural capacity.

Pavement Distresses

As discussed earlier, pavements are categorized into flexible or rigid, but only flexible pavement is discussed since it is the main interest of this study. The major distresses for flexible pavement include fatigue cracking, rutting, longitudinal/transverse cracking, raveling, stripping, and the loss of skid resistance.

Fatigue cracking

Fatigue cracking is prevalent among aged flexible pavements. It gets another name, "alligator cracking", from its appearance in severely-damaged condition (Figure 2.1). The cracking initializes at the bottom of asphalt mixture layers and propagates upward to the surface, so it is also called "bottom-up cracking". The cracks allow moisture infiltration, roughness, and may further deteriorate to a pothole (*Fatigue cracking*, 2009). Thin HMA layers, stiff mixtures, and soft base are more likely to intensify the potential of bottom-up cracking (Schwartz and

Carvalho, 2007). The Highway Performance Monitoring System (HPMS) uses the percent of cracking area divided by the total area to measure the severity level of fatigue cracking. For example, the cracking of 500 ft length by 2 ft width in each wheelpath can be reported as 5% if the sample section is a single lane, 12 ft width by 1 mile length. In addition to these causes, cold weather often quickens the propagation of cracking. In the laboratory, the flexural beam test is typically performed to investigate the fatigue of a HMA material, which can be related to its resistance to fatigue cracking.

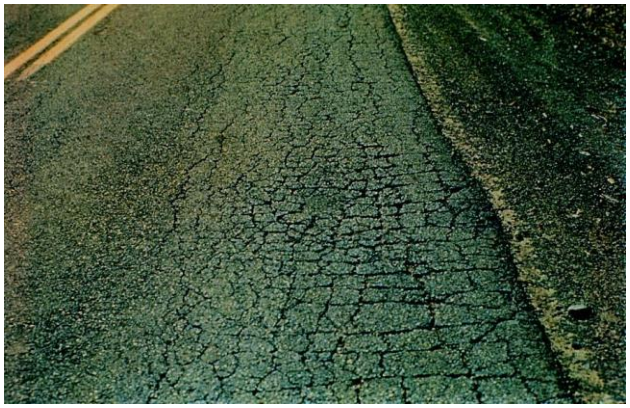

Figure 2.1 Fatigue cracking (*Fatigue cracking*, 2009)

Rutting

Rutting, also known as permanent deformation, is observed as surface depression in the wheel path, sometimes accompanied by pavement uplift along the sides of the rut (Figure 2.2). Ruts tend to steer a vehicle towards the rut path as its tires are riding on the rut, which can cause vehicle hydroplaning if ruts are filled with water (*Rutting*, 2008). It is a load-induced distress caused by consolidation or lateral movement of the materials due to cumulative traffic loading at moderate to high temperatures (Schwartz and Carvalho, 2007). The rut depth is usually measured by Straight Edge, Dipstick Profile, or Automated Laser Profile. In the laboratory, the tests for predicting the HMA rutting characteristics include the static creep test, the repeated load test, dynamic modulus test, empirical tests (i.e., the Hveem and Marshall mix design tests), and

wheel-tracking simulative tests. Each of them has limitations related to equipment complexity, expense, running time, and material parameters.

Figure 2.2 Rutting (*Rutting*, 2008)

Longitudinal/Transverse cracking

Longitudinal cracking (Figure 2.3) often develops parallel to the pavement centerline when the paving lane joint is poorly constructed. Transverse cracking (Figure 2.4) usually propagates across the centerline. These types of cracks are not usually load-associated. They may be caused by the shrinkage of asphalt surface due to low temperatures, asphalt hardening, or result from reflective cracking caused by cracks beneath the asphalt surface (Huang, 1993).

Figure 2.3 Longitudinal cracking (*Longitudinal cracking*, 2008)

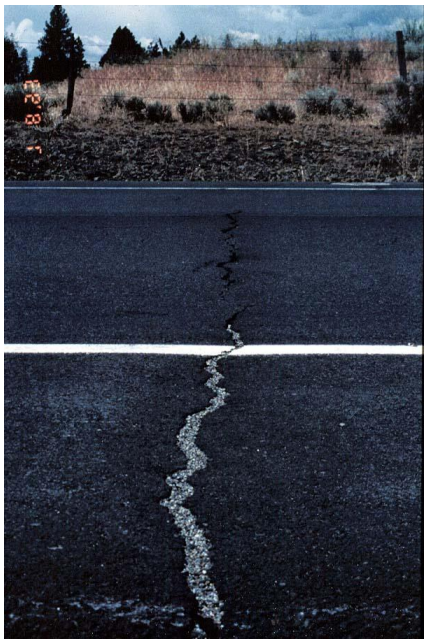

Figure 2.4 Transverse cracking (*Transverse cracking*, 2006)

Ride Quality

Ride quality represents the overall performance of a pavement. The ride quality is evaluated by pavement roughness, which is defined as an expression of irregularities in the pavement surface. The roughness adversely affects the ride quality, delay costs, fuel consumption, and maintenance costs (*Roughness* 2007). The typical metrics of pavement roughness are Present Serviceability Rating (PSR) developed by AASHO Road Test, International Roughness Index (IRI) developed by World Bank, or other indexes, with IRI being the most prevalent (*Roughness* 2007). The measurement of IRI is made using a profilometer, which can measure small surface variations in vertical displacement as a function of longitudinal position.

State highway agencies usually use the International Roughness Index (IRI) to rate pavement roughness, and schedule maintenance and rehabilitation plans. The lower the IRI is, the smoother the pavement surface.

Design Factors

Design factors were briefly discussed in Chapter 1; however, they are an essential part in the design method and crucial to the determination of a final design (i.e., thickness design). Thus, design factors are further specified with details in regard to traffic, the environment, material, failure criteria, and reliability herein.

Traffic

Traffic is the major cause of pavement distresses. It poses external forces to induce fatigue cracking progress and rutting accumulation during repetitive loadings. The effect of traffic is considered in terms of axle loads and the number of repetitions, contact pressure, vehicle speed, and traffic volume distribution.

Axle loads and number of repetitions

The response of pavement to applied traffic is determined by the magnitude of loads, axle types, and the spacing between axles. Load magnitude is a primary factor in the determination of damage; the relationship between axle weight and inflicted pavement damage is not linear but exponential. For instance, a 44.4 kN (10,000 lbs) single axle needs to be applied to a pavement structure more than 12 times to inflict the same damage caused by one repetition of an 80 kN (18,000 lbs) single axle (*Loads*, WSDOT Pavement Guide). As for axle types, two axles, if not grouped closely as tandem, tridem, or quad axle, should be considered independently because they are too far apart to superpose their effects (i.e., stresses or strains); otherwise, the influenced areas of these axles begin to overlap, as a result, the concern is no longer the single load but rather the combined effect of all the interacting loads. Obviously, it is not appropriate to treat those axles as one group as a single axle, nor is appropriate to treat each axle independently (Huang, 1993). In the AASHTO method, the load of an axle (i.e., single, tandem, tridem, or

quad) with a specific magnitude is normalized to a number of "standard" loads based on its damaging effect on the pavement. The "standard" loads are named as Equivalent Single Axle Loads (ESALs). In the M-E method, "load spectra" replaced the ESALs to characterize traffic directly by numbers of axles, axle configuration, and axle weight. It provides precise load data for each passing axle in the mechanistic analysis.

The number of repetitions describes how many axle loads are imposed during a long term. In the AASHTO method, the number of ESALs describes the repetitive traffic loadings in a uniform manner, serving as a fundamental input in pavement design. In the M-E method, the ratio of the number of actual loads over the number of allowable loads is used to quantify a long term effect of traffic loadings under the Miner's hypothesis (Miner, 1945). It is assumed in Miner's hypothesis that each axle load inflicts a certain amount of incremental damage, and the total damage can be estimated by a known number of load repetitions. If the pavement is imposed with a variety of load magnitudes, the damage ratio for each load magnitude can be specified separately based on its number of repetitions and then they can be combined together for predicting the total pavement damage.

Contact pressure

The contact pressure is the force spread over the interface between the tire and pavement, which equals to the force distributed to the pavement. In fact, the contact pressure is the result of composition of tire pressure and pressure due to tire wall. The contact pressure is greater than the tire pressure for low-pressure tires (Figure 2.5) because the wall of tires is in compression and the sum of vertical forces due to wall and tire pressure must be equal to the force due to contact pressure; otherwise, the contact pressure is smaller than the tire pressure for high-pressure tires

(Figure 2.5) (Huang, 1993). In mechanistic-empirical methods, the contact pressure is usually assumed to be the tire inflation pressure with a circular tire/pavement interface.

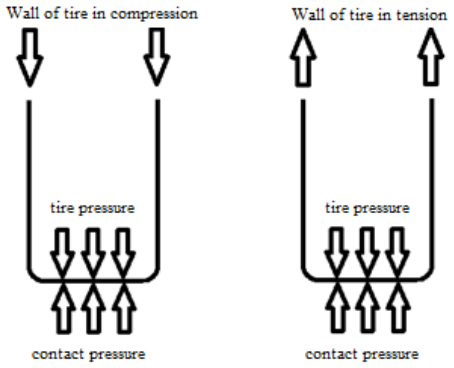

Figure 2.5 Low pressure tire (left) and high pressure tire (right) (Huang, 1993)

Vehicle speed

The vehicle speed determines the frequency of moving loads, which may affect the properties of pavement materials. For example, the stiffness of asphalt mixture is sensitive to the frequency of loading. Slower speeds typically result in lower modulus values in asphalt concrete which, in turn, increase strain levels.

Traffic volume distribution

On any given road, one direction typically carries more traffic than the other. Furthermore, within one direction, each lane carries a different portion. The outer lane often carries most of the trucks and therefore is usually subjected to heavier loading, especially for Interstate highways. This requires the outer lane to be more resilient to load-induced damage.

To prepare traffic data for designing a new pavement, agencies may need to monitor the characteristics of former traffic loads (i.e., past traffic volume, weight data, speed) along or near the roadway segment to be designed, thus, they can best forecast the traffic inputs for design purpose. Four main sources of traffic data are typically used for the traffic characterization in the MEPDG: weigh-in-motion (WIM) data, automatic vehicle classification (AVC), vehicle counts,

and traffic forecasting and trip generation models (NCHRP 1-37A Report, Part 2, Chapter 4, 2004).

Environmental effects

The environment provides an independent medium that affects material properties. The environment can vary much across different regions in a country with seasonal or monthly changes. The key environmental concerns in the pavement design are typically temperature and precipitation, which are usually recorded by local weather stations.

Temperature

Temperature greatly affects the behavior of asphalt materials. When the pavement gets cold, the HMA becomes stiffer and tends to have fatigue damage because stiff materials often have a shorter fatigue life. The extreme low temperature even induces low-temperature cracking, which could happen regardless of traffic loading (Ksaibati and Erickson, 1998). In practice, this problem can be avoided by adopting modified asphalt materials. Otherwise, when the pavement gets hot, the HMA becomes softer and tends to deform under traffic loading so rutting is more likely to occur at wheel paths.

Precipitation

Precipitation impacts the quantity of surface water, which can change the location of the groundwater table once it infiltrates into the subgrade. The groundwater table should be kept at least 3 feet below the pavement surface (Huang, 1993); otherwise, the seasonal frost will have a detrimental effect on pavements. Also, excessive moisture will cause the loss of bond between aggregates and binder, resulting in distresses, such as bottom-up cracking, stripping, and raveling.

Materials

As mentioned previously, the properties of materials determine the inherent capability to resist damage caused by traffic and environmental effects; thus, they need to be accurately characterized. The properties generally include mechanistic properties, such as stiffness and Poisson's ratio, and some other properties, for example, the related properties for low-temperature cracking: the tensile strength, creep compliance, and coefficient of thermal expansion.

The characterization of material properties differs in asphalt mixture and unbound materials. The discussion mainly covers the mechanistic properties for these two components since they are key roles in the pavement behavior.

Asphalt mixture

Asphalt mixtures are often modeled as elastic materials in elastic layered systems. The elastic modulus and the Poisson ratio were used to characterize asphalt mixture (Yoder & Witczak, 1975). Sometimes the resilient modulus was used instead of elastic modulus, which differed in the testing method. However, neither moduli accounted for the visco-elasticity of asphalt mixture. As a result, the dynamic modulus (|E*|) was proposed to characterize asphalt mixture so as to compute stress and strain in flexible pavements.

Elastic modulus

The elastic modulus, or Young's modulus, is a measure of the elasticity of a material, which is equal to the constant ratio of stress over strain within its elastic range of loading (i.e., a load range where the relationship between the stress and strain is linear) (*Elastic Modulus*, 2007). If the elastic modulus of asphalt mixture is higher, it will bend or deform less.

Resilient modulus

The resilient modulus of a material is an estimate of its elastic modulus (*Resilient Modulus*, 2007). The resilient modulus is determined by the tri-axial test, in which a repeated axial cycle stress of fixed patterns (i.e., magnitude, load duration, and cycle duration) is applied to a cylindrical test specimen. The cyclic load application can simulate actual traffic loading more accurately than constant load applications. The resilient modulus can be calculated as the ratio of the repeated deviator axial stress to the recoverable axial strain.

Dynamic modulus

The dynamic modulus uses a complex number with two components, a viscous part and an elastic part, to relate stress to strain for linear visco-elastic materials subjected to continuously-applied sinusoidal loading in the frequency domain (Witczak et al., 2002). The complex number is defined as the ratio of the amplitude of the sinusoidal stress (σ) at any given time (t) and the angular load frequency (ω), and the amplitude of the sinusoidal strain (ε) at the same time and frequency (Witczak et al., 2002).

$$E^* = \frac{\sigma}{\varepsilon} = \frac{\sigma_0 e^{i\omega t}}{\varepsilon_0 e^{i(\omega t - \theta)}} = \frac{\sigma_0 \sin \omega t}{\varepsilon_0 \sin(\omega t - \theta)} = |E^*| \cos\theta + |E^*| \sin\theta * i \qquad (2\text{-}1)$$

where,

σ_0 = peak (maximum) stress

ε_0 = peak (maximum) strain

θ = phase angle

ω = angular velocity

t = time

i = imaginary component of the complex modulus

This type of characterization for asphalt mixtures is under Level Input 1 in the MEPDG to account for the interaction between material properties and environmental conditions. It can be determined by the Asphalt Mixture Performance Test (AMPT).

Unbound materials

The unbound materials are not as frequency-temperature sensitive as asphalt mixtures. The characterization of unbound materials mostly focuses on resilient modulus, Poisson ratio, and the coefficient of lateral pressure. The resilient modulus can be measured from backcalculation based on FWD data or through the use of correlations with other material strength properties, such as California Bearing Ratio (CBR).

Moreover, only a few design methods, such as the MEPDG, require gradation, Atterberg limits, and hydraulic conductivity to predict temperature and moisture conditions within the pavement system.

Failure criteria

Failure criteria define the indicators related with the pavement failure (i.e., the occurrence of major distresses) and their thresholds. In the AASHTO method, the present serviceability index (PSI), which indicates the general condition of a pavement, is used as the criterion to judge whether the pavement fails or not. The failure criteria for M-E method are described in detail below.

Fatigue cracking

The failure criterion for fatigue cracking is the allowable number of load repetitions before “significant” cracking (or failure) occurs. In other words, if the number of applied load repetitions exceeds the allowable number of load repetitions, significant fatigue cracking is expected to occur. To identify and measure cracking, some visually evaluate the level of

cracking severity into low (no or a few cracks), moderate (interconnected cracks), and high (severely interconnected cracks) categories (Oregon DOT Distress Survey Manual, 2010). The definition of significant cracking (or failure) is often established on agencies' identification perspective, engineering experience, management strategy, and funding availability. The Asphalt Institute recommended an area greater than 45 percent of the wheel path or an equivalent 20 percent of the total lane as failure in their transfer functions (Priest and Timm, 2006). The MEPDG considered 50 percent fatigue cracking of the total lane at a damage percentage of 100 percent as failure (NCHRP 1-37A Report, Appendix II-1, 2004).

Rutting

The failure criterion for rutting is the allowable number of load repetitions before critical rut depth is formed. If the actual number of repetitions exceeds the allowable number of repetitions, rutting will cause driving discomfort and even potential safety hazards. The evaluation for rutting condition is based on the average depth of rutting, and varies by type of road. Usually, rut depth less than 0.2" is good, and rut depth larger than 0.5" is poor. The rut depth between 0.2" and 0.5" is fair (Pavement Preservation Manual, 2009). The definition of critical rut depth is often established on agencies' engineering experience, management strategy, and funding availability.

IRI

IRI, as an overall evaluation of pavement performance, can also be taken as a failure criterion. The failure criterion for IRI is usually an allowable level, which represents a combination of different distresses. The FHWA suggests that a road surface with IRI rating below 95 is in good condition, providing a decent ride quality; a road surface with IRI from 95 to 119 is in fair condition; a road surface with an IRI from 120 to 170 is in mediocre condition; and

a road with IRI above 170 is in poor condition, providing an unacceptable ride quality (AASHTO and TRIP 2009, P9). The definition of allowable IRI is often established on agencies' engineering experience, management strategy, and funding availability.

Other criteria

Besides the two failure criteria above, there are also some other criteria for specific distresses, such as low-temperature cracking. The potential of low-temperature cracking for a given pavement can be evaluated if the mix stiffness and fracture strength characteristics are known and temperature data on-site are available to compute the thermal stress. The pavement will crack when the computed thermal stress is greater than the fracture strength.

Reliability

The uncertainty and variability associated with design inputs have always been of great concern to pavement engineers. Uncertainty exists in any prediction of future situations (i.e., traffic and environmental changes). Variability is common because pavement materials are constructed with variance at different spatial locations. These may cause less accurate input characterization, which is the basis of a pavement design. To guarantee the reliability of design, there are two methods to account for uncertainty and variability associated with inputs: deterministic and probabilistic (Huang, 1993). In the deterministic method, each design input has a fixed value based on engineering judgment and experience. The designer assigns a safety factor to each design input to allow more challenging conditions so that the final design can withstand the risks beyond the estimated situation. A more realistic approach is the probabilistic method in which each of the design factors is assigned a mean and a variance. The variability of a design input is determined by characterizing its distribution, and then the reliability of an acceptable design can be estimated (Huang, 1993). The reliability of a pavement design can be defined as

the probability that the performance indicator is acceptable. For example, the reliability in the MEPDG is the probability that the performance of the pavement predicted for that design will be satisfactory over the time period under consideration (Li et al., 2011). It is defined in the design as equation (2-2).

$$R = P\,[\text{performance indicator over design period} < \text{critical indicator level}] \quad (2\text{-}2)$$

where,

P = probability, percent

The basic elements of pavement design as discussed above are accounted for in the pavement design methods which serve the project design. The following will introduce a few traditional and modern design methods that use elements of pavement design.

TRADITIONAL DESIGN METHODS

California Method

The California Method was originally developed in the 1940s based on experience obtained from test roads and pavement theory. It was adopted by the western states and has been modified several times to suit the changes of regional traffic characteristics. The objective of the original design method was to avoid plastic deformation and the distortion of the pavement surface, but a later modification included the minimization of early fatigue cracking due to traffic loads (Garber and Hoel, 2009).

The factors considered in this method are traffic loads and the strength of construction materials. The traffic loads are initially calculated in terms of ESALs and then converted to a traffic index (TI) as equation (2-3) (Garber and Hoel, 2009).

$$TI = 9.0 * \left(\frac{ESAL}{10^6}\right)^{0.119} \quad (2\text{-}3)$$

The strength of the subgrade material is determined by the Hveem Stabilometer test in terms of the resistance value R. The strength characteristics of each layer material are described by a gravel equivalent factor G_f, which is determined based on the type of material.

The thicknesses of respective layers are determined by dividing gravel equivalents (GE) by their factors G_f. The GE can be derived by Equation (2-4) depending on the R value. The R value is the resistance value of the material of the supporting layer (Garber and Hoel, 2009). For subgrade, the R value is normally determined at an exudation pressure of 300 psi.

$$GE = 0.0032 * (TI) * (100 - R) \tag{2-4}$$

The California Method is simple to use but its applicability is highly subject to the local traffic characteristics. Although the method accounts for the strength of supporting materials, it does not consider the seasonal effect of the environment. Different types of distresses are considered together to evaluate whether a pavement fails. It is not efficient to investigate a single type of distress and consider preventive measures.

Asphalt Institute Method

The Asphalt Institute Method establishes its own relationships between subgrade strength, traffic, and pavement structure. The goal of this method is to determine the minimum thickness of the asphalt layer with which the pavement can satisfy the criteria in regard to two types of strains: the horizontal tensile strain at the bottom of the asphalt layer, and the vertical compressive strain at the surface of subgrade (Garber and Hoel, 2009). The AI method is a good example of an early M-E approach to pavement design.

The basic design factors in this method are traffic characteristics, subgrade engineering properties, and base/subbase engineering properties. The annual traffic containing a mix of vehicle axle loads is converted to ESALs. In addition, the subgrade engineering properties

should be determined in the laboratory or relative to with other test values (i.e., CBR and R value). The base/subbase material should satisfy certain quality requirements in terms of CBR, liquid limit, Plasticity Index (PI), particle size distribution, and minimum sand equivalent.

The minimum thickness for various types of materials is determined by using a computer program DAMA or by using the appropriate charts, such as design chart for full-depth asphalt concrete shown in Figure 2.6.

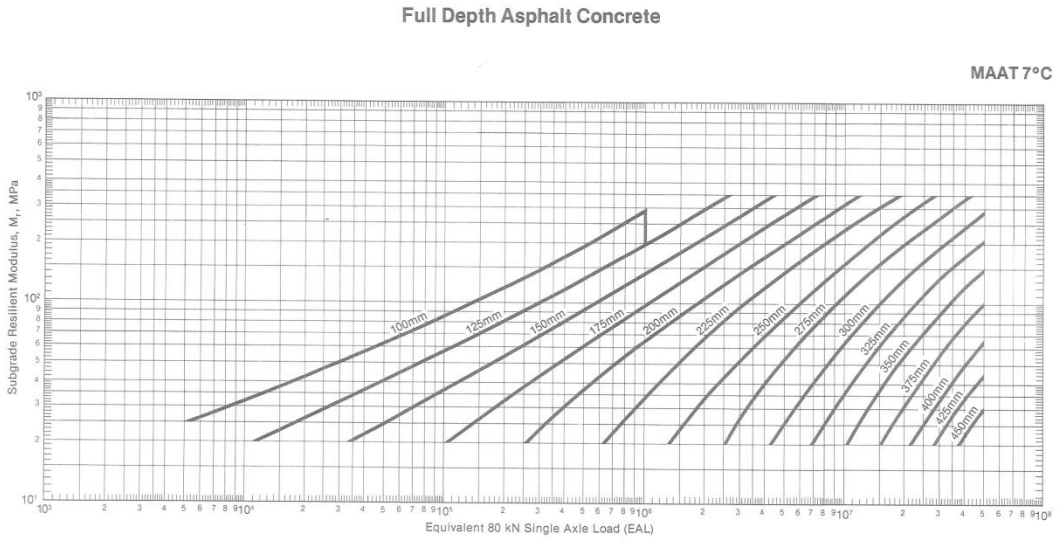

Figure 2.6 Design chart for full depth asphalt concrete (Asphalt Institute, 1983)

The Asphalt Institute method is straightforward and provides a guide for thickness determination for various paving materials. It also accounts for the effect of temperature on the materials when selecting an appropriate design chart based on mean annual air temperature (MAAT) of the local area. More importantly, the Asphalt Institute method is an M-E design method which establishes the design criteria based on the mechanics of materials coupled with the observed performance. The original fatigue transfer function was based on laboratory equation developed by Monismith and Epps (1969). Then, the transfer function was calibrated using field data from AASHO Road Test, considering the failure to be 45 percent cracking of

wheelpaths and then further modified to include a correction factor to account for the volumetrics of the mixture as suggested by Pell and Cooper (1975). Furthermore, only the determination of the soil modulus requires a reliability safety factor to account for the variability from design inputs. The design procedures still lack the consideration of variations associated with material quality, homogeneity, and construction technique, which might cause a non-uniform pavement response at different spatial locations. Also, the options of pavement materials are limited to several given material alternatives.

AASHTO Method

The AASHTO method includes a series of design methods with different versions based on the original AASHO Road Test. It has been widely used by state agencies. According to an FHWA survey (*Asphalt Design Procedure* 2007), 63 percent of the state DOTs were using the 1993 AASHTO method, while 12 percent of them were using the 1972 AASHTO method. In addition, 8 percent of the state DOTs were using a combination of AASHTO methods and state procedures. The AASHTO method aims to achieve a pavement design that allows a tolerable serviceability decrease over the design life. The first version of this design equation directly incorporated the empirical observations under the AASHO Road Test local conditions, and was modified and extended its applicability to other regions (AASHTO 1972, 1986, 1993).

The 1993 AASHTO method empirically evaluates the effects of design factors on pavement performance, with respect to design time constraints, traffic, reliability, serviceability, environmental effect, and effective subgrade modulus. The method adopts the design equation, as Equation (2-5) for flexible pavements, or a nomograph (Figure 2.7) to derive a thickness design based on the evaluation of those design factors. In either the design equation or the

nomograph, the Structural Number (SN) is usually targeted as the result which can generate the thicknesses of layers (AASHTO guide, 1993).

$$\log W_{18} = Z_R * S_0 + 9.36 * \log_{10}(SN+1) - 0.20 + \frac{\log_{10}[\frac{\Delta PSI}{4.2-1.5}]}{0.4 + \frac{1094}{(SN+1)^{5.19}}} + 2.32 * \log M_R - 8.07 \qquad (2\text{-}5)$$

where,

W_{18}= predicted number of 80kN (18,000 lbs) ESALs

Z_R = standard normal deviate at chosen percent reliability (R)

S_0 = combined standard error of the traffic prediction and performance prediction

SN = structural number

ΔPSI = difference between the initial design serviceability index, p_0, and the design terminal serviceability index, p_t

M_R = the resilient modulus of material used for the lower layer, psi

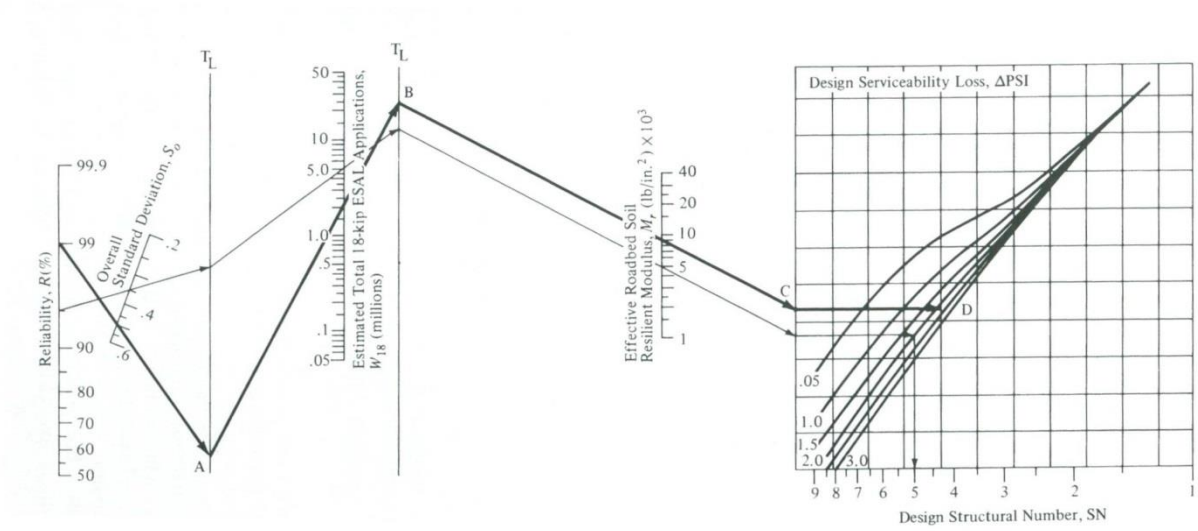

Figure 2.7 Nomograph (AASHTO guide, 1993)

Two variables are adopted for design time constraints: analysis period and performance period. The analysis period is the length of time over which the whole pavement maintenance

strategy is designed to apply. It includes both the design life of use after initial construction and the prolonged life due to planned rehabilitation. The performance period is the length of time during which a pavement structure deteriorates from the initial serviceability to terminal serviceability before rehabilitation, or the performance time between rehabilitation operations. The analysis period is used for evaluating alternative long-term strategies based on the life-cycle cost analysis (Huang, 1993).

The ESAL concept is used to quantify traffic loadings. The ESALs that a pavement will encounter over the design life is determined by counting truck traffic, predicting traffic growth, and converting this to ESALs (AASHTO Guide, 1993).

The reliability is determined by the functional classification of the pavement. For example, for an Interstate highway in an urban area, the recommended reliability should lie between 85 to 99.9 percent. The reliability is related to the "normal deviate", which is a statistic adopted in the design equation (AASHTO Guide, 1993).

The change of serviceability represents the capacity of pavement to withstand damage experienced between initial construction and terminal failure. The serviceability is evaluated by PSI, which is derived based on the original PSR from the AASHO Road Test. The initial PSI is a function of pavement classification and construction quality; and the terminal PSI is a design index that can be tolerated until rehabilitation, resurfacing, or reconstruction (AASHTO Guide, 1993).

The effect of the environment is accounted for by applying an excessive reduction of serviceability in the design equation. Since the AASHTO methods are derived based on the two-year AASHO Road Test, the long-term effect of temperature and moisture on the pavement structure cannot be precisely evaluated (AASHTO Guide, 1993).

The subgrade is characterized by one elastic modulus. This modulus would result in the same damage as predicted by using the multiple moduli which account for its seasonal (or monthly) fluctuation due to temperature, moisture, or load damage. In the Figure 2.8, the monthly soil modulus is transferred to relative damage, and then the relative damages are averaged. The average relative damage is used to derive the effective soil modulus, which accounts for the monthly fluctuation of soil modulus.

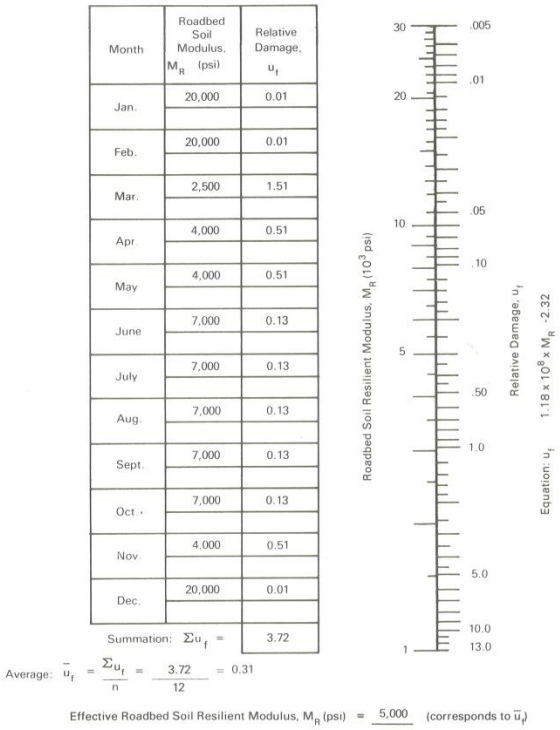

Figure 2.4. Chart for estimating effective roadbed soil resilient modulus for flexible pavements designed using the serviceability criteria.

Figure 2.8 Chart for estimating effective subgrade resilient modulus (FHWA, 2006)

The structural number is used to determine the thickness of respective layer. It is a function of layer thicknesses, layer coefficients, and drainage coefficients as Equation (2-6) shows, and it accounts for all the layers above the layer that M_R characterizes (Figure 2.9).

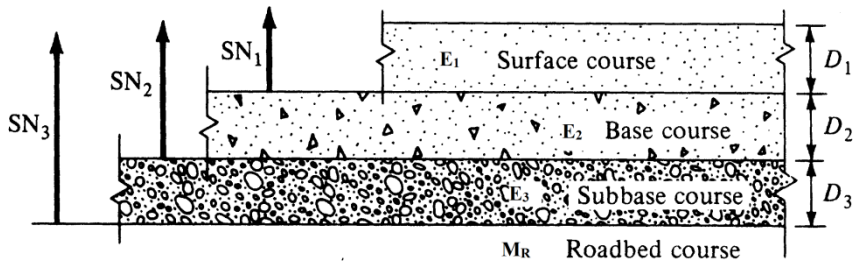

Figure 2.9 Pavement structure (Garber and Hoel, 2009)

For example, if M_R in the Equation (2-6) is substituted by the modulus of the base course (E_2) in Figure 2.9, the SN_1 only accounts for the surface layer; if M_R is substituted by the modulus of the subbase course (E_3), the SN_2 accounts for the surface and base layer. Therefore, the thickness of each layer can be derived by dividing a_i from the corresponding $a_i * D_i$.

$$SN_n = a_1 * m_1 * D_1 + a_2 * m_2 * D_2 + a_3 * m_3 * D_3 + \cdots + a_n * m_n * D_n \quad (2\text{-}6)$$

where,

SN_n = structural number for the combined n-layer structure

a_i = layer coefficient for surface, base, or subbase (i = 1, 2, 3, ⋯, or n)

m_i = dainage coefficient for surface, base, or subbase (i = 1, 2, 3, ⋯, or n)

D_i = the thickness of surface, base, or subbase (i = 1, 2, 3, ⋯, or n), in.

The AASHTO methods first adopted the concept of ESALs to quantify the effect of traffic loadings and the concept of PSI to evaluate the serviceability of pavement condition. Additionally, the AASHTO methods have specific variables in the design procedure to account for the effect of climate and subgrade. However, these methods are empirically-based because they are proposed based on the AASHO Road Test. Therefore, the efficiency of the AASHTO methods cannot be well-guaranteed in different regions with characteristics of modern traffic, climate, and materials.

MEPDG

Introduction

The Mechanistic-Empirical Pavement Design Guide (MEPDG) is a pavement design guide associated with its computer software that applies the mechanistic-empirical design to analyze input data and to predict the damage accumulation over the design life. It is applicable to designs for new or rehabilitated pavements, in any type of flexible, rigid, and semi-rigid pavement. The typical predicted distresses for flexible pavement designs are alligator cracking, rutting, thermal cracking; and for rigid pavement designs, faulting, cracking, and continuously reinforced concrete pavement (CRCP) punch-outs. Design performance can be compared with the threshold values, or comparisons of performance may be made for alternate designs with varying traffic, structure, and materials (Sharpe, 2004).

The MEPDG is one of the most sophisticated design methods because it not only characterizes design inputs in all-inclusive details, but also incorporates the M-E design structure with advanced features in reliability, input hierarchy, and distress analysis. It is not as straightforward as the older AASHTO methods, which derive pavement thicknesses directly from design equation or the nomograph; it requires an iterative process in which the pavement structure configuration is adjusted until the predicted performance of pavement satisfies the design criteria.

Input Characterization

The MEPDG employs a hierarchical approach for selecting design inputs based on the designer's knowledge of input parameters and importance of project (Li et al., 2011). The input Level 1 requires measured data directly, either in-situ or project-specific. This level represents the most familiar situation for a specific project. The input Level 2 needs a lower accuracy of

input information. The input parameters could be estimated by correlations or regression equations. The input Level 3 is the easiest one to determine just using estimated or default values. Most of the inputs in this study were provided at input Level 1, which helps to minimize the error in the estimation of design inputs.

Material characterization

The MEPDG characterize materials using many properties, which are required by the mechanistic model, transfer functions, and the climatic model (NCHRP Project 1-37A Report, Part 2, Chapter 2, 2004).

For asphalt concrete, the mechanistic model requires two basic properties: dynamic modulus and Poisson's ratio. The Poisson's ratio can be assumed but the dynamic modulus is a variable affected by temperature and loading frequency. The dynamic modulus is provided by lab data at input Level 1. The properties for transfer functions are tensile strength, creep compliance, and coefficient of thermal expansion (NCHRP 1-37A Report, Part 2, Chapter 2, 2004). In addition, the parameters required for the climatic model are mainly thermal properties of HMA and binder viscosity.

For unbound materials, the resilient modulus and the Poisson's ratio are used in the mechanistic model. The unit weight and the coefficient of thermal expansion are needed if the unbound material is considered to be stress-sensitive at input Level 1. No inputs are required by transfer functions for flexible pavement designs. In addition, the gradation parameters, plasticity index, optimum moisture contents are needed for climatic models (NCHRP Project 1-37A Report, Part 2, Chapter 2, 2004).

Environmental effects characterization

The MEPDG adopted the Enhanced Integrated Climate Model (EICM) to characterize environmental effects. The EICM is a one-dimensional heat and moisture flow program that simulates changes in the behavior and characteristics of pavement and subgrade materials in conjunction with climatic conditions. The major output from the EICM is a set of adjustment factors for unbound layer materials, which accounts for the effects of environmental conditions. Also, three additional outputs of importance are the temperatures at midpoints of each bound layer, the temperature profiles within the asphalt for every hour, and the average moisture content for each sub-layer (NCHRP 1-37A Report, Part 2, Chapter 3, 2004). These outputs are incorporated into the design framework regarding materials characterization, structural response, and performance prediction. The EICM enables hourly characterization of temperature, moisture, and frost throughout the pavement structure, considerably enhancing the quality of pavement design. The source of environmental data comes from more than 800 weather stations of the National Climatic Data Center (NCDC) throughout the United States, which allows the user to select a given station or generate a climatic data file for local use (Li et al., 2011).

Traffic characterization

The MEPDG no longer uses the ESAL concept to evaluate traffic, but adopts the load spectra for analyzing traffic directly in a series of load ranges of axles. The inputs accounting for axle type, load magnitude, and traffic volume jointly define the number of loading repetitions for each axle group classified by axle configuration and magnitude; and the numbers of loading repetitions will be analyzed for the damage accumulation.

Mechanistic Models

The MEPDG utilizes the JULEA multilayer elastic theory program to calculate mechanistic responses of the pavement structure assuming that all materials can be treated as linearly elastic (NCHRP 1-37A Report, Part 3, Chapter 3, 2004). Each pavement layer (i.e., asphalt, base, and subgrade) is actually divided into thinner sub-layers so that the varying properties at different depths can be captured. The JULEA program can predict stress, strain or deflection at any point in a particular layer or sub-layer based on material properties, layer structure, and loading conditions; meanwhile, it provides a combination of analysis features, theoretical rigor, and computational speed (NCHRP 1-37A Report, Part 3, Chapter 3, 2004). The load-induced responses are analyzed at critical locations with various depths and the most damage-vulnerable points are used to predict pavement distress performance (Schwartz and Carvalho, 2007). In addition, the Finite Element Model (FEM) would be applied to the special situation that the non-linear behavior of unbound materials is simulated (e.g., Input Level 1 for subgrade materials).

Distress Prediction Models

Fatigue cracking

The fatigue cracking model for asphalt concrete in the MEPDG was obtained based upon the Asphalt Institute's equation, which was derived by modifications to constant stress laboratory fatigue criteria (Asphalt Institute, 1982). The Asphalt Institute's equation was calibrated to Equation (2-7) using data from 82 LTPP sections including new and rehabilitated pavements across the country with different climatic locations and diverse range of site features. The calibration process included collecting the LTPP calibration data, running the MEPDG simulation using different sets of coefficients, comparing the predicted damage to the measured

cracking, and minimizing the square of errors between predicted damage and the measured cracking (NCHRP 1-37A Report, Appendix II-1, 2004). The standard error of model predictions was 6.2% (NCHRP 1-37A Report, Appendix II-1, 2004). The local calibration coefficients β_{f_i} were set to be 1 in the nationally-calibrated models.

$$N_f = 0.00432 * C * \beta_{f_1} * \varepsilon_t^{-\beta_{f_2} * 3.9492} * E^{-\beta_{f_3} * 1.281} \quad (2\text{-}7)$$

where,

N_f = number of repetitions of a given magnitude of load to failure

β_{f_1}, β_{f_2}, β_{f_3} = local calibration coefficients

C = laboratory to field adjustment factor, $C=10^M$ and

$$M = 4.84 * \left(\frac{V_{beff}}{V_a + V_{beff}} - 0.69\right)$$

V_{beff} = the effective binder content, percent by volume

V_a = the air voids, percent by volume

ε_t = tensile strain at the critical location in the asphalt layer, in./in.

E = asphalt concrete stiffness at given temperature, psi

Then, the damage caused by a given magnitude of load will be accumulated in terms of the ratio between the actual load repetitions and allowable load repetitions based on the Miner's Law (1945):

$$D_k = \sum \frac{n_{ij}}{N_{ij}} \quad (2\text{-}8)$$

where,

D_k = damage for layer k

n_{ij} = actual load repetitions for load i within period j

N_{ij} = allowable load repetitions for load i within period j

In order to provide in-situ representation for cracking, the MEPDG adopted another model, called alligator cracking model, to relate the accumulated damage (D_k) to the cracked area. Fatigue cracking is measured in terms of cracking area as the percentage of the lane area in the MEPDG, and 50% of the total lane area is considered as failure (NCHRP 1-37A Report, Appendix II-1, 2004). This model was calibrated to be as followed using the same LTPP database.

$$FC = \left(\frac{6000}{1+e^{(C1*C1'+C2*C2'*\log(D_k*100))}}\right)*\left(\frac{1}{60}\right) \quad (2\text{-}9)$$

$$C_2' = -2.40874 - 39.748(1+h_{AC})^{-2.856} \quad (2\text{-}10)$$

$$C_1' = -2*C_2' \quad (2\text{-}11)$$

where,

FC = alligator fatigue cracking, percent

$C_1 = C_2 = 1$

D_k =damage for layer k, percent

h_{AC} = total thickness of asphalt layer, in.

Rutting

In the MEPDG, rutting is evaluated for asphalt concrete and unbound materials, respectively. For asphalt concrete, the adopted rutting model was initially based on Leahy's model, modified by Ayes, and last by Kaloush (Schwartz and Carvalho, 2007). For unbound materials, the model was first derived by Tseng and Lytton, which was modified by Ayres and later on by El-Basyouny and Witczak (NCHRP 1-37A Report, Appendix GG-1, 2004). The national calibration was performed using the identical LTPP sections used for the fatigue

cracking model calibration. The calibration process included collecting the LTPP calibration data, running the MEPDG simulation using different sets of coefficients, selecting the best coefficients based on the reasonableness of the results, adjusting functions for confining pressure, and minimizing the square of errors between predicted damage and the measured cracking. As a result, the predictions produced a SE of 0.055 inch for the asphalt concrete model (NCHRP 1-37A Report, Appendix GG-1, 2004). The SE was 0.014 inch for the base/subbase model, and 0.056 inch for the subgrade model (NCHRP 1-37A Report, Appendix GG-1, 2004). For asphalt rutting prediction in the MEPDG, the asphalt concrete layer is subdivided into thinner sublayers, so the total predicted rut depth for the asphalt concrete layer can be achieved by:

$$Rut_{AC} = \sum_{i=1}^{n} (\varepsilon_p)_i * \Delta h_i \quad (2\text{-}12)$$

where,

Rut_{AC} = rut depth at the asphalt concrete layer, in.

n = number of sublayers

$(\varepsilon_p)_i$ = vertical plastic strain at mid-thickness of sublayer i, in./in.

Δh_i = thickness of sublayer i, in.

The vertical plastic strain (ε_p) in the sublayer i can be determined by the nationally-calibrated model below, which was calibrated using identical LTPP pavement sections used for asphalt concrete fatigue cracking model calibration (NCHRP 1-37A Report, Appendix GG-1, 2004). The resilient strain is derived by the mechanistic model.

$$\frac{\varepsilon_p}{\varepsilon_r} = \beta_1 * 10^{-3.35412} * T^{1.5606*\beta_2} * N^{0.4791*\beta_3} \quad (2\text{-}13)$$

where,

ε_r = computed vertical resilient strain at mid-thickness of the sublayer i, in./in.

k_1, k_2, k_3 = regression coefficients derived from laboratory testing

β_1, β_2, β_3 = local calibration coefficients

T = temperature, °F

N = number of repetitions from a given load group

The unbound granular materials are also divided into sublayers, and the total rut depth is the summation of rut depth appeared in each of sublayers. The rut depth (δ_i) appeared in any given sublayer is computed as:

$$\delta_i = \beta_1 * k_1 * (\frac{\varepsilon_p}{\varepsilon_r}) * e^{-(\frac{\rho}{N})^{\beta}} * \varepsilon_v * h_i \quad (2\text{-}14)$$

where,

δ_i= rut depth or plastic deformation of the sublayer i, in.

β_1 = local calibration coefficient

k_1 = regression coefficient determined from the laboratory permanent deformation test

ε_P = intercept for the sublayer i determined from laboratory repeated load permanent deformation tests, in./in.

ε_r = resilient stain for the sublayer i imposed in laboratory test to obtain material properties (i.e., ε_P, β, and ρ), in./in.

β, ρ = material properties

N = number of load applications

ε_v = average vertical resilient strain in the sublayer i for a given load and calculated by the mechanistic model, in./in.

h_i = thickness of the sub-layer i, in.

It is not computationally feasible to divide the subgrade into sublayers so as to estimate the total subgrade rut depth because the subgrade is regarded as a semi-infinite layer in the structural response models (NCHRP 1-37A Report, Appendix GG-1, 2004). An adjustment on the rutting models is therefore required for computing the plastic strains in a semi-infinite layer. The plastic strain at different depths can be computed with a simpler method as Equation (2-15), and it will be used to determine the total subgrade rutting (Schwartz and Carvalho, 2007).

$$\varepsilon_p(z) = (\varepsilon_{p0}) * e^{-\alpha * z} \quad (2\text{-}15)$$

where,

$\varepsilon_p(z)$ = plastic vertical strain at the depth z (measured from the top of the subgrade), in./in.

ε_{p0} = plastic vertical strain at the top of the subgrade (i.e., z=0), in./in.

Z = depth measured from the top of the subgrade, in.

α = regression coefficient

With regard to determine the value of α, two depths in the subgrade were utilized to fit Equation (2-15) and solve a system of two equations. The MEPDG uses the top of the subgrade (z=0) and 6 inches below the top (z=6). The plastic strains at these two depths can be derived by Equation (2-14) given that the plastic strain is also the ratio of the rut depth over the sublayer thickness (i.e., δ_i/h_i).

The total subgrade (δ_{sb}) rut depth can be computed by integrating Equation (2-16) over the whole subgrade down until the bedrock (Schwartz and Carvalho, 2007).

$$\delta_{sb} = \left(\frac{1 - e^{-\alpha h_{bedrock}}}{k}\right)\varepsilon_{p0} \quad (2\text{-}16)$$

where,

$h_{bedrock}$ = depth to the beckrock, in.

Roughness

The MEPDG roughness models were developed for flexible pavements with three types of base layers: relatively thick granular base, asphalt-treated base, and cement-treated base (NCHRP 1-37A Report, Appendix OO-3, 2004). The IRI model considered over 350 LTPP sections in the calibration. The SE was 0.387 m/km. The equation for conventional flexible pavement with thick granular base is shown as Equation (2-17). The calibration coefficients shown in the MEPDG were specified regarding rutting, fatigue cracking, transverse cracking, and site factors (Darter, Titus-Glover, and Von Quintus, 2009).

$$IRI = IRI_0 + 40\,(RD) + 0.400\,(FC_{Total}) + 0.008\,(TC) + 0.015\,(SF) \quad (2\text{-}17)$$

where,

RD = average rut depth, in.

FC_{Total} = total area of load-related cracking (combined alligator, longitudinal, and reflection cracking in the wheel path), percent of wheel path area

TC = total length of transverse cracks, ft./mile

SF = site factor

$$SF = Frosth + Swellp * Age^{1.5} \quad (2\text{-}18)$$

where,

Frosth = Ln [(Precip+1) * Fines * (FI + 1)]

Swellp = Ln [(Precip+1) * Clay * (PI + 1)]

Fines = Fsand + Silt

Age = pavement age, year

PI = subgrade soil plasticity index, percent

Precip = average annual precipitation or rainfall, in

FI = average annual freezing index, °F days

Fsand = amount of fine sand particles (between 0.074 and 0.42 mm) in subgrade, percent

Silt = amount of silt particles (between 0.074 and 0.002 mm) in subgrade, percent

Clay = amount of clay particles (less than 0.002 mm) in subgrade, percent

Local Calibration

The MEPDG, like all mechanistic-empirical design methods, relies on predictions of pavement responses under load correlated to empirical predictions of distress. The distress prediction models in the MEPDG were derived based on a national calibration of previously-developed equations using LTPP data from the entire U.S. Thus, the models reflect a wide range of traffic conditions, climates, and structural configurations, rather than a state-specific or local design scenario. Furthermore, modern advancements in asphalt technology, such as polymer-modified materials and warm-mix asphalt were not included in the LTPP sections during the MEPDG national calibration. Since state and regional differences, in addFition to material characteristics, can strongly influence pavement performance, there is a need for local calibration of the transfer functions prior to implementation of the MEPDG.

The aim of local calibration is to reduce the difference between an observed result and a predicted result to a minimum value. The calibration process is performed on pavement sections that are characterized in traffic, climate, material, and field performance. The stepwise procedure recommended for a local calibration includes (AASHTO's Guide for the Local Calibration of the MEPDG, 2010):

a. Select hierarchical input levels for use in local calibration
b. Develop experimental design & matrix
c. Estimate sample size for each distress simulation model
d. Select roadway segment
e. Extract and evaluate roadway segment/test section data
f. Conduct field investigation of test sections to define missing data
g. Assess bias for the experimental matrix or sampling template
h. Determine local calibration coefficient to eliminate bias of transfer function
i. Assess standard error for transfer function
j. Improve precision of model; Modify coefficients and exponents of transfer functions or develop calibration function
k. Interpretation of results; Decide on adequacy of calibration coefficients

The recommended procedure by AASHTO provides a systematic guidance for performing local calibration of the MEPDG. The methodology of this study is discussed in Chapter 4 including local calibration and validation. The following section details local calibration efforts conducted by several states.

LOCAL CALIBRATION CASE STUDIES

Washington

The Washington State Department of Transportation (WSDOT) initiated MEPDG local calibration for the replacement of the 1993 AASHTO Design Guide by the MEPDG. The research utilized a total of 38 weight-in-motion stations with different locations and traffic patterns throughout Washington. The climate data recorded by the weather stations in Washington were tested, inspected, and judged to be acceptable for calibration efforts (Li et al.,

2009). The traffic data were obtained from the WSDOT project design records. The structural information and pavement performance were provided by the Washington State Pavement Management System (WSPMS).

The use of the calibration dataset combined two statistical approaches: split-sample approach and jackknife testing approach (Li et al., 2009). The split-sample approach is to split the sample into two subsets: one for the local calibration and the other for the validation. The datasets for local calibration and validation need to be independent of each other to ensure validity of analysis. The jackknife approach is to re-compute the statistic estimate leaving out one or more observations at a time from the sample set. In the new set of replicates of the statistic, an estimate for the bias and an estimate for the variance of the statistic can be calculated.

The local calibration process was implemented by five basic steps: bench testing, model analysis, calibration, validation, and iteration (Li et al., 2009). For the bench testing, it aimed to evaluate the MEPDG regarding the run-time issues and the reasonableness of model predictions, and to identify the needs of local calibration. The reasonableness of the models was checked by varying key design parameters of traffic loading, climate, layer thickness, and soil properties; and then comparing results with expected pavement performance.

The local calibration should be performed in an appropriate order among different distress models (Li et al., 2009). First, the asphalt mixture fatigue model needed to be calibrated before the longitudinal and alligator cracking models. Second, the cracking and rutting models needed to be calibrated before calibrating the roughness model. Also, the team conducted a sensitivity analysis on the calibration coefficients of the models, which intends to evaluate how

much each calibration coefficient affects the results of pavement distress models (Li et al., 2009). The sensitivity was defined as follows:

$$E_{distress}^{C_i} = \frac{\partial(distress)/distress}{\partial(C_i)/C_i} \quad (2\text{-}19)$$

where,

$E_{distress}^{C_i}$= sensitivity of calibration coefficient C_i for the associated distress condition

∂ (distress)= change in estimated distress associated with a change in factor C_i

∂ (C_i)= change in the calibration coefficient C_i

distress = estimated distress using default calibration coefficients

C_i = default value

Table 2.1 shows the sensitivity of each calibration coefficient based on typical pavement characteristics in Washington State. A positive value implies that the prediction increases as the calibration coefficient increases, and a negative value implies that the prediction decreases as the coefficient increases. Zero implies that the coefficient has no impact on the model prediction.

Table 2.1 Sensitivity of the MEPDG calibration coefficients (Li et al., 2009)

Local calibration coefficients	Sensitivity values	Related variables in the MEPDG distress models
AC fatigue		
β_{f1}	-3.3	Effective binder content, air voids, AC thickness
β_{f2}	-40	Tensile strain
β_{f3}	20	Material stiffness
Longitudinal cracking		
C_1	-0.2	Fatigue damage, traffic
C_2	1	Fatigue damage, traffic
C_3	0	No related variable
C_4	$\approx$0	No related variable
Alligator cracking		
C_1	1	AC thickness
C_2	0	Fatigue damage, AC thickness
C_3	$\approx$0	No related variable
Rutting		
β_{r1}	0.6	Layer thickness, layer resilient strain
β_{r2}	20.6	Temperature
β_{r3}	8.9	Number of load repetitions
IRI		
C_1	Not available	Rutting
C_2	Not available	Fatigue cracking
C_3	Not available	Transverse cracking
C_4	Not available	Site factor

Only new flexible pavement sections were selected in this study. The local calibration results were derived by minimizing the root-mean-square error (RMSE) between the MEPDG predictions and WSPMS measured data on all selected sections.

The local calibration was performed based on two representative sections, while the local calibration results were validated by using a broad dataset which are independent of the two sections. Thirteen flexible pavement stations for validation were selected from three different data sources based on traffic level, soil, and climate conditions. Five pavement sections from a previous WSDOT study covered high/medium/low traffic with strong subgrade in western Washington, medium traffic with strong subgrade in eastern Washington, and medium traffic with weak subgrade in eastern Washington. Six representative sections were from WSPMS

accounting for high/low traffic with strong subgrade for both western and eastern Washington, low traffic with weak subgrade in eastern Washington, and medium traffic with strong subgrade on mountain area. In addition, two sections in Washington were used in the original MEPDG national calibration, which was classified as medium traffic with strong subgrade in eastern Washington and high traffic with strong subgrade in western Washington (Li et al., 2009).

For the calibration, an initial set of calibration coefficients was assumed in the MEPDG for each of the two selected sections for the local calibration. Then, one of the calibration coefficients with a higher sensitivity value was varied and run iteratively to evaluate the RMSE (Li et al., 2009). Once no significant improvement for RMSE was made, another coefficient with the higher sensitivity among the rest was adjusted in the MEPDG. The results of local calibration should be a set of calibration factors that lead to the lowest RMSE between the MEPDG predictions and WSPMS observations. Then, the local calibration results were validated by using other sections. Table 2.2 below shows the final calibration results of this study.

Table 2.2 Final local calibration coefficients (Li et al., 2009)

Calibration Factor	MEPDG Default	After Local Calibration
AC fatigue		
β_{f1}	1	0.96
β_{f2}	1	0.97
β_{f3}	1	1.03
Longitudinal cracking		
C_1	7	6.42
C_2	3.5	3.596
C_3	0	0
C_4	1000	1000
Alligator cracking		
C_1	1	1.071
C_2	1	1
C_3	6000	6000
AC rutting		
β_{r1}	1	1.05
β_{r2}	1	1.109
β_{r3}	1	1.1
Subgrade rutting		
β_{s1}	1	0
IRI		
C_1	40	N/A
C_2	0.4	N/A
C_3	0.008	N/A
C_4	0.015	N/A

In this study, it was found that the alligator cracking was significant in WSDOT flexible pavements; and the locally-calibrated alligator cracking curve showed the same trend as the measured data (Li et al., 2009). The plots below show the measured and predicted alligator cracking in western and eastern Washington.

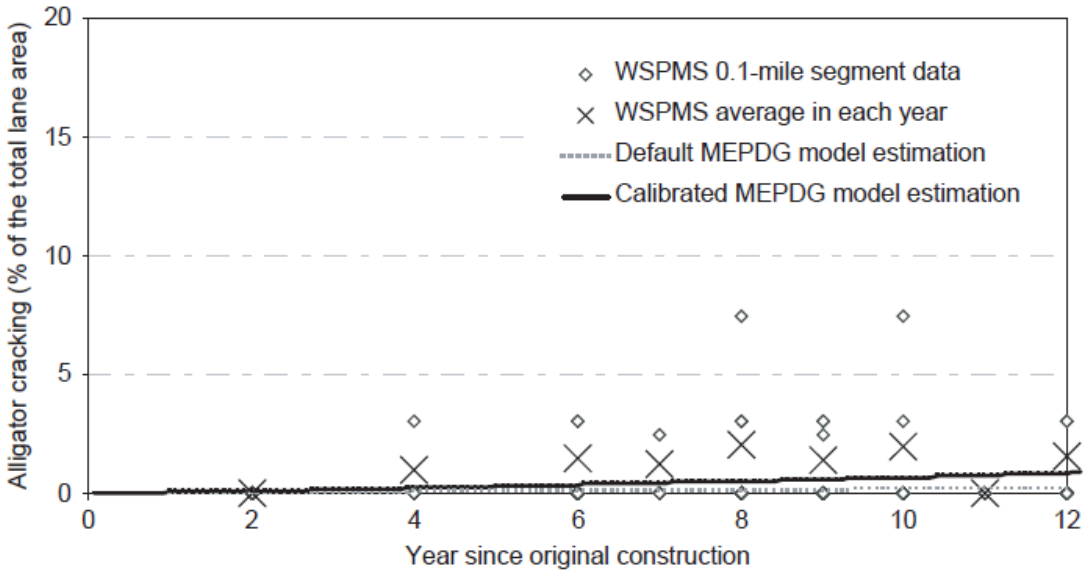

Figure 2.10 Measured and predicted alligator cracking in western Washington (Li et al., 2009)

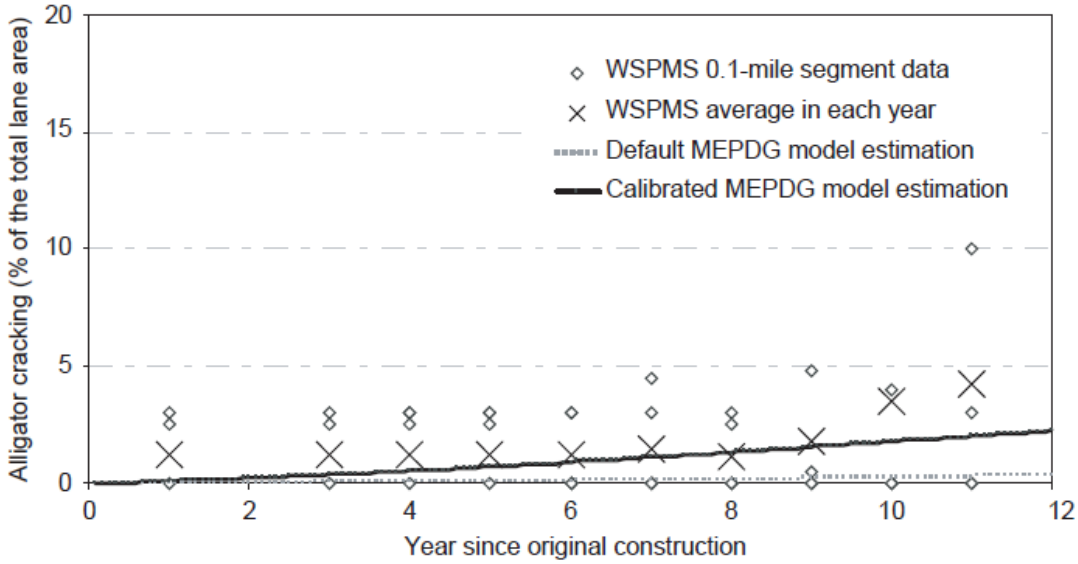

Figure 2.11 Measured and predicted alligator cracking in eastern Washington (Li et al., 2009)

The longitudinal cracking was significant and the locally-calibrated model provided a reasonable prediction of longitudinal cracking (Li et al., 2009). The plots below show the measured and predicted longitudinal cracking in western and eastern Washington.

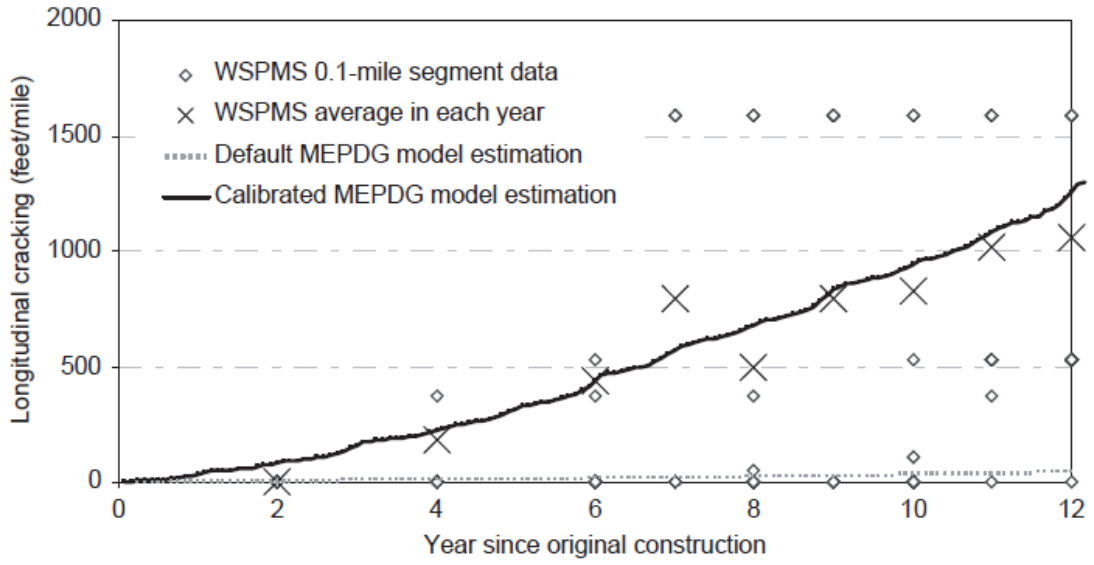

Figure 2.12 Measured and predicted longitudinal cracking in western Washington (Li et al., 2009)

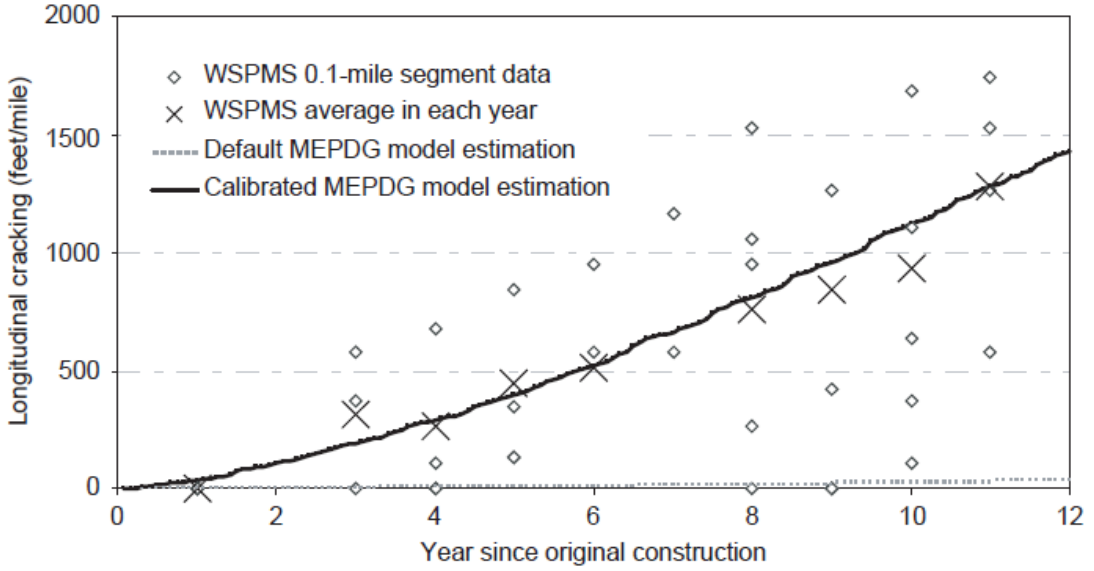

Figure 2.13 Measured and predicted longitudinal cracking in eastern Washington (Li et al., 2009)

As for the transverse cracking, WSPMS data showed no transverse cracking in Western Washington but a significant amount in eastern Washington (Li et al., 2009). The predicted transverse cracking by the nationally-calibrated model matched well with the WSPMS data and

WSDOT observations. The plots below show the measured and predicted transverse cracking in western and eastern Washington.

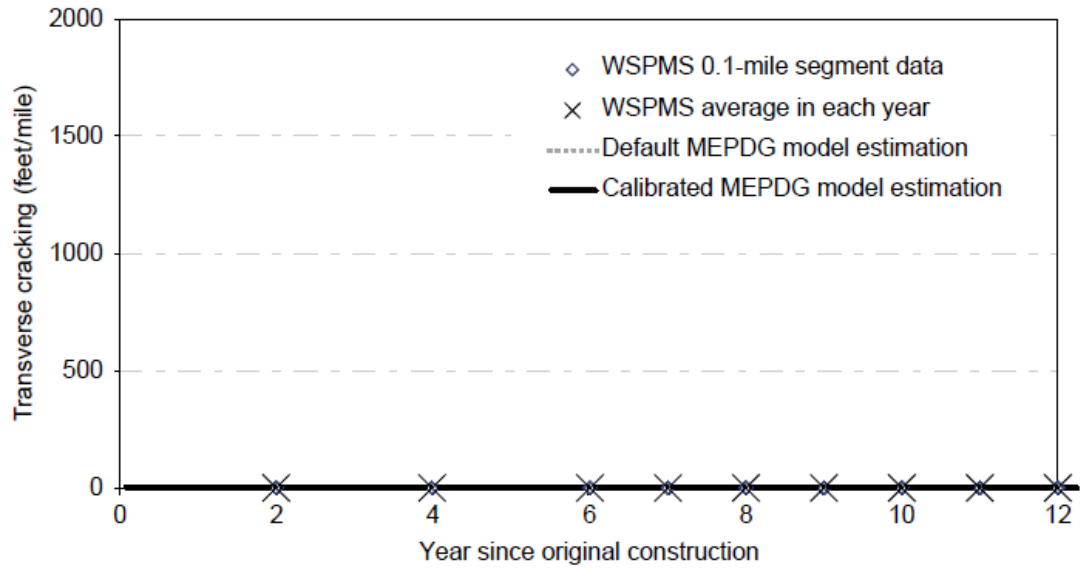

Figure 2.14 Measured and predicted transverse cracking in western Washington (Li et al., 2009)

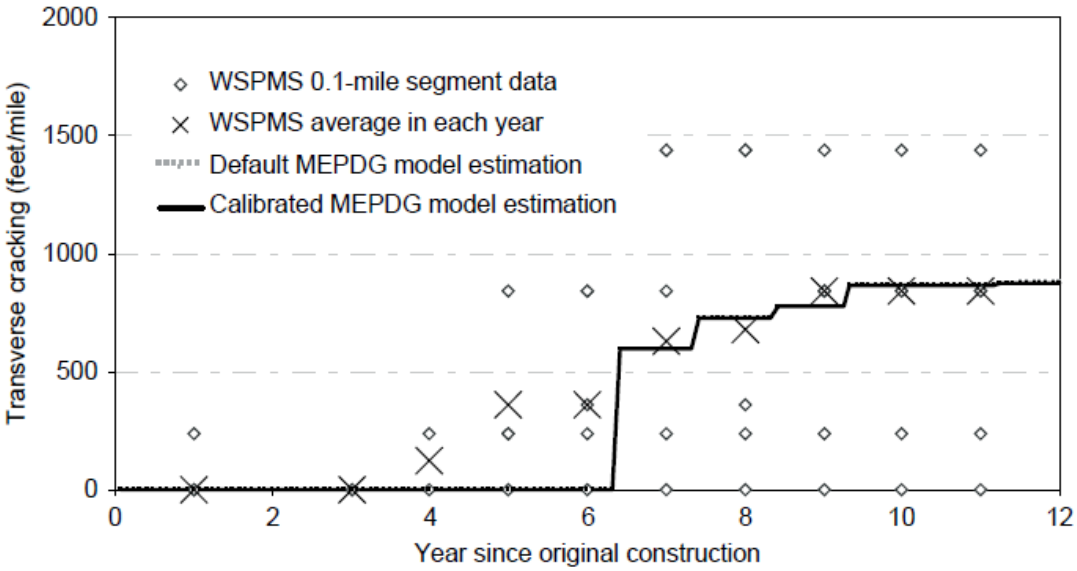

Figure 2.15 Measured and predicted transverse cracking in eastern Washington (Li et al., 2009)

In addition, the rutting predictions of the locally-calibrated model matched well with WSPMS data throughout the design life. The plots below show the conformity of the measured rutting with predicted rutting in western and eastern Washington.

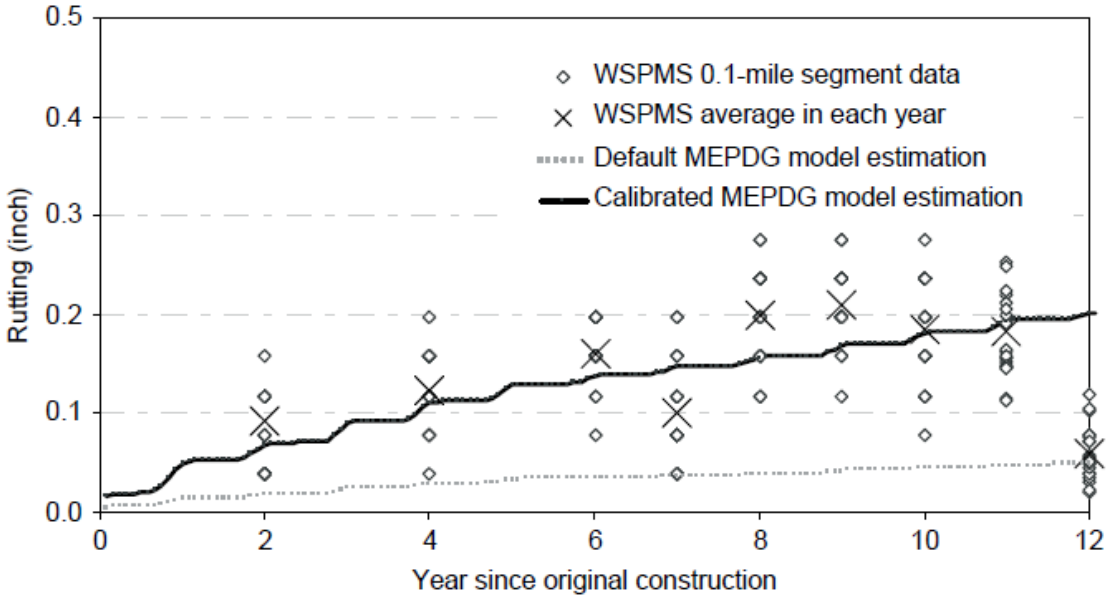

Figure 2.16 Measured and predicted rutting in western Washington (Li et al., 2009)

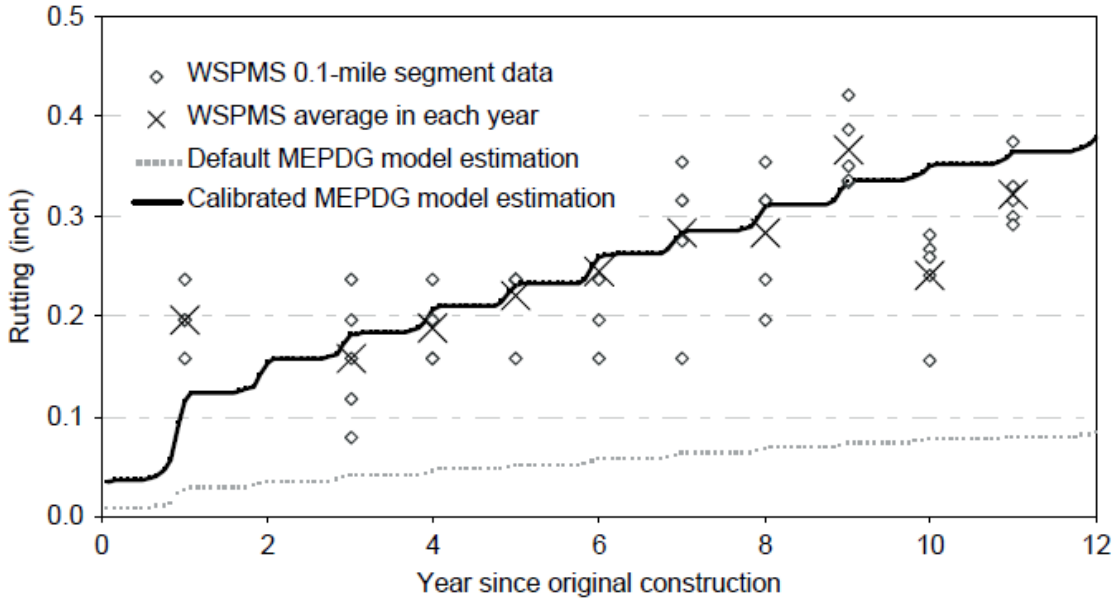

Figure 2.17 Measured and predicted rutting in eastern Washington (Li et al., 2009)

For the roughness, the measured values of WSDOT flexible pavements tended to be higher than the nationally-calibrated model predictions. However, the difference between the MEPDG predictions and measurements can be minimized by the roughness local calibration (Li et al., 2009). The plots below show the comparison between the measured and predicted IRI in western and eastern Washington.

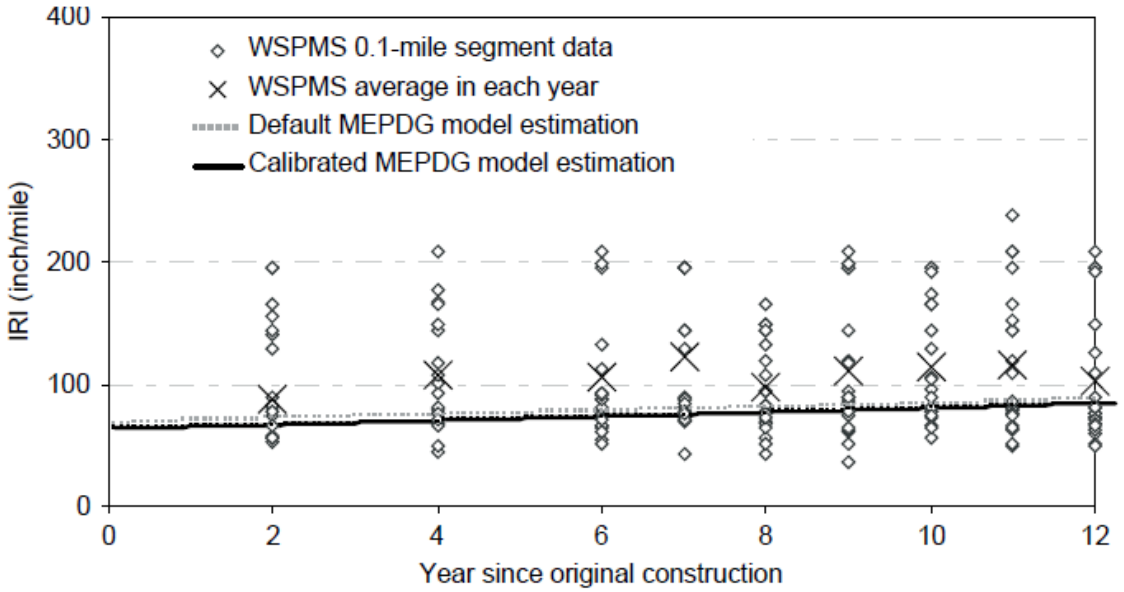

Figure 2.18 Measured and predicted IRI in western Washington (Li et al., 2009)

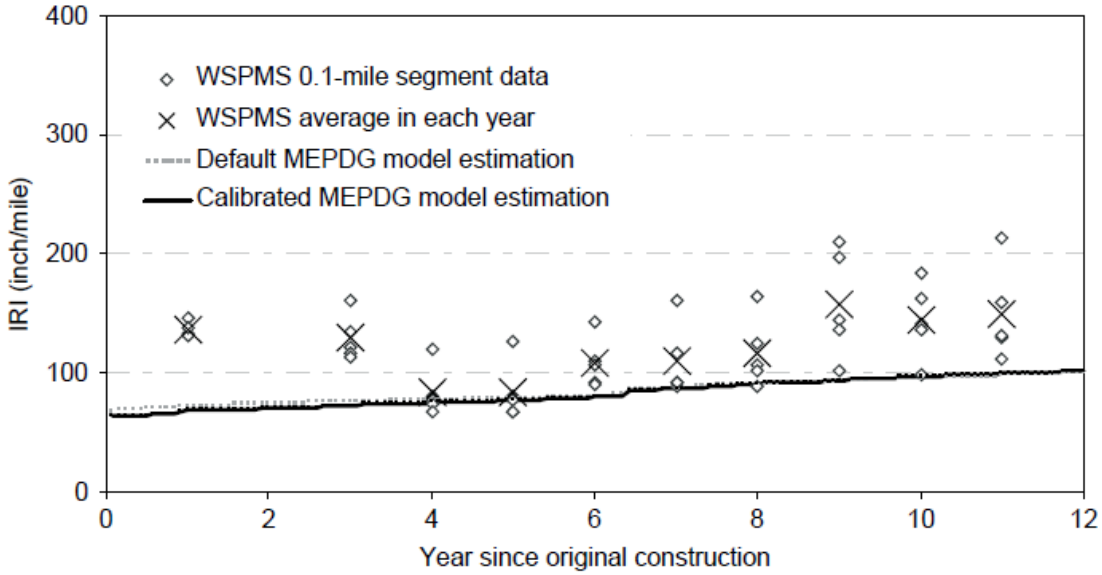

Figure 2.19 Measured and predicted IRI in eastern Washington (Li et al., 2009)

North Carolina

The North Carolina Department of Transportation (NCDOT) conducted a local calibration of the MEPDG for asphalt pavements in terms of the rutting model and bottom-up fatigue cracking model (Muthadi and Kim, 2008). In terms of the calibration dataset, 30 LTPP pavement sections (i.e., 16 new flexible pavement sections and 14 rehabilitated sections) were chosen from the LTPP database, and 23 NCDOT pavement sections were selected from the NCDOT data system. A total of 53 sections were selected from three geographic areas: mountain, piedmont, and coastal regions. The climatic data for these sections was obtained by interpolating the data from weather stations nearby based on the local geographic information (Muthadi and Kim, 2008).

An experimental matrix was developed to classify all sections based on their pavement types and structures (Muthadi and Kim, 2008). 39 new sections (i.e., 11 sections with thin HMA, 11 with intermediate HMA, and 17 with thick HMA) and 14 rehabilitated sections (i.e., 8 sections with intermediate HMA and 6 sections with thick HMA) were selected in this study. Approximately 80% of the dataset (including data from 53 sections) were utilized for the calibration and the remaining 20% were for the validation.

The local calibration plan included three steps (Muthadi and Kim, 2008): first, run the MEPDG based on the local traffic, climate, and material information using the nationally-calibrated models. Second, calibrate the coefficients in the models to minimize the bias between the predicted and the measured distresses and reduce the standard error, if any exists. Third, validate the recommended calibration coefficients by evaluating the accuracy of prediction models. The following are major concerns and important findings in this study.

For the rutting model, it was recognized that the appropriate value of calibration coefficient k_1 can be solved by using the Microsoft Excel Solver program instead of running the MEPDG many times (Muthadi and Kim, 2008). Furthermore, β_{GB} was varied to reduce the error between the predicted and measured granular base rutting; and β_{SG} was varied for the subgrade rutting (Muthadi and Kim, 2008). However, the measured rut depth distributed in each layer (i.e., asphalt, granular base, and subgrade) cannot be directly obtained in the field like the total rut depth, so the measured rut depth must be estimated. It was assumed that the portion of the predicted rut depth distributed in each layer was the same as the portion of the measured rut depth distributed in each layer. So the measured granular base rut depth and subgrade rut depth can be calculated based on their proportions accounted in the total predicted rut depth (Muthadi and Kim, 2008).

In the local calibration, a Chi-square test was performed to determine whether the standard error provided by the local calibration results was significantly different from that provided by the national calibration results (Muthadi and Kim, 2008). For the rutting model, the standard error provided by local calibration results was not significantly different from that by national calibration results (Table 2.3). For the fatigue cracking model, the results of local calibration (i.e., $R^2 = 0.11$ and standard error = 3.64) were still considered to be better than the results of national calibration (i.e., $R^2 = 0.03$ and standard error = 6.02), but Figure 2.20 revealed that neither of them looked satisfactory. One possible reason identified was that the cracks outside the wheel path were usually ignored in the measurements by NCDOT, which caused the under-estimation of fatigue cracking.

Table 2.3 Statistical summary of the rutting model local calibration results (Muthadi and Kim, 2008)

	AC		GB	
	National calibration	Local calibration	National calibration	Local calibration
Average Rut depth (in)	0.1178	0.1030	0.0442	0.0344
SE(in)	0.054	0.047	0.027	0.021
Bias(in)	-0.0149	0	-0.0098	0
p-value	0.00622, <0.05	0.499, >0.05	0.0002, <0.05	0.5, >0.05
N	111	111	111	111
	SG		**Total**	
	National calibration	Local calibration	National calibration	Local calibration
Average Rut depth(in)	0.1551	0.1026	0.3171	0.2399
SE(in)	0.084	0.056	0.154	0.109
Bias(in)	-0.0525	0	-0.0771	0
p-value	1.6E-9, <0.05	0.5, >0.05	2.9E-7, <0.05	0.499, >0.05
N	111	111	111	111

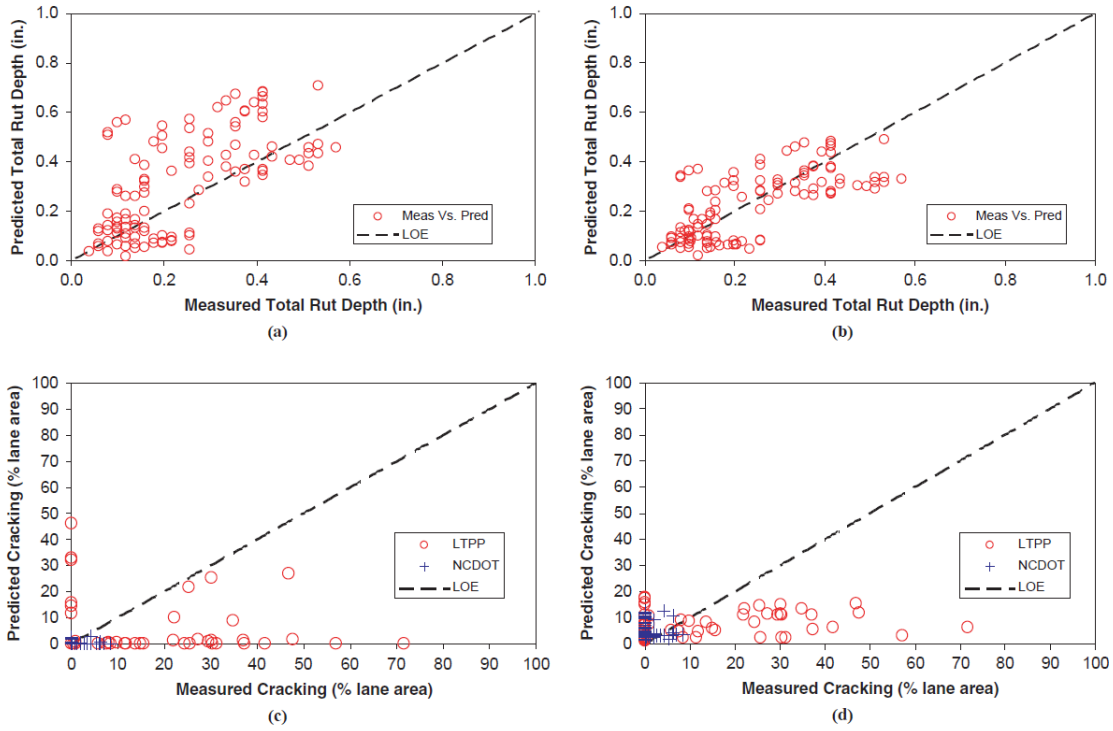

Figure 2.20 Measured versus predicted distresses: (a) total rut depth predicted by nationally-calibrated rutting model (b) total rut depth by locally-calibrated rutting model (c) fatigue cracking by nationally-calibrated rutting model (d) fatigue cracking by locally-calibrated rutting model (Muthadi and Kim, 2008)

Then, the remaining 20% of the dataset were used to validate the reasonableness of the final calibrated models. The results of the validation were shown in Table 2.4.

Table 2.4 Statistical summary of validation results (Muthadi and Kim, 2008)

	rutting model	fatigue cracking model
SE	0.145 in	4.86 %
bias	0.033 in	-5.04%
N	26	32
chi-square Statistic	36.82	5.66
degree of freedom	25	31
p-value	0.0599, >0.05	0.9999, >0.05

Finally, the recommendation regarding the calibration coefficients was exhibited in Table 2.5. It was concluded that the rut depth values predicted by the locally-calibrated model matched well the observed rut depth values in LTPP sections; the locally-calibrated alligator cracking

model under-predicted the percentage of alligator cracking for most of the sections (Muthadi and Kim, 2008).

Table 2.5 Recommended calibration coefficients (Muthadi and Kim, 2008)

	calibration coefficient	national calibration	local calibration
Rutting			
AC	k_1	-3.4488	-3.41273
	k_2	1.5606	1.5606
	k_3	0.479244	0.479244
GB	β_{GB}	1.673	1.5803
SG	β_{SG}	1.35	1.10491
Fatigue			
AC	k_1	0.00432	0.007566
	k_2	3.9492	3.9492
	k_3	1.281	1.281
	C_1	1	0.437199
	C_2	1	0.150494

Ohio State

Mallela et al. composed guidelines of implementing the MEPDG for Ohio. They collected input data using information from the LTPP sections. The sensitivity analysis was first performed to evaluate how the variation in the output of a model can be apportioned, qualitatively or quantitatively, to different sources of variation in the input of a model (Mallela et al., 2009). Then, the local calibration of performance prediction models were conducted by modifying calibration coefficients. The adequacy of the local calibration was evaluated by checking the results of prediction with the measured data. The statistical analysis was provided to evaluate the difference between predictions and measured data.

In this study, the alligator cracking model was not calibrated because the field measurement of the alligator cracking was often disturbed by the early generated longitudinal cracking during construction. For the HMA transverse cracking, a non-statistical comparison was performed between measured and predicted values after the local calibration, and a further evaluation was recommended by using data from northern Ohio sites (Mallela et al., 2009). The

nationally-calibrated rutting model consistently over-predicted the rut depth. Considering the fact most of the sections used for local calibration have relatively thick HMA layers, the proportion of HMA layer rutting (about 17 to 44 percent) in the total rutting was proportionately higher. Therefore, they attempted to reduce the proportion of unbound layers in the total rutting by adjusting the sub-model coefficients β_{s1} and β_{s2}. Also, the MEPDG over-predicted rutting for lower magnitudes of measured rutting and under-predicted rutting for the higher magnitudes of measured rutting. This requires an adjustment to β_{r2} and β_{r3} of the HMA rutting sub-model (Mallela et al., 2009). The results of the statistical analysis before local calibration are presented in Table 2.6 and Figure 2.21.

Table 2.6 Hypothesis testing before local calibration of the rutting model (Mallela et al., 2009)

Hypothesis	DF	Parameter Estimate	Std. Error	t Value	p-value	95 Percent Confidence Limits	
H0: Intercept =0	1	0.2178	0.0059	36.8	<0.0001	0.21	0.23
H0: Slope = 1	1	1.0228	0.0571	13.49	<0.0001	0.65	0.88
H0: Measured-Predicted Rutting =0	101			-52.7	<0.0001		

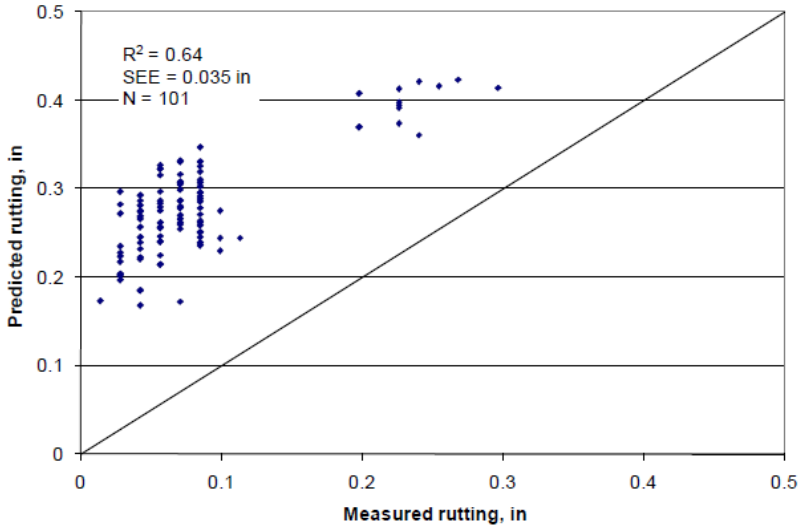

Figure 2.21 Measured versus predicted HMA total rutting before local calibration (Mallela et al., 2009)

The total rutting model was locally-calibrated using Equation (2-20) (Mallela et al., 2009). The results of the statistical analysis after local calibration are presented in Table 2.7.

$$Rut_{total} = 0.51 * Rut_{AC} + 0.32 * Rut_{Base} + 0.33 * Rut_{Subgrade} \quad (2\text{-}20)$$

where,

Rut_{total}= total rut depth, in.

Rut_{AC}= asphalt rut depth, in.

Rut_{Base}= base rut depth, in.

$Rut_{Subgrade}$= subgrade rut depth, in.

Table 2.7 Hypothesis testing after local calibration of the rutting model (Mallela et al., 2009)

Hypothesis	DF	Parameter Estimate	Std. Error	t Value	p-value	95 Percent Confidence Limits	
H0: Intercept =0	1	0.083	0.0024	34.4	<0.0001	0.078	0.087
H0: Slope = 1	1	0.952	0.049	19.4	0.3395	0.855	1.05
H0: Measured-Predicted Rutting =0	101			-5.62	<0.0001		

The measured and predicted HMA total rutting are shown in Figure 2.22. It can be seen that the number of data points was the same as that in Figure 2.21 but the R^2 was 0.63. It was found previously in Figure 2.21 that the predicted rutting was generally 0.2 in. higher than the measured rutting. However, the R^2 was reported to be 0.64, which was even higher than the R^2 value of 0.63 in Figure 2.22. Therefore, the local calibration did improve the prediction but did not increase the R^2. It suggested that the R^2 was not an efficient statistic to evaluate the improvement of MEPDG predictions.

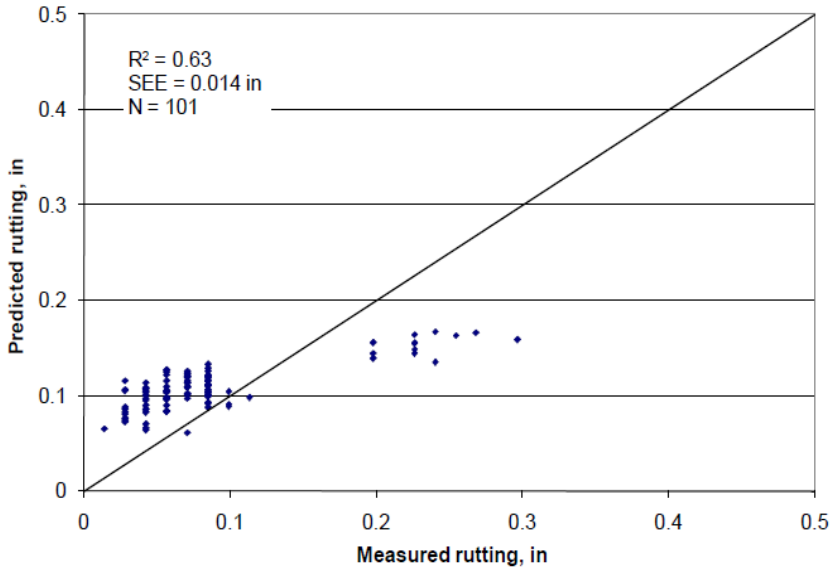

Figure 2.22 Measured versus predicted HMA total rutting after local calibration (Mallela et al., 2009)

It was found that the goodness of fit of the locally-calibrated model was adequate, but the model predictions were still with bias. A more comprehensive evaluation of HMA pavement mixtures and a larger calibration dataset would be necessary to calibrate the models for ODOT in the future (Mallela et al., 2009). Besides, the nationally-calibrated IRI model for HMA provided a poor correlation ($R^2 = 0.008$) between the measured and MEPDG predicted values. Through a local calibration, the R-square value increased to 0.69 while the SEE was about the same as the nationally-calibrated model (Mallela et al., 2009). The bias produced by the locally-calibrated model was considered to be acceptable compared with the nationally-calibrated model.

Minnesota State

Minnesota utilized the data from the MnROAD project for their local calibration (Hoegh et al., 2010). They mainly compared the actual measurement of rutting data from 31 test sections located on I-94 highway with the MEPDG predicted rutting data for those sections. It was found that the total rut depth predicted by the nationally-calibrated model was far higher than measured total rut depth (Hoegh et al., 2010). The predicted base and subgrade rutting was found

unreasonably high as Figure 2.23 shows. However, the HMA rut depth predicted by the nationally-calibrated model was quite similar to the measured total rut depth. Therefore, their local calibration modified the nationally-calibrated model predictions by subtracting the predicted value in the first month. This can reduce the bias between the predicted and measured rut depth. The following local calibration of the MEPDG rutting model was proposed as below (Hoegh et al., 2010).

$$Rut_{total} = Rut_{AC} + Rut_{Base}* + Rut_{Subgrade}* \quad (2\text{-}21)$$

$$Rut_{Base}* = Rut_{Base} - Rut_{Base1} \quad (2\text{-}22)$$

$$Rut_{Subgrade}* = Rut_{Subgrade} - Rut_{Subgrade1} \quad (2.23)$$

where,

Rut_{total} = predicted surface rut depth using the nationally-calibrated model, in.

Rut_{AC} = predicted asphalt rut depth using the nationally-calibrated model, in.

Rut_{Base}*= predicted base rut depth after model local calibration, in.

$Rut_{Subgrade}$*= predicted subgrade rut depth after model local calibration, in.

Rut_{Base} = predicted base rut depth using the nationally-calibrated model, in.

$Rut_{Subgrade}$ = predicted subgrade rut depth using the nationally-calibrated model, in.

Rut_{Base1} = predicted base rut depth using the nationally-calibrated model in the first month, in.

$Rut_{Subgrade1}$= predicted subgrade rut depth using the nationally-calibrated model in the first month, in.

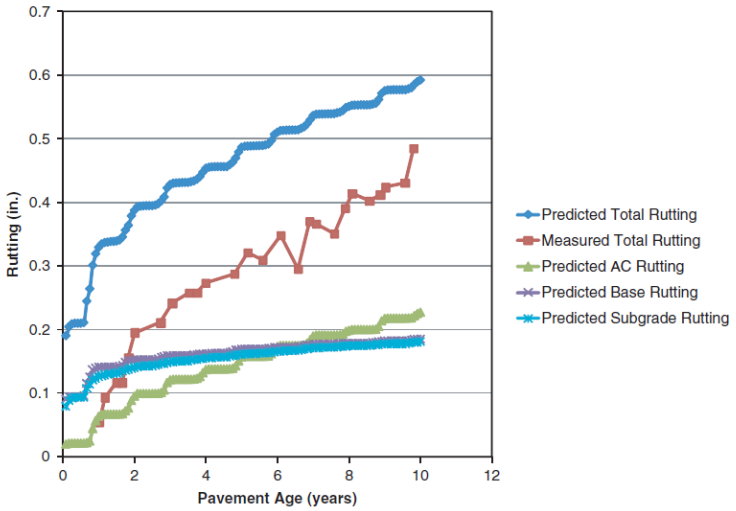

Figure 2.23 Measured and predicted rutting for Section 2 before local calibration (Hoegh et al., 2010)

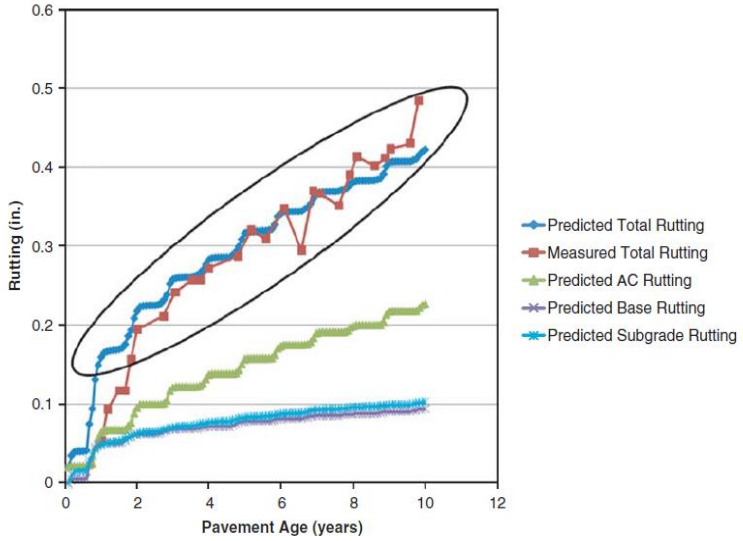

Figure 2.24 Measured and predicted rutting for Section 2 after local calibration (Hoegh et al., 2010)

So the predicted rutting curve after local calibration had a better correlation with measured rutting curve for the entire life of pavement and this trend was observed for most of the sections (Figure 2.24). It was suggested that the locally-calibrated rutting model was an improvement for the Minnesota conditions despite a wide range of local design features, such as different traffic mixes, and different pavement ages (Hoegh et al., 2010).

SUMMARY

The local calibration of the MEPDG needs to be performed based on a comprehensive understanding of pavement design concepts. Therefore, this chapter gathers the basic knowledge from literature to equip the study toward pavement designs. It can help to inform the fundamentals of pavement design and illuminate the modern trend of design needs before getting into the presentation of the study. The next chapter introduces the dataset of the study including input characterization and pavement performance measurements.

CHAPTER 3

MEPDG INPUT CHARACTERIZATION AND PERFORMANCE DATA COLLECTION

TEST FACILITY INTRODUCTION

The National Center for Asphalt Technology (NCAT) at Auburn University has been devoted to exploring and advancing asphalt technology to fulfill the pavement industry needs since 1986. The main task of NCAT is to perform asphalt material testing and research and to investigate real-world pavement performance.

Test Track

Research cycle

The Test Track began in 2000 with 46 sections comprising a 1.7 mile track. In 2003, 23 of 46 original sections were rebuilt to facilitate another round of research. Of these sections, eight were rebuilt and utilized for a structural experiment; fifteen were shallow milled and inlaid (i.e., between ¾ and 4 inches deep), while the other 23 sections remained in place to serve as a continuation of the original experiment. In 2006, eleven structural sections were newly built with varied thicknesses, and other sections from the past cycle were rehabilitated with shallow milling (i.e., less than 4 inches) or left in place. In 2009, the fourth research cycle began. Seventeen of the test sections were either reconstructed or rehabilitated, while the remaining 29 were left in place to allow for additional traffic loading (West et al., 2012). In this research, the data used was mainly from the 2003 and 2006 research cycles.

Structural study

NCAT initiated the structural study of pavements in the 2003 research cycle to study dynamic response and long-term performance of various pavement structures, and to validate and calibrate performance prediction models based on Test Track conditions (Priest, 2013). In the 2003 research cycle, eight sections were designed, instrumented, and investigated to be used

for the initial structural study (Timm, 2009). In the 2006 research cycle, five structural sections (i.e., N3, N4, N5, N6, and N7) from 2003 were left in-place, and three structural sections (i.e., N1, N2, and N8) from 2003 were rebuilt; moreover, three new structural sections (i.e., N9, N10, and S11) were added.

Materials Laboratory

The NCAT materials laboratory is equipped with state-of-the-art facilities to perform all routine mix design and quality control tests for asphalt binders and mixtures. The laboratory provided sufficient material characterization for inputs into the MEPDG.

MEPDG INPUTS CHARACTERIZATION

Introduction

A variety of input parameters were characterized to describe the design scenarios based on the results of lab testing, field measurement, and theoretical correlation. Level 1 inputs required by the MEPDG were developed, when possible, to ensure the highest accuracy of model predictions of pavement performance.

General Information

From the construction records of the 2003 and 2006 research cycle, the base/subgrade construction month for each section was retrieved, as well as the asphalt layer construction month (Table 3.1). This information was to provide the project starting point in the MEPDG. Once pavement construction finished, traffic loading started for the whole track in the next month. At that point, the initial pavement smoothness was measured in terms of IRI (Table 3.2).

Table 3.1 Construction and traffic months

Section	Test Cycle	Base/Subgrade Construction Month	Asphalt layer Construction Month	Traffic Opening Month
N1	2003	June	July	October
N2	2003	June	July	October
N3	2003	June	July	October
N4	2003	June	July	October
N5	2003	June	July	October
N6	2003	June	July	October
N7	2003	June	July	October
N8	2003	June	July	October
N1	2006	August	September	November
N2	2006	August	September	November
N8	2006	August	October	November
N9	2006	August	October	November
N10	2006	August	October	November
S11	2006	August	October	November

Table 3.2 Initial IRI values

Section	Test Cycle	Initial IRI (in/mile)
N1	2003	57
N2	2003	56
N3	2003	35
N4	2003	48
N5	2003	59
N6	2003	52
N7	2003	44
N8	2003	42
N1	2006	115
N2	2006	106
N8	2006	95
N9	2006	105
N10	2006	65
S11	2006	67

Traffic

The truck fleet at the Test Track runs at a target speed of 45 mph, and operates 16 hours daily, six days a week for each two-year cycle. Each of the trucks completes about 680 miles per day so as to apply 10 million ESAL collectively in two years. Thanks to simple truck patterns

and running schedule, input Level 1 for traffic information were precisely characterized for the MEPDG analysis. The details of traffic inputs are explained as below.

Truck types and axle loads

In the 2003 research cycle, five of the trucks, termed "triple trailers", consisted of a steering axle, a tandem axle, and five trailing single axles (Figure 3.1). The sixth truck, termed "box trailer", consisted of a steer axle and two tandems (Figure 3.2). In the 2006 cycle, only five triple trailers were used to apply traffic loads.

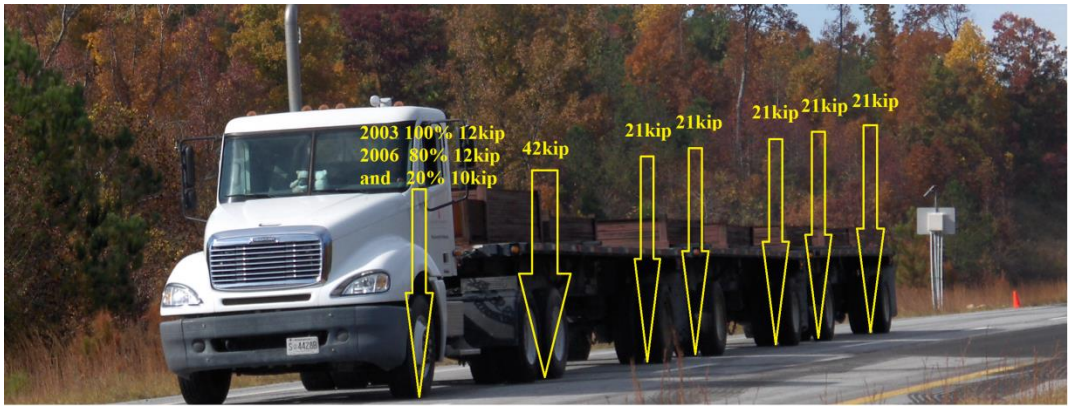

Figure 3.1 Triple trailer truck

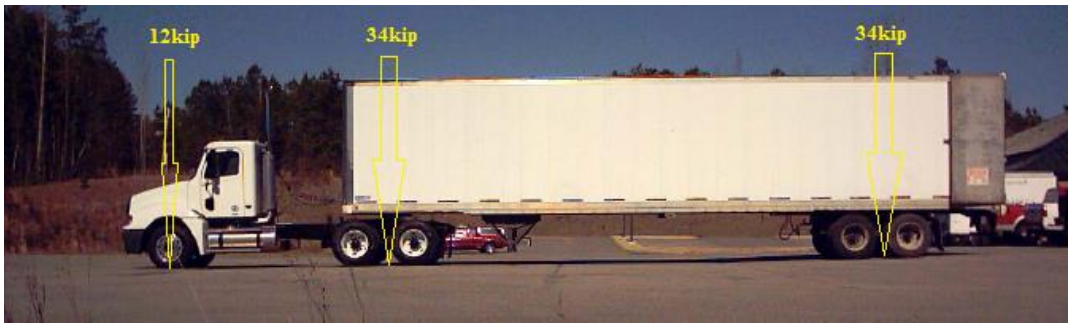

Figure 3.2 Box trailer truck

The axle weight of trucks is needed by the MEPDG as well. In the 2003 research cycle, five triple trailers had the same axle weights distribution. The single and tandem axles weighed approximately 21,000 lb and 42,000 lb respectively, while the steer axle weighed around 12,000 lb. The box trailer had 2 tandem axles that weighed around 34,000 lb. each and a steer axle that weighed around 12,000 lb. In the 2006 cycle, the box trailer was no longer used. Five triple

trailers had the same weights of axles as those in the 2003 research cycle; however, one of the five had a steer axle that weighed 10,000 lb, which was 2,000 lb less than steer axles of the other four. In other words, 80% of the steer axles weighed 12,000 lb and 20% weighed around 10,000 lb. It is noted that the MEPDG does not differentiate between steer and single axles so all steer axles were modeled as single axles with different weights.

Number of axles per vehicle

Another required input was the average number of axles for each vehicle classification (i.e., FHWA Truck Class 4 through 13). Though the box trailer in the 2003 research cycle could be easily modeled as a Class 9 vehicle with one steer and two tandem axles, the triple trailer had six single axles, including the steer axle and trailing single axles. It exceeded the maximum number of single axles (i.e., five axles) among all the vehicle classes allowed in the MEPDG v1.1. In order to represent a triple trailer, two fictitious vehicle classes were used together with five single axles and one tandem axle from the Class 13, and the remaining one single axle from the Class 12. The same inputs were used to model the triple trailers in the 2006 research cycle. The inputs in the MEPDG are shown in Figure 3.3.

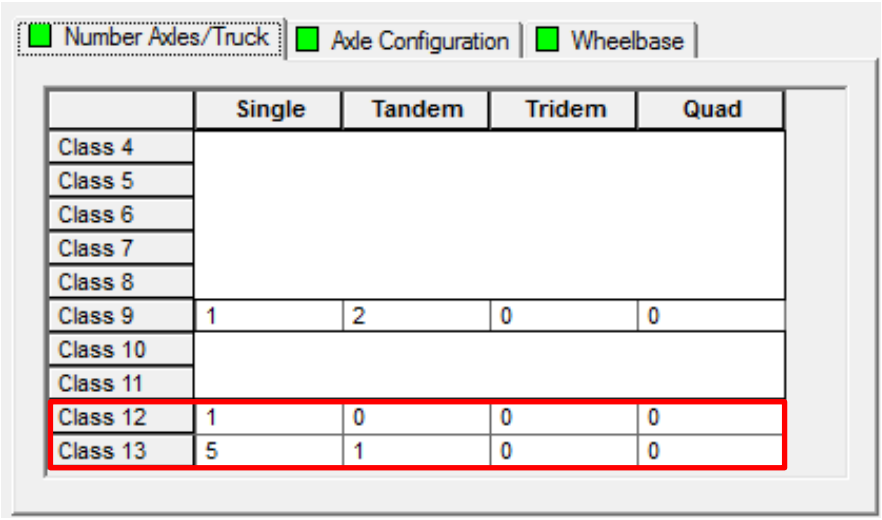

	Single	Tandem	Tridem	Quad
Class 4				
Class 5				
Class 6				
Class 7				
Class 8				
Class 9	1	2	0	0
Class 10				
Class 11				
Class 12	1	0	0	0
Class 13	5	1	0	0

Figure 3.3 Number of axles per vehicle

Axle configuration

The truck axle configurations were specified by Powell and Rosenthal (2011), and the average value of trucks used in the 2003 and 2006 research cycle were entered into the MEPDG. The average axle width was 8.5 ft, the dual tire spacing was 13.5 in, and the tire pressure was approximately 100 psi. Other traffic inputs (i.e., lateral traffic wander) were assumed to be routine design values, and they were left as the defaults provided by the MEPDG.

AADTT and traffic distribution

The volume of traffic on highways is often evaluated depending on the truck traffic because it is not necessary to consider the minor damage on pavement caused by vehicles with less than six tires (i.e., motorcycles, passenger cars, buses, and other vehicles). All the heavily-loaded vehicles used at the Test Track were regarded as the truck traffic. The annual average daily truck traffic (AADTT) is a major input regarding traffic information in the MEPDG. According to traffic records, the daily truck passes was determined to be 1,155 trucks per day on average for the 2003 research cycle and 1,541 trucks per day for the 2006 cycle.

The heavily-loaded vehicles were simulated in the MEPDG by utilizing existing vehicle classes, but adjusting the number of truck passes or AADTT. For example, a triple trailer was equivalently treated as a Class 13 vehicle and a Class 12 vehicle; as a result, the number of daily truck passes describing the amount of triple trailers was doubled. In the 2003 research cycle, 5/6 of the total truck passes was completed by triple trailers, so 962.5 out of 1,155 were double counted as 1,925. The remainder of the truck passes by the box trailer, 193, was added by the doubled value of 1,925 to reach a final AADTT of 2,118 per day. As for the 2006 research cycle, the box trailer was not used, so the AADTT of 1,541 was doubled to 3,082 per day. For the vehicle class distribution, in the 2003 research cycle, the Class 9 comprised 9%, and the Class 12

together with the Class 13 equally comprised 91%; for the 2006 research cycle, the Class 12 represented 50% and the Class 13 represented 50%.

The MEPDG also allows users to specify the average hourly distribution of traffic on a daily basis. The hourly traffic distribution for the Test Track is shown in Figure 3.4 (for the 2003 research cycle) and Figure 3.5 (for the 2006 research cycle). The fluctuation of volume over the hours was the result of shift changes, truck refueling, driver breaks, and truck maintenance stops. The monthly traffic applied was consistent over research cycles, so the monthly distribution factors were all 1.0 and there was no annual traffic growth.

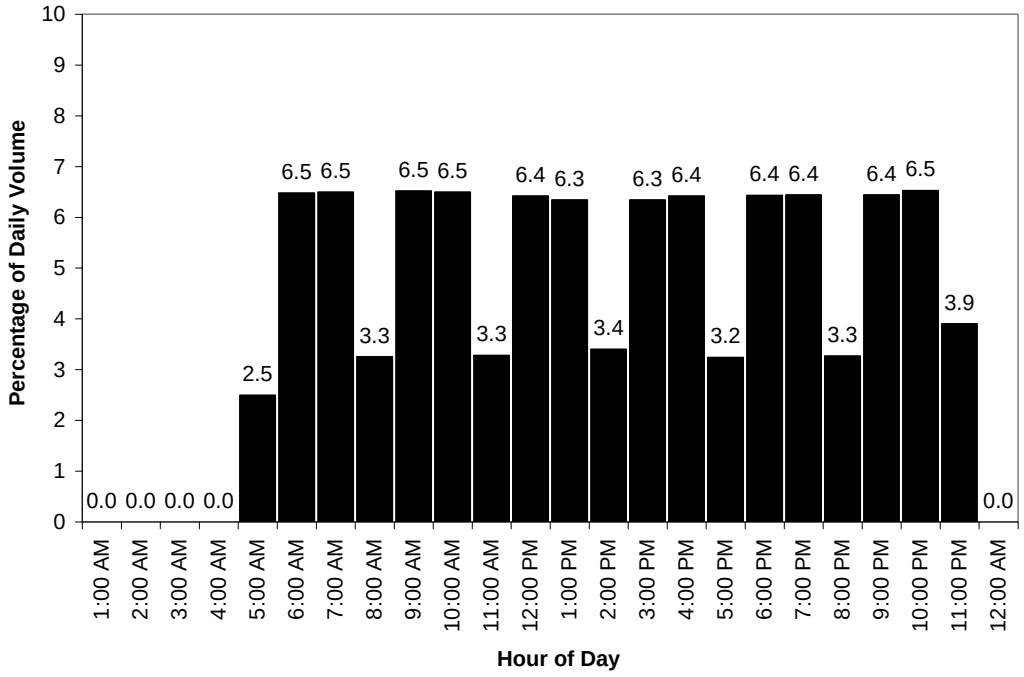

Figure 3.4 Hourly traffic distribution for the 2003 research cycle

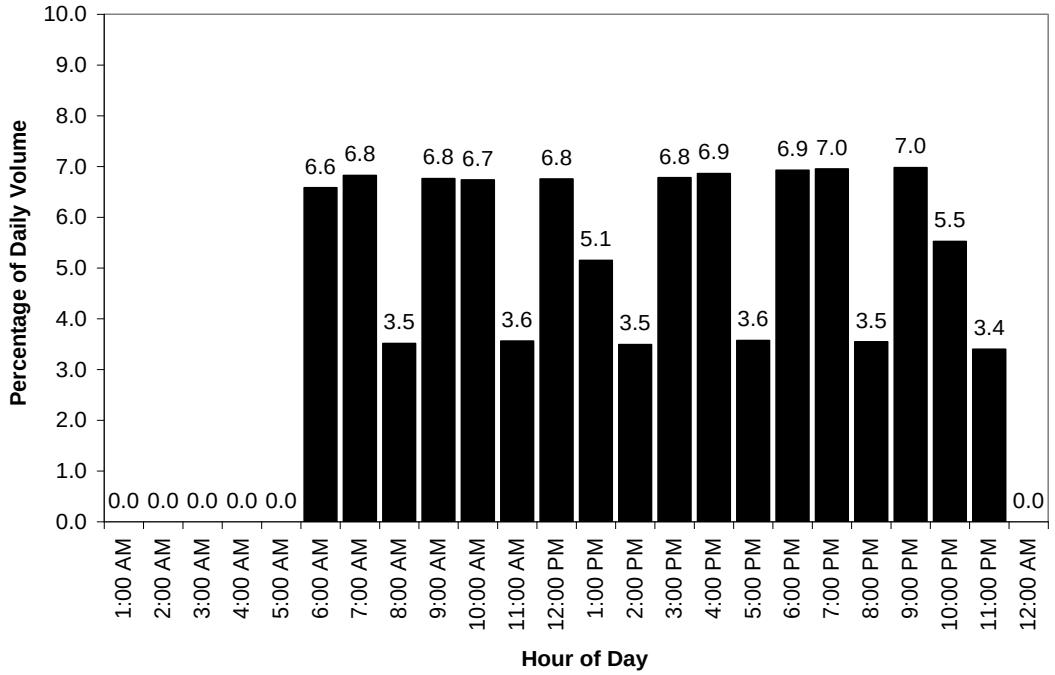

Figure 3.5 Hourly traffic distribution for the 2006 research cycle

Climate

Introduction

The climatic data required in the MEPDG is used by the Enhanced Integrated Climate Model (EICM) to calculate changes in the temperature and moisture profile throughout the pavement cross section. The climatic input for the MEPDG is actually a file that contains a recorded history of temperature, rainfall, wind speed, humidity, and sunlight conditions for a specific area. There are two ways to prepare the climatic inputs for the MEPDG, either by selecting a climatic data file for representative areas or by preparing a new climatic data file based on a local weather station. The latter was adopted in this study because the Test Track has an on-site weather station (Figure 3.6), which is responsible for collecting environmental information on an hourly basis. The Test Track is at a geographic coordinate of 32°59´N, -85°30´W, and an elevation of 600ft. The next section will cover the method to prepare a climate file for a particular condition.

Figure 3.6 Test Track on-site weather station

Generating the climate file for the Test Track

It is noted that two formats of files function in the MEPDG; one is the ICM file and the other is the hourly climatic database file. The ICM file was generated by the MEPDG calculation based on an hourly climatic database file. In fact, the hourly climatic database file was either given for those representative areas or can be self-developed. The required form of the hourly climatic database file is shown in Figure 3.7. Each row of the data file contains the elements explained in parentheses.

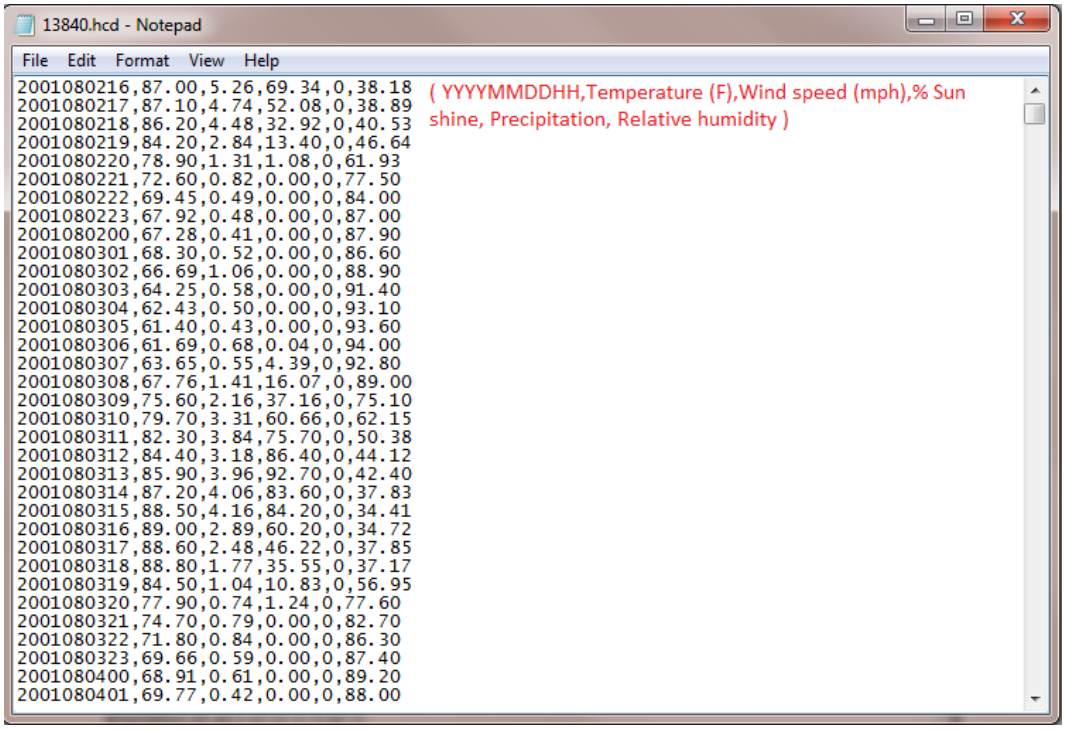

Figure 3.7 Hourly climatic database file

The procedure of preparing an hourly climatic database file is detailed in three steps as follows:

1. Extract useful elements from the station data file. Microsoft Excel can help to generate climatic data in an hourly order.

2. Check the raw data to see whether some hourly records were missing or replicated. This temporary collection error may be the result of a battery problem. If one hour's data was missing, the data record of the same month, day and hour in the previous or the next year was used to supplement the missing data. If one hour's data replicated, the data collected at the first time were kept as valid in the file. The data file can be finally exported to a CSV file and copied into a HCD file by Microsoft Notepad for later use.

3. Fill in basic information into the station.dat file which outlines a basic description of weather station such as station number, location, and first date in file. The station.dat file was written in the format defined by the MEPDG.

4. Place the “station.dat” file into a folder named “default” under the directory of the MEPDG and copy the HCD file into the “hcd” folder; then, upload these files into the climate module in MEPDG by a “generate” command. Finally, the climatic data for the NCAT Test Track weather station was generated for climatic inputs.

Structure

When it comes to the pavement structure, the MEPDG requires detailed inputs in terms of the layer thickness, material types, and structural capacity. The investigated pavement sections were discussed below.

Cross sections

The cross sections of the investigated test sections in the 2003 and 2006 research cycle are shown in Figures 3.8 and 3.9.

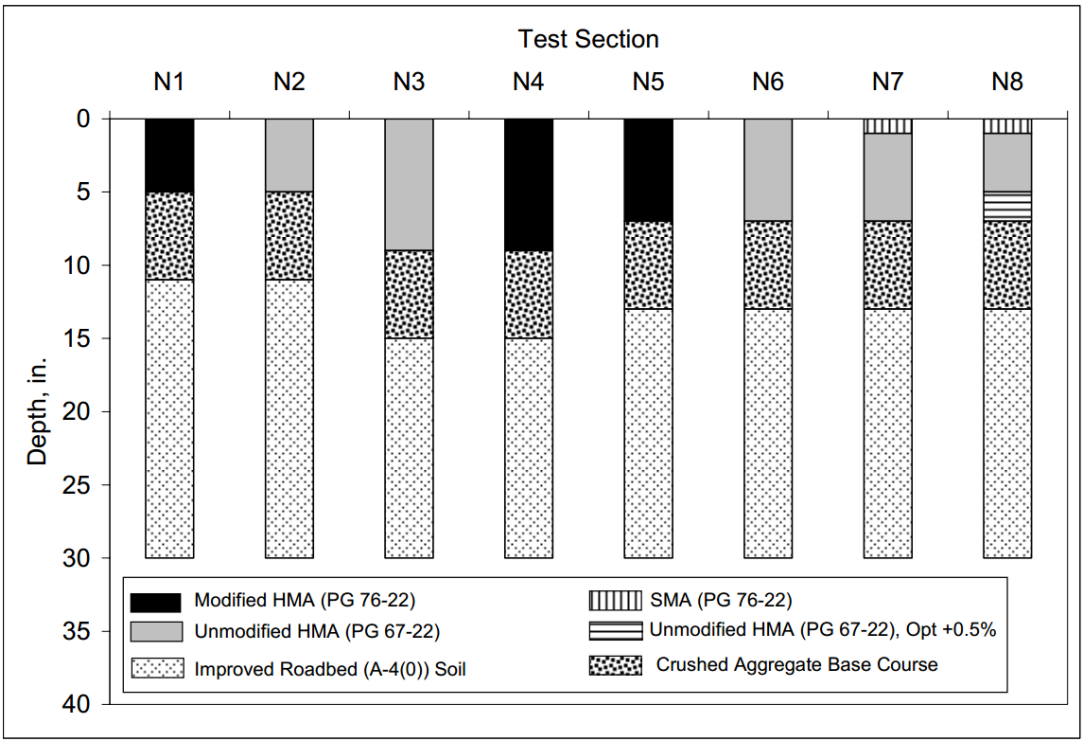

Figure 3.8 Cross section of structural sections in the 2003 research cycle (Timm and Priest, 2006)

In Figure 3.8, eight structural sections (i.e., N1 through N8) in the 2003 research cycle were designed in pairs to compare HMA mixtures difference, but all sections had the same subgrade soil and 6-inch crushed aggregate base. The shared subgrade soil, commonly termed the "Track soil" was excavated from the west curve of the Test Track, which can be classified as an AASHTO A-4(0) soil (Timm and Priest, 2006). Sections N1 through N6 were built in such a pairwise manner that a pair had similar HMA thicknesses; one contained modified asphalt binder while the other contained unmodified binder. Section N7 was topped with a 1 inch wearing layer made with stone matrix asphalt (SMA). Section N8 was topped with a 1 inch SMA as well, but had a 2-inch rich bottom PG 67-22 layer with an additional 0.5% binder (Timm and Priest, 2006).

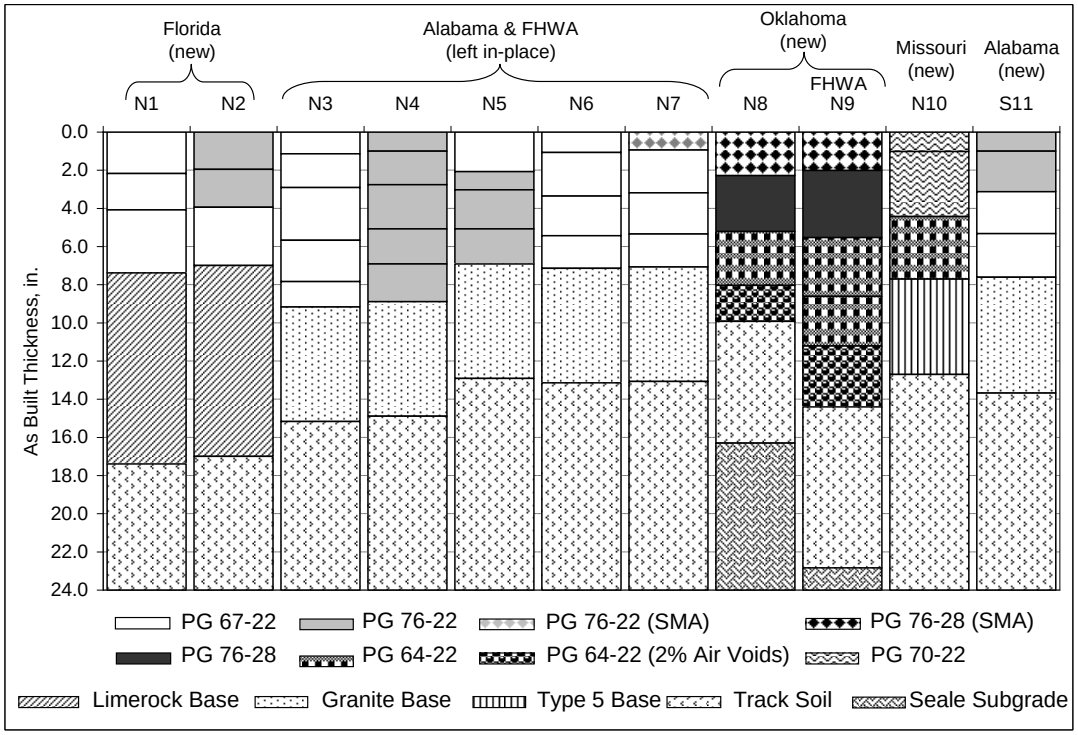

Figure 3.9 Cross section of structural sections in the 2006 research cycle (Timm, 2009)

For the 2006 research cycle, the structural experiment was expanded to eleven sections including Florida, Oklahoma, Missouri, and additional Alabama sections. Among eleven structural sections, five of the original eight structural sections (i.e., N3 through N7) were left in place from the 2003 cycle. It is noted that section N5 was milled and inlaid 2 inches in an

attempt to control extensive top-down cracking throughout the section. Three of the sections from the 2003 research cycle (i.e., N1, N2, and N8) were reconstructed with new pavement structure designs and three new sections were added in the structural study (i.e., N9, N10, and S11). As Figure 3.9 shows, among all sections only N8 and N9 were newly built with the Seale subgrade material, which was classified as an AASHTO A-7-6 soil (Taylor and Timm, 2009). The other sections continued to use the Test Track soil as subgrade material.

Section N1 and N2 both used 10 inches of limerock, rather than crushed aggregate, as the base material. N1 had 3 lifts of HMA made with unmodified PG 67-22 binder, while N2 differed in the upper 2 lifts made with modified 76-22 binder. Five sections (i.e., N3 through N7) were left with the same structure in the 2003 research cycle. Section N8 had 10 inches of HMA, including a top lift of PG 76-28 SMA, a lift of PG 76-28 HMA, and a lift of PG 64-22 HMA, and base HMA made with PG 64-22 binder designed with 2% air voids. Section N9 was topped with SMA with PG 76-28 binder, followed by a lift of PG 76-28 HMA and two lifts of unmodified HMA, with a PG 64-22 HMA base lift designed to 2% air voids. Section N10 used 4 inches of Missouri Type 5 base, which is a dolomitic limestone base material. The upper 8-inch HMA layers were made by one lift of PG 64-22 HMA and one lift of PG 70-22 HMA. Section S11 also consisted 8 inches of HMA including the upper lift made with modified PG 76-22 binder over bottom lifts made with unmodified PG 67-22 binder.

Thickness input

The measured thickness for each layer was recorded during construction, and these values were input into the MEPDG. The measured thicknesses of structural sections for both the 2003 and 2006 research cycles are shown in Table 3.3 and Table 3.4.

When entering lift thicknesses into the MEPDG, there are a few requirements for users. First of all, the minimum value for lift thickness is one inch. There were two sections (i.e., N1 and N5 in 2003 research cycle) with lifts thinner than one inch. For this case, the thickness of the top lift was specified as one inch, and then the thickness increase of the top lift was deducted from the lift below; therefore, those lifts thinner than one inch were entered without changing overall HMA thickness.

Another requirement is that a layer of pavement can only have 4 asphalt lifts at most. There were three test sections placed with an asphalt layer of more than 4 lifts (i.e., N3 and N4 in the 2003 research cycle, and N9 in the 2006 research cycle). For these sections, the fourth and fifth lifts were combined together and a thickness equal to the sum was assigned. In these test sections with five lifts, the combined two lifts shared the same mix design, so the accuracy of structure characterization did not decrease by making this adjustment.

Table 3.3 Surveyed layer thicknesses of the 2003 sections

Test Section &Year	Layer ID	Layer Thickness (in)	Input Thickness (in)
N1 2003	HMA-1	0.6	1.0
N1 2003	HMA-2	2.1	1.7
N1 2003	HMA-3	2.2	2.2
N1 2003	GB	6.0	6.0
N2 2003	HMA-1	1.1	1.1
N2 2003	HMA-2	2.0	2.0
N2 2003	HMA-3	1.8	1.8
N2 2003	GB	6.0	6.0
N3 2003	HMA-1	1.2	1.2
N3 2003	HMA-2	1.8	1.8
N3 2003	HMA-3	2.7	2.7
N3 2003	HMA-4	2.1	3.4
N3 2003	HMA-5	1.3	-
N3 2003	GB	6.0	6.0
N4 2003	HMA-1	1.0	1.0
N4 2003	HMA-2	1.7	1.7
N4 2003	HMA-3	2.3	2.3
N4 2003	HMA-4	1.8	3.8
N4 2003	HMA-5	2.0	-
N4 2003	GB	6.0	6.0
N5 2003	HMA-1	0.9	1.0
N5 2003	HMA-2	2.2	2.1
N5 2003	HMA-3	2.0	1.8
N5 2003	HMA-4	1.8	2.0
N5 2003	GB	6.0	6.0
N6 2003	HMA-1	1.1	1.1
N6 2003	HMA-2	2.3	2.3
N6 2003	HMA-3	2.2	1.8
N6 2003	HMA-4	1.6	2.0
N6 2003	GB	6.0	6.0
N7 2003	HMA-1	1.0	1.0
N7 2003	HMA-2	2.3	2.3
N7 2003	HMA-3	2.1	1.8
N7 2003	HMA-4	1.7	2.0
N7 2003	GB	6.0	6.0
N8 2003	HMA-1	1.1	1.1
N8 2003	HMA-2	2.1	2.1
N8 2003	HMA-3	1.9	1.8
N8 2003	HMA-4	1.9	2.0
N8 2003	GB	6.0	6.0

Table 3.3 Surveyed layer thicknesses of the 2006 sections

Test Section &Year	Layer ID	Layer Thickness (in)	Input Thickness (in)
N1 2006	HMA-1	2.2	2.2
N1 2006	HMA-2	1.9	1.9
N1 2006	HMA-3	3.3	3.3
N1 2006	GB	10.0	10.0
N2 2006	HMA-1	2.0	2.0
N2 2006	HMA-2	2.0	2.0
N2 2006	HMA-3	3.1	3.1
N2 2006	GB	10.0	10.0
N8 2006	HMA-1	2.3	2.3
N8 2006	HMA-2	2.9	3.0
N8 2006	HMA-3	2.8	2.8
N8 2006	HMA-4	1.9	2.0
N8 2006	GB	6.4	6.4
N9 2006	HMA-1	2.0	2.0
N9 2006	HMA-2	3.5	3.5
N9 2006	HMA-3	3.1	3.1
N9 2006	HMA-4	2.6	5.8
N9 2006	HMA-5	3.2	-
N9 2006	GB	8.4	8.4
N10 2006	HMA-1	1.0	1.0
N10 2006	HMA-2	3.4	3.4
N10 2006	HMA-3	2.2	2.2
N10 2006	GB	5.0	5.0
S11 2006	HMA-1	1.0	1.0
S11 2006	HMA-2	2.1	2.1
S11 2006	HMA-3	2.2	2.2
S11 2006	HMA-4	2.3	2.3
S11 2006	GB	6.1	6.1

Material properties

After specifying the layer thickness of the pavement, the material properties were input to the MEPDG. Because sufficient information was collected, the input Level 1 was used for most material properties.

Asphalt mixtures

At input Level 1, the MEPDG requires users to characterize asphalt material regarding dynamic modulus (E*), complex binder modulus, volumetric properties, and general properties.

E test data*

The input for the dynamic modulus (E*) is a minimum of 3*3 matrix (temperature vs. frequencies) for each asphalt mixture or HMA lift. These data were obtained by the dynamic modulus test in the laboratory. For the 2003 research cycle, the dynamic modulus testing was performed in an unconfined state by Purdue University (Timm and Priest, 2006). The range of test temperatures starts at a minimum temperature between -12.2 ℃ (10°F) and -6.6 ℃ (20°F), and ends at a maximum temperature between 51.6℃ (125°F) and 57.2℃ (135°F). For the 2006 cycle, the testing was performed at the NCAT laboratory under the guidance of AASHTO TP 62-07 (Robbins, 2013). The range of temperatures tested were from a low temperature of 4.4℃ (40°F) to a high temperature of 37.7℃ (100°F). The testing temperature range for the 2006 cycle was determined based on the climatic conditions for Alabama pavements. However, the temperature range for the 2006 cycle was not as wide as that for the 2003 cycle. To keep consistency of test temperature ranges, the raw data from the laboratory was used to extrapolate to the extreme temperatures of -9.4℃ (15°F) and 54.4℃ (130°F) using non-linear regression equations of the following form (Timm et al., 2009):

$$E^* = a \cdot b^{Temperature} \cdot Frequency^c \quad (3\text{-}1)$$

where,

E* = the mixture dynamic modulus, psi

Temperature = test temperature in the lab, °F

Frequency = test frequency in the lab, Hz

a, b, c = regression constants

The models for predicting E* at the extreme temperatures generally have high R^2 values so it is reasonable to perform extrapolation on raw data. Table 3.5 and Table 3.6 show the

regression model constant and corresponding R^2 value for each test lift mixture in the 2003 and 2006 research cycle.

Table 3.5 E* regression coefficients for the 2003 research cycle (Davis, 2009)

Mixture (Section-Lift Number)	a	b	c	R^2
1 (N1-1, N4-1 & N5-1)	3,776,660	0.9705	0.1601	0.99
2 (N1-2, N1-3, N4-2, N4-3, N4-4, N4-5, N5-2, N5-3, N5-4 & N5-5)	4,370,389	0.9696	0.1619	0.99
3 (N2-1, N3-1 & N6-1)	3,750,543	0.9708	0.1517	0.99
4 (N2-2, N2-3, N3-2, N3-3, N3-4, N3-5, N6-2, N6-3, N6-4, N7-2, N7-3, N7-4, N8-2, & N8-3)	4,967,657	0.9668	0.1447	0.85
5 (N7-1 & N8-1)	4,546,113	0.9712	0.1464	0.98
6 (N8-4)	4,636,938	0.9740	0.1313	0.97

Table 3.6 E* regression coefficient for the 2006 research cycle (Davis, 2009)

Mixture (Section-Lift Number)	a	b	c	R^2
1 (N1-1 & N1-2)	3,776,660	0.9705	0.1601	0.99
2 (N1-3, N2-3, S11-3 & S11-4)	4,370,389	0.9696	0.1619	0.99
3 (N2-1 & N2-2)	3,750,543	0.9708	0.1517	0.99
4 (N8-1 & N9-1)	4,967,657	0.9668	0.1447	0.85
5 (N8-2 & N9-2)	4,546,113	0.9712	0.1464	0.98
6 (N8-3, N9-3 & N9-4)	4,636,938	0.9740	0.1313	0.97
7 (N8-4 & N9-5)	3,342,206	0.9692	0.1734	0.99
8A (N10-1)	4,555,840	0.9683	0.1484	0.99
8B (N10-2)	5,992,918	0.9704	0.1546	0.97
9 (N10-3)	4,152,065	0.9710	0.1542	0.98
28A (S11-1)	3,112,030	0.9699	0.1646	0.98
28B (S11-2)	4,702,712	0.9726	0.1635	0.98

The goodness-of-fit is further illustrated by the graph comparing the measured and predicted E* data in the Figure 3.10.

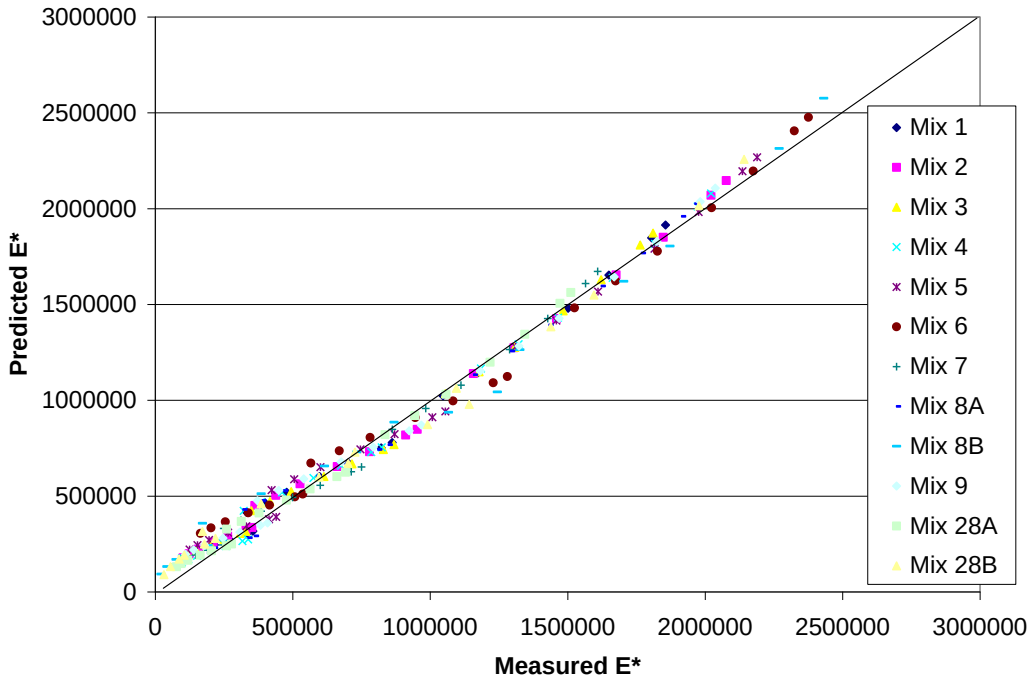

Figure 3.10 Measured vs. predicted E* data (Davis, 2009)

Another stipulation of the MEPDG is that E* values are not allowed to exceed 5,000,000 psi. Only two lifts had E* values that were greater than this value, which means they were too stiff under test conditions. The two values were not considered in the data. Once the data were input into the software, master curves were automatically generated, and the reasonableness could be easily checked. Figure 3.11 shows a sample E* master curve generated for N1-1 lift in the 2003 research cycle. In some cases, certain values were contradictory to common sense. For example, E* values did not increase with a decrease in temperature at certain test frequencies. These data were not input because they cannot generate an accurate master curve. The E* value for each lift mixture in the 2003 and 2006 research cycle are shown in Appendix A.

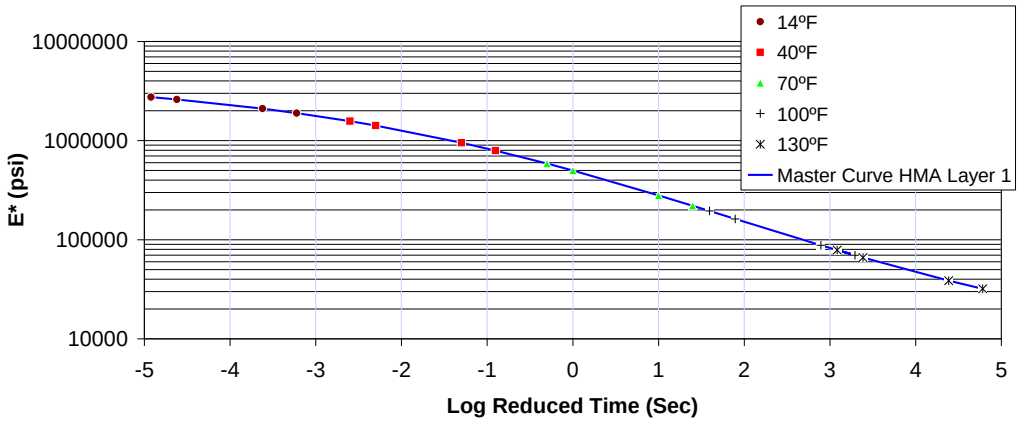

Figure 3.11 The MEPDG E* master curve for N1-1 lift in the 2003 research cycle (Davis, 2009)

G test data*

The binder characterization at input Level 1 requires shear modulus (G*) and phase angle (δ), which are measured in the dynamic shear rheometer (DSR) test. This test can be performed in three phases of binder aging: no aging, short-term aging, and long-term aging. The MEPDG requires the characterization of short-term aged binder (i.e., through the Rolling Thin Film Oven test).

Although G* and δ were provided as inputs, they had a minimal effect on the results of the analysis. This assumption was tested by running a baseline case for one of the test sections, and then changing only the G* or the phase angle values (i.e., doubling values). There was very little difference found between the predicted performances (in terms of rutting, bottom-up fatigue cracking, and IRI) of the two cases. The reason for this result was that the MEPDG does not use G* and δ to construct the master curves to characterize the mixture performance if the E* test data are provided. In addition, although the G* and δ were used in aging calculations, the binder only functioned in a short term (two years) so binder aging had a minimal effect on the distress predictions. Therefore, the G* and δ values under representative testing conditions were used in the MEPDG, and these values are shown in Appendix B.

Mixture volumetric determination

The MEPDG requires some general information for HMA lifts to capture their volumetric compositions, and mechanical and thermal properties. Some of these inputs were entered as the default values because they are typical, including the master curve reference temperature (70°F), Poisson ratio (0.35), thermal conductivity (0.67 BTU/hr·ft·°F), and heat capacity (0.23 BTU/lb·°F). However, the as-built volumetric properties were provided by construction and lab reports for each mix type, regarding in-place air voids, mixture unit weight, and effective binder content. A sample of construction records is presented in Figure 3.12 for lift N1-1 of the 2006 research cycle.

Quadrant: N
Section: 1
Sublot: 1

Laboratory Diary

General Description of Mix and Materials

Design Method:	Super
Compactive Effort:	100 gyrations
Binder Performance Grade:	67-22
Modifier Type:	NA
Aggregate Type:	Grn/Lms
Design Gradation Type:	Dense

Avg. Lab Properties of Plant Produced Mix

Sieve Size	Design	QC
1":	100	100
3/4":	100	100
1/2":	97	97
3/8":	82	82
No. 4:	60	59
No. 8:	50	49
No. 16:	38	39
No. 30:	28	30
No. 50:	19	22
No. 100:	12	14
No. 200:	7.0	8.8
Asphalt Content:	4.8	4.9
Pill Bulk Gravity:	2.413	2.431
TMD (Rice):	2.514	2.499
Avg Air Voids:	4.0	2.7
Avg VMA:	14.4	13.3

Construction Diary

Relevant Conditions for Construction

Completion Date:	September 29, 2006
24 Hour High Temperature (F):	73
24 Hour Low Temperature (F):	48
24 Hour Rainfall (in):	0.00
Planned Mill / Lift Thickness (in):	2.00
Paving Machine:	Roadtec

Plant Configuration and Placement Details

Component	% Setting
Asphalt Content (Plant Setting)	4.7
78 LaGrange Granite	45.0
M10 Columbus Granite	45.0
8910 Opelika Limestone Screenings	10.0

Approximate Length (ft):	200
Survey Mill / Lift Thickness (in):	2.1
Type of Tack Coat Utilized:	67-22
Target Tack Application Rate (gal/sy):	0.05
Avg Temperature at Plant (F):	305
Avg Section Compaction:	94.6%

Figure 3.12 Construction and lab record for N1-1 lift in 2006 research cycle

Based on this record, the in situ air voids was obtained by subtracting the average section compaction from 100%. For example, the air voids for N1-1 lift in the 2006 research cycle was

5.4% by subtracting the section compaction rate 94.6% from 100%. The unit weight was calculated using the QC G_{mm} value and the average section compaction. First, the G_{mm} of 2.499 was multiplied by 94.6% to get a bulk specific gravity of the compacted mixture (G_{mb}) of 2.364; then, this value was multiplied by 62.4 lb/ft^3 to yield a mixture unit weight of 147.5 lb/ft^3. The compacted mixture (G_{mb}), percent aggregate in the mixture (P_s), and the bulk specific gravity of the aggregate blend (G_{sb}) were used to find the voids in mineral aggregate (VMA) of the mixture as equation (3-2).

$$VMA = 100 - \left[\frac{G_{mb} \times P_s}{G_{sb}} \right] \tag{3-2}$$

The G_{sb} was calculated by the mass percent in total (f_A) and bulk specific gravity (G_A) of each mixture component. The equation used is shown as below:

$$\frac{1}{G_{sb}} = \frac{f_A}{G_A} + \frac{f_B}{G_B} \tag{3-3}$$

Then, the volume of effective binder was calculated by subtracting air voids from VMA. For example, the P_s and G_{sb} were 95.1% and 2.669, respectively. Using those values with the G_{mb} of 2.364, the VMA was calculated as 15.78% by equation (3-2), with effective volumetric binder content as 10.38%. The same computation was performed on other lifts of test sections and the results of volumetric inputs are shown in Appendix C. As mentioned earlier in the section "Thickness Input", for those test sections consisted of five HMA lifts, a weighted average was taken of the volumetric properties of the bottom two lifts for input as the "fourth" layer.

Unbound materials

The unbound layers, specifically the base and subgrade layers were characterized at the input Level 3 in the MEPDG. The reason that the input Level 1 or 2 was not used was due to a software running error in the analysis in the version 1.1 of MEPDG. The level 3 inputs for

unbound layers are material type, gradation, Poisson ratio, coefficient of lateral earth pressure, and a representative resilient modulus (M_R).

2003 test sections

For the 2003 research cycle structural sections, only two types of unbound material were used: the crushed aggregate base and the Test Track soil subgrade. In the MEPDG, the "crushed stone" was selected as the base material, and a typical value of 0.4 was adopted for the Poisson ratio of this material. The coefficient of lateral earth pressure was specified as 0.3572 for each material to calculate horizontal stresses (Taylor, 2008). For the Test Track soil, an A-4 material was used with a Poisson ratio of 0.45. The gradations for the crushed aggregate base and the Track soil are shown in Table 3.7.

Table 3.7 Unbound materials gradations for the 2003 research cycle (Timm and Priest, 2006)

	Percent passing (%)	
Sieve size (mm)	**Crushed aggregate base**	**Test Track soil subgrade**
37.5	100	100
25	96	83
19	90	81
12.5	80	78
9.5	76	75
4.75	59	71
2.36	49	68
1.18	40	66
0.6	32	64
0.3	23	61
0.15	15	56
0.075	10	48

For input Level 3, the representative M_R values were needed for different kinds of unbound materials. The M_R values were obtained from the backcalculation of falling weight deflectometer (FWD) deflection data. The backcalculation was performed by the software EVERCALC 5.0 developed by Washington State DOT. It was found that the software accuracy

depends on the number of pavement layers being analyzed, and the optimal number of pavement layers for backcalculation was three. For the 2003 sections, the three-layer structure consisted of HMA as the top layer, the granular base, and "new fill" material (Test Track soil) combined as the second layer, and the remainder of the subgrade from the 2000 research cycle being the third layer (Timm and Priest, 2006). The new fill material was used to fill the gap depth between the granular base and the existing subgrade from the 2000 research cycle. Therefore, a level road surface for each test section can be ensured once the granular base and HMA lifts had been placed. The new fill material was excavated from the same embankment as the subgrade material which was already in place for those sections. So the same Poisson ratio, gradation, and material classification were used for the new fill.

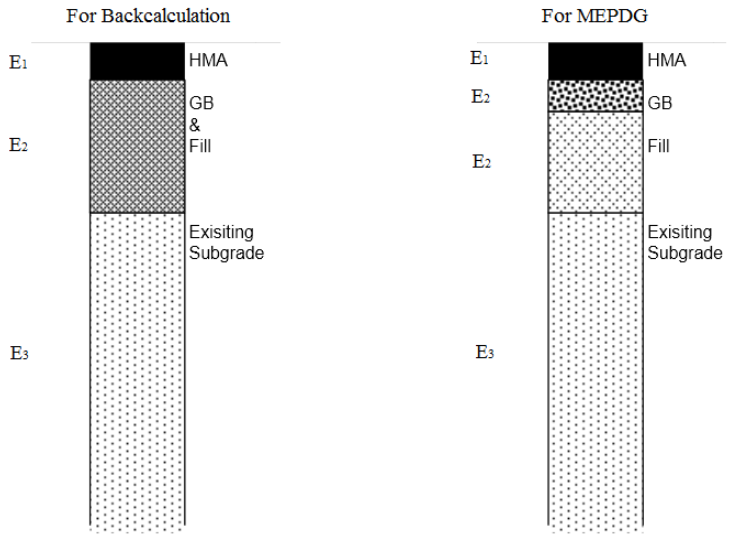

Figure 3.13 Cross sections comparison

However, in order to provide a three-layer structure for backcalculation, there was only one M_R value for the granular base and new fill material collectively, and a different M_R value for the remainder of the subgrade material. In the MEPDG, since good predictions are based on good characterization of pavement structure, it is better to specify a four-layer structure as built in reality than three-layer structure as considered in backcalculation (Figure 3.13). To rectify the

issue, three layers, instead of two layers, were assumed to be underneath the last HMA lift in the MEPDG: one 6-inch granular base layer, one layer of new fill material using the thickness designated in Table 3.8, and finally the subgrade with an assumed infinite thickness. The backcalculated modulus found for the combined base and new fill was taken as representative modulus for each of those two layers, while backcalculated subgrade modulus was the input for the last Test Track soil subgrade layer. The backcalculated moduli values are shown in Table 3.9. Although it may be unusual that the subgrade moduli are significantly higher than the base moduli, this trend is consistent with other findings regarding the Test Track materials (Timm and Priest, 2006; Taylor and Timm, 2009).

Table 3.8 New fill depths for the 2003 research cycle (Taylor and Timm, 2009)

Test section	depth of new fill (in)
N1	19
N2	19
N3	15
N4	15
N5	17
N6	17
N7	17
N8	17

Table 3.9 Unbound materials moduli for the 2003 research cycle (Timm and Priest, 2006)

Test section	Granular base & new fill M_R (psi)	Subgrade M_R (psi)
N1	8,219	26,958
N2	10,061	27,482
N3	13,083	32,516
N4	11,717	33,889
N5	7,852	30,564
N6	11,153	34,682
N7	12,243	33,817
N8	10,258	30,859

2006 test sections

For the 2006 research cycle structural sections, five different unbound materials were used as base or subgrade layers: the Test Track soil discussed previously, the crushed aggregate base used in the 2003 structural sections, a poor quality subgrade material for sections N8 and N9, a Florida limerock base material for sections N1 and N2, and a dolomitic limestone base material (termed the Type 5 base) for section N10. For the Test Track soil and the granular base material used in the previous test cycle, the same material selections and gradations were used as previously discussed. The poor quality subgrade soil used for sections N8 and N9, termed the Seale subgrade, was classified as an AASHTO A-7-6 soil within the MEPDG. The Florida limestone and Type 5 base materials were both classified as crushed stone within the MEPDG. The Poisson ratio was commonly assumed to be 0.40 for all three materials. The gradations used in the MEPDG for the three new materials are shown in Table 3.10.

Table 3.10 Unbound materials gradations 2006 research cycle (Taylor and Timm, 2009)

	Percent Passing (%)		
Sieve Size (mm)	**Seale Subgrade**	**Florida Limestone**	**Type 5 Base**
37.5	100	100	100
25	100	100	99
19	100	100	97
12.5	100	88	92
9.5	100	81	88
4.75	100	61	79
2.36	100	44	71
1.18	99	32	64
0.6	98	26	58
0.3	92	23	49
0.15	82	21	36
0.075	58	19	25

A different procedure was explained to calculate the representative M_R values for the base and subgrade materials used in the 2006 test cycle. The in-situ stress state of each material was monitored by dynamic pavement response measurements, namely vertical pressure, made

throughout the 2006 test cycle. Figure 3.13 shows an example of these measurements made over one year for section N1.

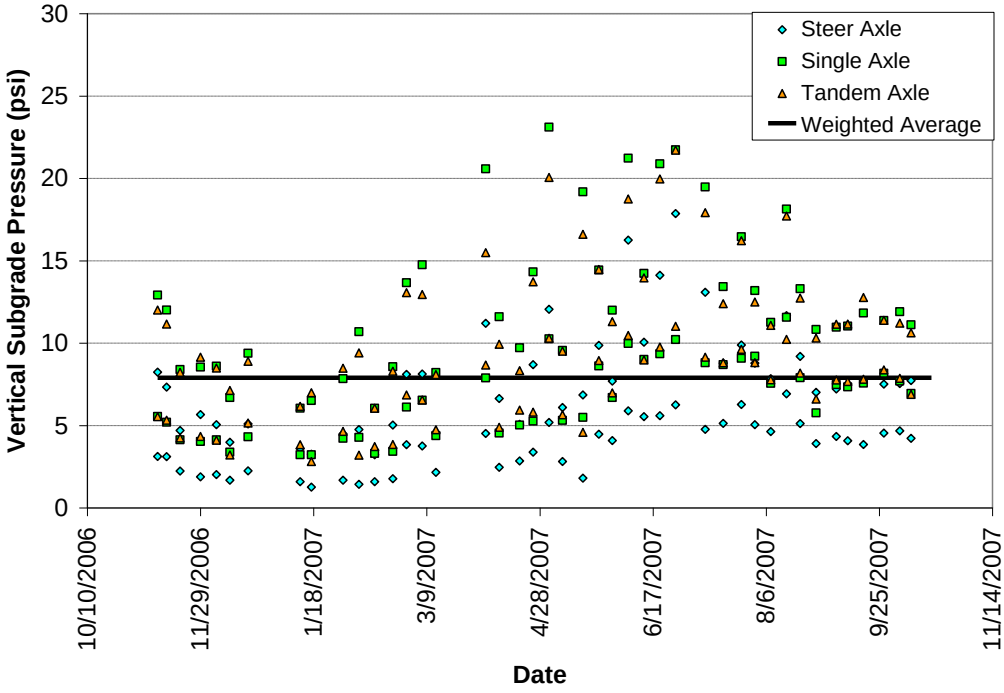

Figure 3.14 Vertical pressures in N1 subgrade in the 2006 research cycle(Davis, 2009)

As seen in Figure 3.14, the pressures for each axle type increase during warmer months when the HMA is softer, and the pressures correspondingly decrease during cooler months. Using the relative frequency of each axle type (14.3% steer axles, 14.3% tandem axles, and 71.4% single axles), a weighted average vertical stress due to traffic loading was used to calculate the representative M_R of each unbound material. It was combined with the overburden pressure to obtain the total average vertical stress (σ_1). The overburden pressure existed due to the weight of overlying material, which can be computed from the overlying layer thicknesses and unit weights. Finally, the corresponding horizontal stresses (σ_3) were calculated by multiplying the vertical stress by the lateral earth pressure coefficient 0.3572 (Taylor, 2008). The vertical and horizontal stresses were then used in Equation (3-4) to estimate a representative M_R for each unbound

material (Taylor and Timm, 2009). The M_R input for MEPDG was finally calculated and shown in Table 3.12.

$$M_R = k_1 p_a * \left(\frac{\theta}{p_a}\right)^{k_2} * \left(\frac{\sigma_d}{p_a}\right)^{k_3} \quad (3\text{-}4)$$

where,

M_R = the resilient modulus, psi

k_1, k_2, and k_3 = regression coefficients (Table 3.11)

p_a = the atmospheric pressure (14.6 psi)

θ = the bulk stress (σ_1+2*σ_3), psi

σ_d = the deviator stress ($\sigma_1 - \sigma_3$), psi

Table 3.11 Regression coefficients for unbound materials (Taylor and Timm, 2009)

Material Type	k_1	k_2	k_3
Track Soil	1095.43	0.5930	-0.4727
Crushed Granite	581.08	0.8529	-0.1870
Florida Limestone	717.04	1.2338	-0.5645
Type 5	643.69	1.0318	-0.2833
Seale Subgrade	225.09	0.3598	-0.7751

Table 3.12 Unbound materials moduli for the 2006 research cycle (Davis, 2009)

Test Section	Granular Base MR (psi)	Subgrade MR (psi)
N1	23,597	29,701
N2	25,605	29,638
N8	26,020	9,801
N9	24,155	14,804
N10	16,752	28,174
S11	12,530	28,873

PERFORMANCE MONITORING

Introduction

Performance data were observed and recorded weekly in regard to fatigue cracking, rutting, and IRI over the research cycle. It was usually scheduled on every Monday when trucks

were paused to facilitate performance testing and any needed track or truck maintenance (Priest, 2005).

Fatigue Cracking

Inspection method

Fatigue cracking was monitored using a crack mapping method. First, the cracks were identified by its alligator-like appearance. Only interconnected areas of cracks were considered as alligator cracking. Either longitudinal or transverse cracking was not accounted as alligator cracking. The identified cracking were carefully inspected and marked. Second, the marked pavement was photographed using a digital camera. The picture was transferred to a digital map (Figure 3.15). Then, the percentage of cracking area divided by the total area was used to measure the severity level of fatigue cracking. It is important to note that fatigue cracking was only measured over the middle 150 feet length area of each test section; the first and last 25 feet were considered as a "transition zones" between two sections, and the distresses may be caused by the transition of materials. In addition, the fatigue cracking only refers to "bottom-up" cracking that initiates from the bottom of asphalt layer in the study. It was verified by cutting cores during trafficking phase (i.e., the first two years of each research cycle) or cutting trenches after the trafficking phase.

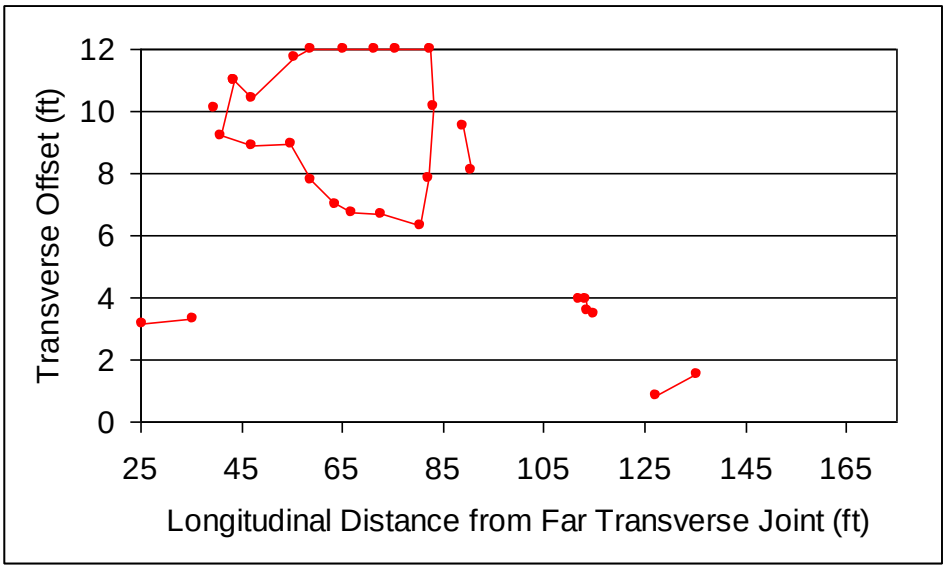

Figure 3.15 Sample crack map from section N6 at the end of the 2006 research cycle

Rutting and IRI

Inspection method

For the 2003 research cycle, the rut depth measurement was made periodically with a dipstick profiler (Figure 3.16), and the roughness measurements was performed occasionally by an Automatic Road Analyzer (ARAN) Inertial Profiler (Figure 3.17) owned by NCAT. This profiler can measure the small wavelengths in the longitudinal profile in the pavement surface at high speeds for each wheel path, which can be converted into IRI or rut depth measurements through models. For the 2006 research cycle, NCAT used the ARAN van to measure rut depths and IRI three times per month.

Figure 3.16 Dipstick profiler

Figure 3.17 ARAN inertial profiler

SUMMARY

This chapter covers the generation of MEPDG inputs regarding traffic, climate, and material properties. The dataset was prepared at the highest input level of MEPDG when possible, mostly at input Level 1, which provided the highest confidence for prediction accuracy. Also, because of the detailed dataset, the local calibration can be performed to the most specific local condition. The next chapter will discuss the methodology of local calibration and validation in this study.

CHAPTER 4

THE METHODOLOGY OF LOCAL CALIBRATION AND VALIDATION

INTRODUCTION

Calibration

Calibration is defined as a process to improve the goodness of fit or accuracy of prediction models in the MEPDG. The goodness of fit indicates how well the model predictions correspond with field-measured values. It can be graphically assessed by evaluating similarity of prediction and measurement trend lines.

Figure 4.1 and Figure 4.2 provide an example to illustrate the concept of goodness of fit. The fatigue cracking at a pavement is investigated over 20 months in this example. The solid line is the trend line for predicted fatigue cracking, and the dashed line is for measured fatigue cracking. Figure 4.1 shows a correspondence between the predicted and measured values, which suggests predictions are reasonable. However, Figure 4.2 presents a disparity between the predicted and measured trend lines, which indicates the predictions are not reliable. In this case, the model is overpredicting the actual cracking progression.

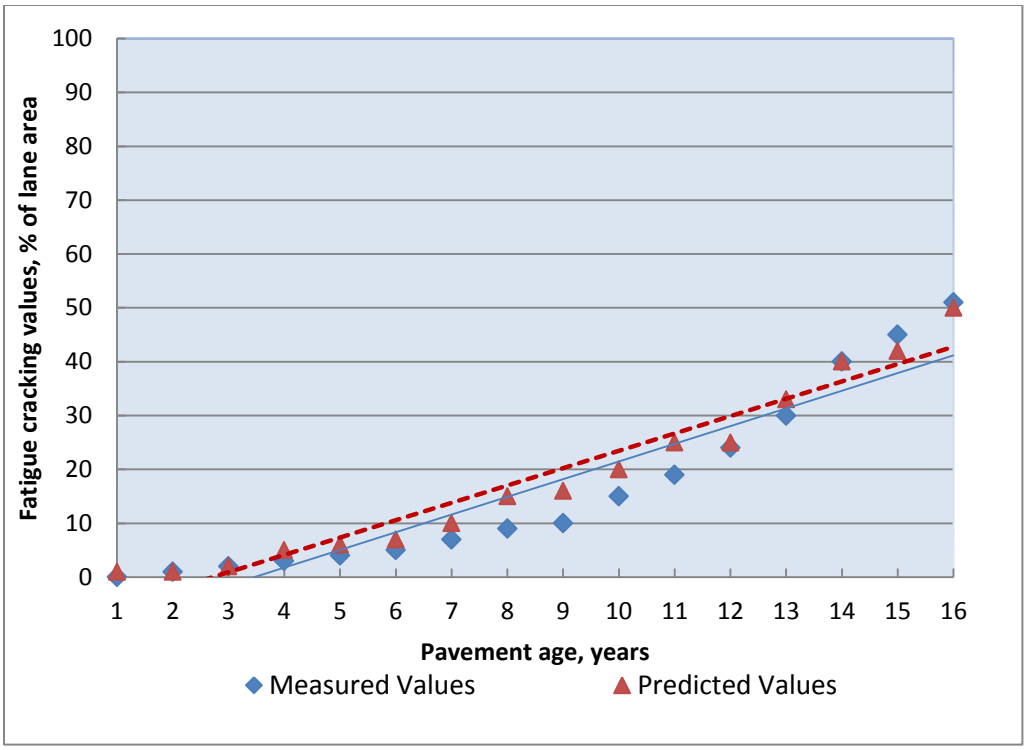

Figure 4.1 Reasonable goodness of fit for model predictions

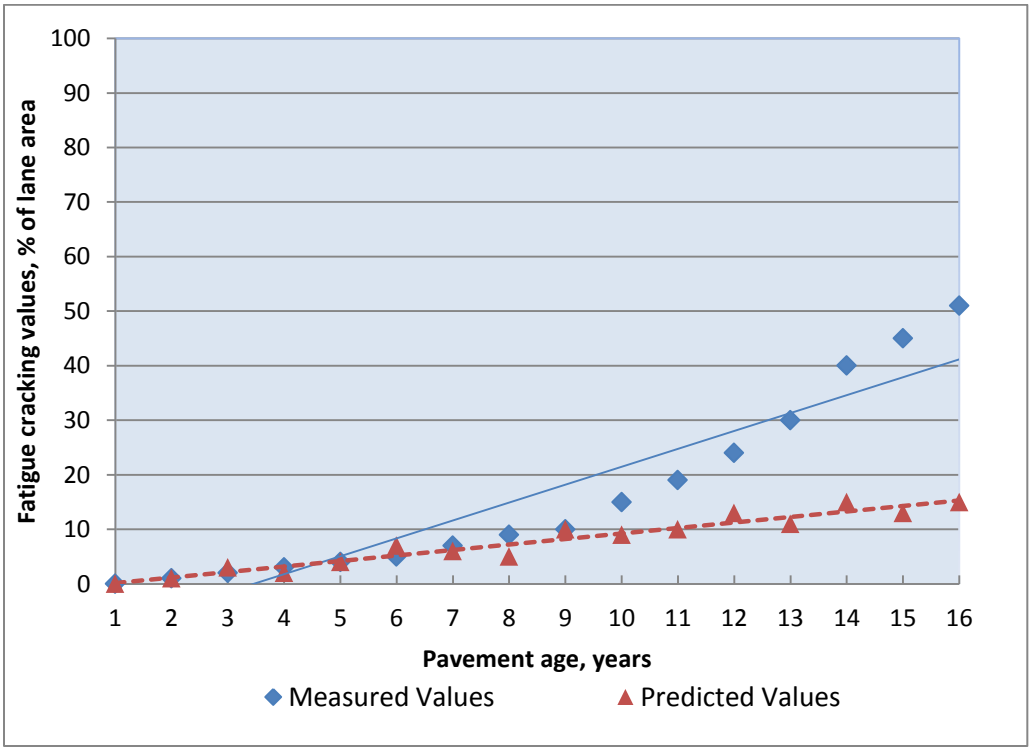

Figure 4.2 Unreasonable goodness of fit for model predictions

Validation

Validation is usually performed after the calibration process, and it aims to verify the goodness of fit and precision of the calibrated models. The data used for validation must be independent from those used for the calibration so as to maintain the objectivity of validation. The results of validation determine whether the calibrated models can be applied to broader scenarios.

LOCAL CALIBRATION

Goal of Calibration

The local calibration was designed to gain an improvement in the MEPDG performance predictions by adjusting the calibration coefficients built in prediction models (i.e., transfer functions) to reflect actual, locally-measured, field performance. The calibrated models with best-fit calibration coefficients could fairly predict the performance of a local pavement, which would contribute to an efficient pavement design. The final result of calibration in this study is the best-fit set of calibration coefficients for the fatigue cracking, rutting, and IRI models.

Calibration Methods

It was found in the literature review that two approaches are commonly used in the local calibration. One was to calibrate prediction models by varying its calibration coefficients (Li et al., 2009; Muthadi and Kim, 2008; Schram and Abdelrahman, 2010; Banerjee et al., 2009). The other was to adjust the results of the model predictions directly (Hoegh et al., 2010). For example, the calibration was performed by subtracting a certain constant value from the prediction results of the nationally-calibrated models.

The first approach (Figure 4.3) included several steps: build project templates with section inputs, assign trial calibration coefficients, run the MEPDG, evaluate predictions, and

repeat the process if necessary. In order to minimize the number of trials, a sensitivity analysis was performed to obtain a better sense of how the calibration coefficients affect the predictions.

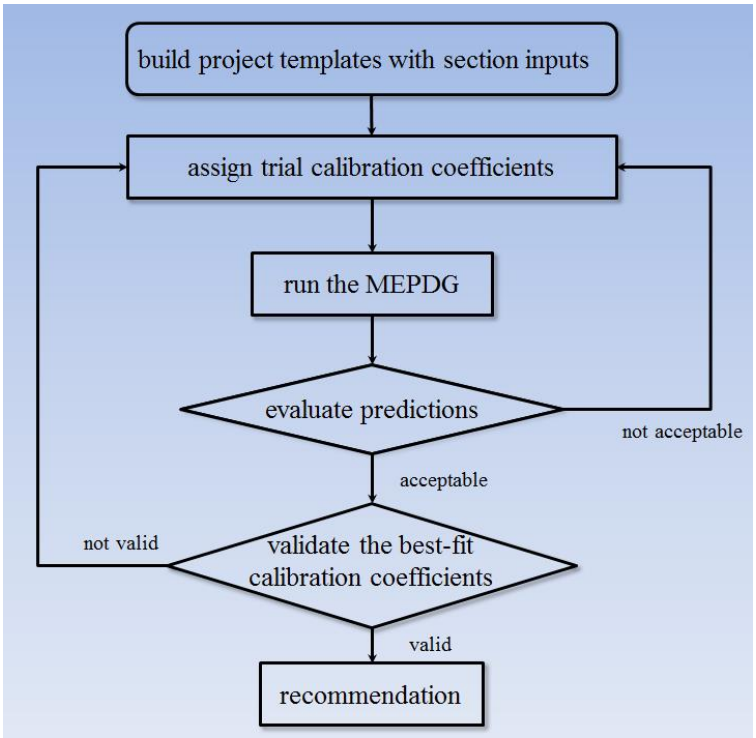

Figure 4.3 Trial and error calibration steps

The second approach was to perform arithmetic adjustment on the predicted values. This approach was useful for the case when a consistent bias was found between predictions and measured values throughout design life (Figure 4.4). It minimized the bias by subtracting a constant value for predicted values. This constant value was determined by "Solver" in Microsoft Excel which can help you find an optimal (maximum or minimum) value for a formula. However, this adjustment shifted the prediction curve without changing its shape, and this approach would not be effective if the prediction curve from the model is not in a similar shape with the curve of measured values (Figure 4.5).

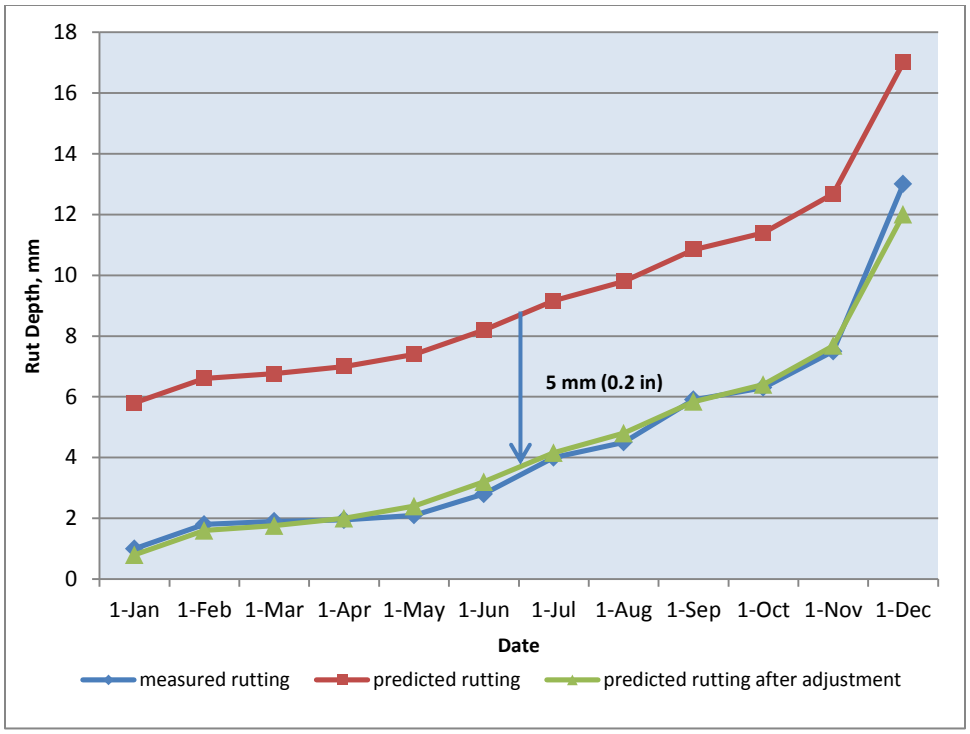

Figure 4.4 Curves in similar shape

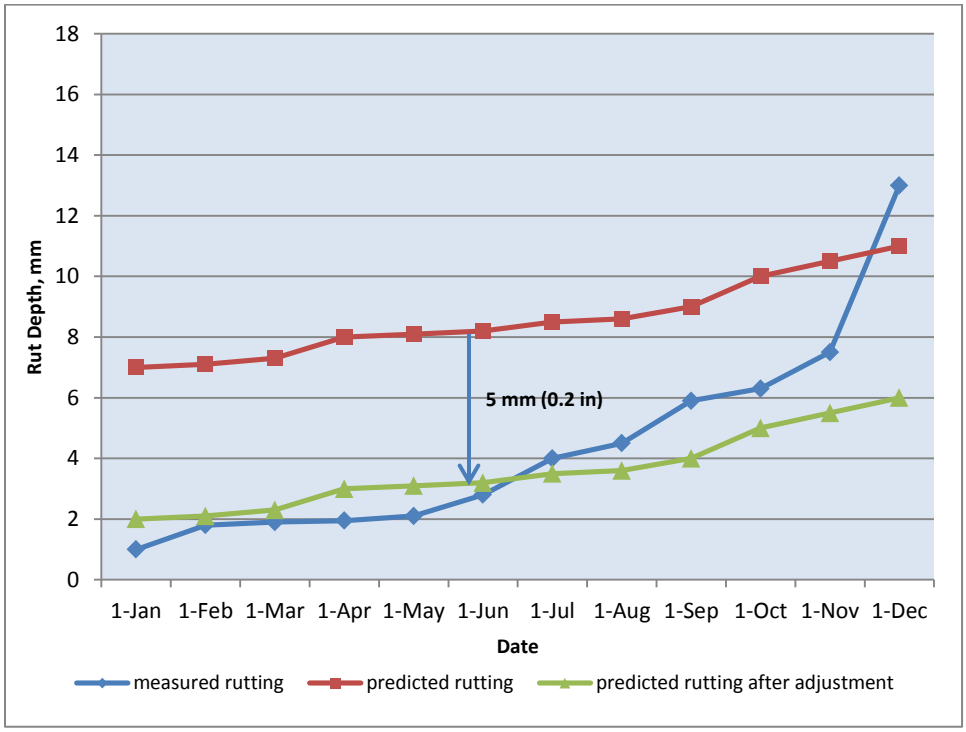

Figure 4.5 Curves not in a similar shape

Methodology of Study

The local calibration adopted in this study was a trial-and-error approach. Before applying "trial" calibration coefficients, the project templates in the MEPDG (Figure 4.6) were set up describing the local condition. The design scenarios (i.e., traffic, climate, and structure) in research cycles were carefully entered into the MEPDG, and they were saved as project templates for all of the investigated sections. Since the investigated sections sustained the same traffic loadings and the same local climate effects, the major difference between project templates was only structural configuration. In total, there were nineteen project templates generated: eight sections in the 2003 research cycle for calibration and eleven sections in the 2006 research cycle for validation. In fact, the project templates in the same research cycle only differed in those inputs describing structure. As introduced in Chapter 3, the traffic inputs and HMA layer properties inputs were entered at input Level 1, and some unbound material properties were entered at input Level 3 or assumed as default values.

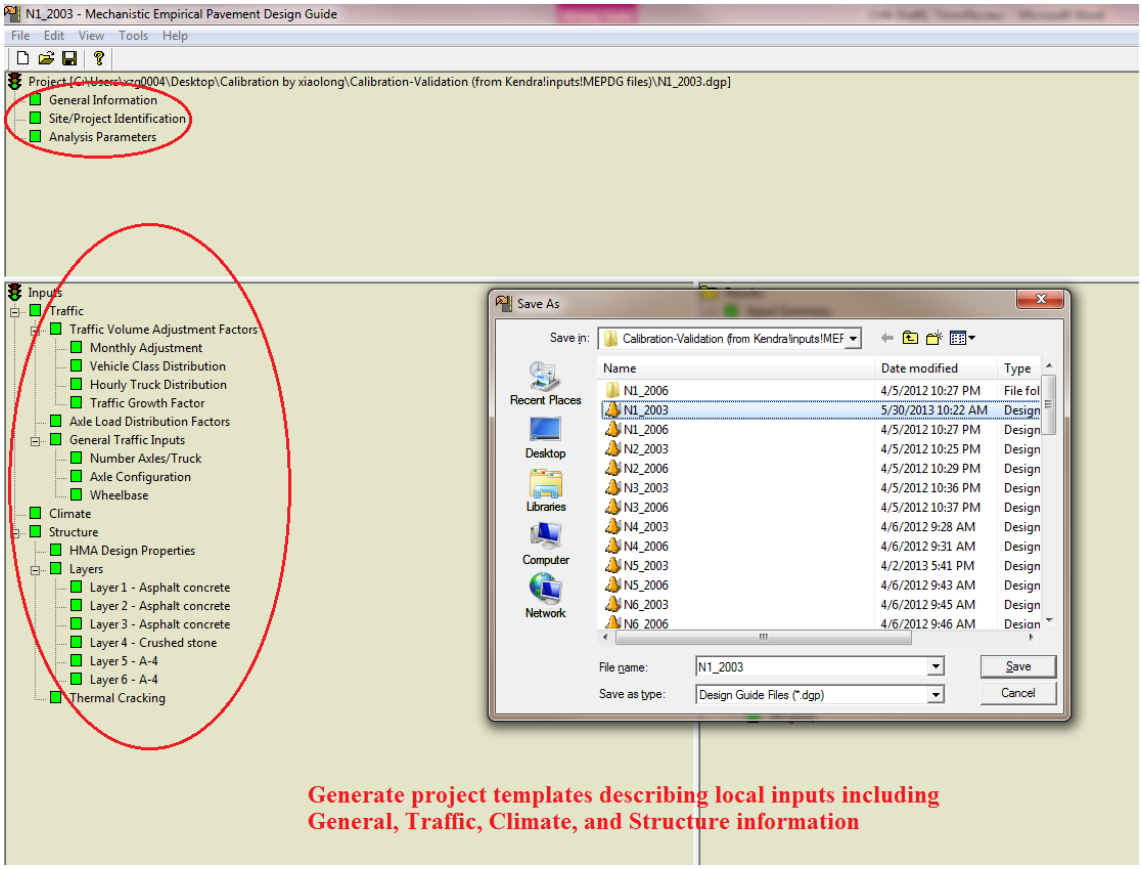

Figure 4.6 Project templates in the MEPDG

By running the project templates, the MEPDG provided the predictions of various distresses for each month during the design life. Then, these predicted values were compared against the measured values during a research cycle. For rutting and IRI, the data recorded on a weekly basis was averaged to monthly readings. For fatigue cracking, the surfaces of sections were inspected weekly, yet the measured cracking data were recorded every several months, which provided cracking development versus time plots. Thus, only a few months' predicted fatigue cracking values by the MEPDG were able to be compared against the available measured values. For a specific performance indicator (i.e., fatigue cracking, or rutting, or IRI), the difference between predicted and measured values was used to evaluate the accuracy of predictions, and whether the calibration coefficients were acceptable. If no other calibration coefficients could be found that could reduce the sum of squared errors (SSE) more than a

certain trial set of calibration coefficients, this trial calibration coefficients was assumed to be the best-fit set of calibration coefficients, and the iteration process was ended.

In statistics, SSE is often used as a quantitative indictor to evaluate the deviation of the fitted values from the actual values. The SSE reflects the accuracy of the model, so it was adopted in this study to quantify the difference between predicted and measured distress values. The MEPDG predicts the development of distresses (i.e., fatigue cracking, rutting, and IRI) on a monthly basis, so the residual (i.e., the difference between the predicted and measured distress) was calculated for each month, and then they were squared and summed up to evaluate MEPDG predictions. Considering all investigated sections, the SSE (Equation 4-1) is regarded as the final indicator of the MEPDG prediction accuracy.

$$SSE = \sum_{n=1}^{8} \sum_{m=1}^{A} (\text{predicted value} - \text{measured value})^2 \quad (4\text{-}1)$$

where,

m = the mth measurement (A is the total number of monthly measurements over the investigated cycle)

n = the nth investigated section (because eight sections involved in the calibration, the maximum of n was eight)

VALIDATION

Goal of Validation

The validation was to verify the reasonableness and robustness of the calibrated prediction models. If the calibrated prediction model was validated to be sufficiently accurate, the calibrated model can be considered by local agencies for future adoption.

Methods of Validation (Criteria)

The prediction results were obtained from the MEPDG using a set of data independent from the calibration. The method of validation was to use the statistical hypothesis test (i.e., Student's *t*-test) to examine whether the calibration results were acceptable. The null hypothesis was that the predicted values and measured values were not significantly different. The α level was assumed to be 0.05 so the p-value was compared with 0.05 to evaluated whether the null hypothesis was rejected. If the p-value was less than 0.05, the null hypothesis was rejected and the calibration results were considered to not be satisfactory. The results of the Student's *t*-test can provide a statistical inference whether the calibration can make a difference on the prediction models.

Methodology of Study

As discussed earlier, eleven sections in the 2006 research cycle were used for validation, and the project template was generated for each of them. The predicted values of distresses were obtained from the MEPDG using the best-fit coefficients, and the measured values were obtained from the Test Track in-field performance. The Student's *t*-test was performed using Excel on two sets of data (i.e predicted and measured) to see if the null hypothesis was rejected.

CHAPTER 5

A METHOD OF RUNNING THE MEPDG AUTOMATICALLY

BACKGROUND

The local calibration of the MEPDG requires iteration to achieve the best-fit calibration coefficients. The performance predictions were achieved through sophisticated models in the MEPDG, so it took considerable time to perform the necessary calculations. For example, a 64-bit system with an Intel Core i7 CPU and 16 GB RAM would take nearly one minute to run a two-year lifetime pavement design. In this study, eight structural sections (or project templates) in the 2003 research cycle were considered in the local calibration. The software operation and results analysis were very time consuming. Therefore, the investment of time and human labor was an important concern in this study.

In this study, one trial set of calibration coefficients took around 18 minutes (calculated as 1 min for each project template multiplied by 8 sections plus 10 minutes used for calculating SSE) to determine whether they could improve the accuracy of a specific distress model. The calculation of SSE usually took at least ten minutes to perform manually for opening files, reading prediction results, and calculating the SSE values. In fact, it also needed considerable time to enter the calibration coefficients in the MEPDG. During this study, 66 sets of calibration coefficients were tried for the fatigue cracking model; 106 sets of calibration coefficients were tried for the rutting model. Therefore, the demand rose to run the MEPDG automatically with little human intervention as possible.

The calibration process in this study included a series of actions: creating project templates, selecting “trial” calibration coefficients, running project analysis, evaluating predictions (i.e., calculating SSE), and repeating this process as necessary. The human labor involved in these steps was finished by mouse-clicking and keyboard-typing. To facilitate

automation of MEPDG operation, these actions could be recorded by using Visual Basic (VB) script language and replayed by VB programs. The following discussion will focus on the method of how to run the MEPDG automatically.

METHOD DESCRIPTION

Software Introduction

The software "Quick Macro v6.60" was adopted, which could record, replay, and edit macros that specify a series of repetitive actions (i.e., mouse-clicking and keyboard-typing). By using this software, human labor was replaced by an execution of programmed macros.

Basic Steps

There were only two steps run by macro: project analysis and results evaluation. Generating the project templates was not included in the macros. The reason was that too much information needed to be input into the MEPDG non-repetitively, so the macro programming cost more effort than doing so manually. Figure 5.1 shows the programmed macros including assigning "trial" calibration coefficients, running project analysis, and evaluating predictions.

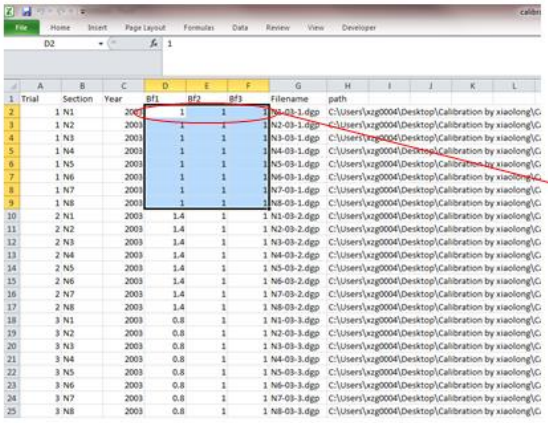

1. Assign trial calibration coefficients in Excel

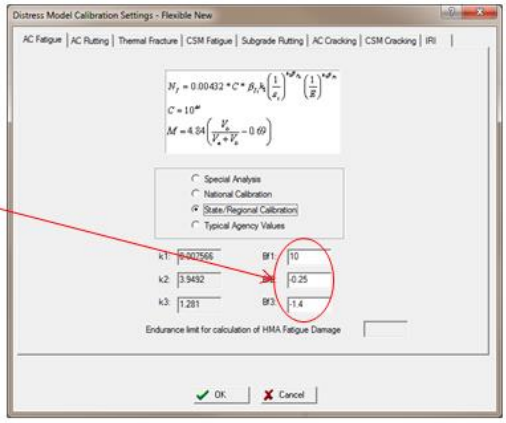

2. Transfer the trial calibration coefficients to project templates

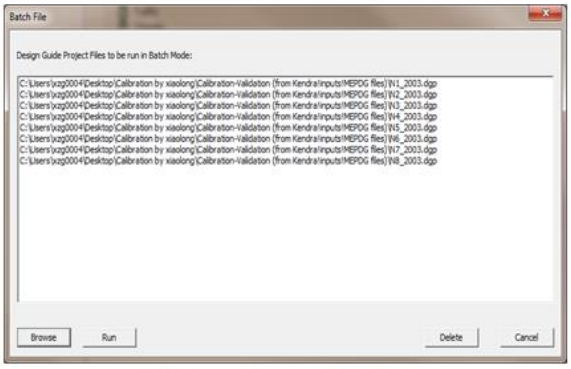

3. Batch up the project templates

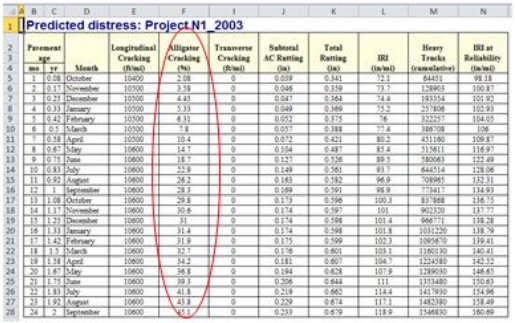

$$SSE = \sum_{n=1}^{\hat{n}} \sum_{m=1}^{d} (\text{predictedvalue} - \text{measuredvalue})^2$$

4. Evaluate predictions by the SSE

Figure 5.1 VB script flow chart

First, the trial calibration coefficients were composed into an Excel file. The Excel file contained the test section information, the project template file name, and the location path. Second, the "trial" calibration coefficients were transferred to the calibration coefficients input textboxes in the MEPDG. Next, eight project templates were compiled into the batch file and ready for a "batch" run. Third, the MEPDG predictions were extracted from the output file and employed for the SSE computation. The result of SSE for one specific set of calibration coefficients was shown in a message box in Quick Macro (Figure 5.2).

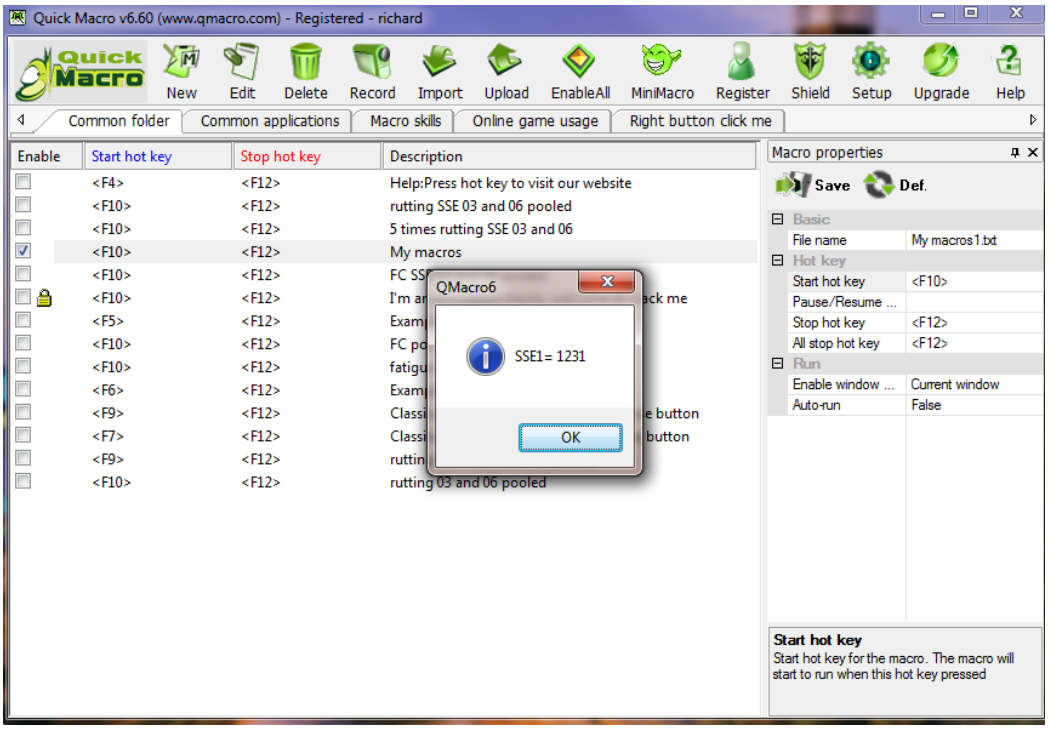

Figure 5.2 SSE result in a message box

Technical Issues

Several technical issues affect the running of macros. These issues were categorized into project analysis delays, foreground/background shift, and excel overrunning error.

Software running delay

Although a two-year project analysis takes nearly one minute to run, the VB script commands were not supposed to initiate the next action (e.g. extracting distress data from the MEPDG output files) before the project analysis was completed. To account for the running delay, the waiting time was set between two actions to coordinate the running pace and it was determined to be one minute in this study. In fact, the longer the design life of the pavement, the longer the waiting time needs to be. The appropriate length of the waiting time is case-specific, and it usually depends on the design scenario of the project and the running speed of the computer.

Foreground/background shift

In the MEPDG, when a new set of calibration coefficients were run, a dialog box will pop up to ask whether you want to reject new calibration coefficients (Figure 5.3). When the dialog box popped up, the focus of the system (i.e., the activated window or menu or textbox) was on this dialog box, in other words, this dialog box was activated as a foreground application. The macro needed to select "No" to move on. However, through considerable times of macro running, the focus of system sometimes shifted from this dialog box to some other applications in the computer system. This could cause erratic running, even wrongly ending the macro. The only remedy was to reinstall the system which brought much inconvenience. An improvement on the macro scripts may be helpful to solve this problem.

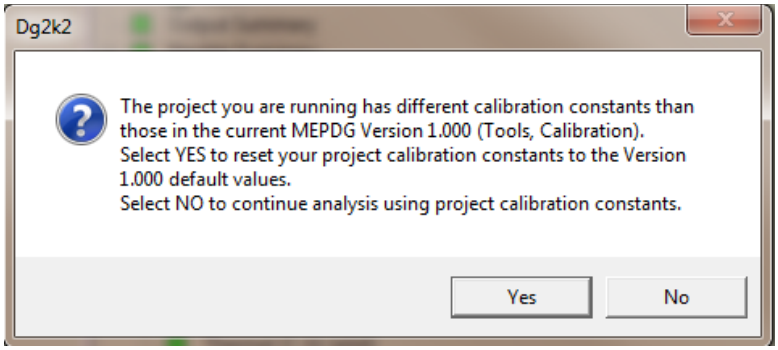

Figure 5.3 Dialog box pop-up

Excel overrunning error

When the macro program finished running, there were numerous MEPDG output files opened in Excel. Before initiating another "trial" set of calibration coefficients, it was necessary to shut down those opened Excel files manually. Otherwise, the MEPDG would have a problem to open Excel after project analysis. If many Excel files are shut down by clicking the "close" button in the upper right corner, an error warning (Figure 5.4) popped up when you ran Excel the next time. It should be noted that it was better to remove the opened files from the list of disabled items as the warning below said, or else, the macro usually had a running problem.

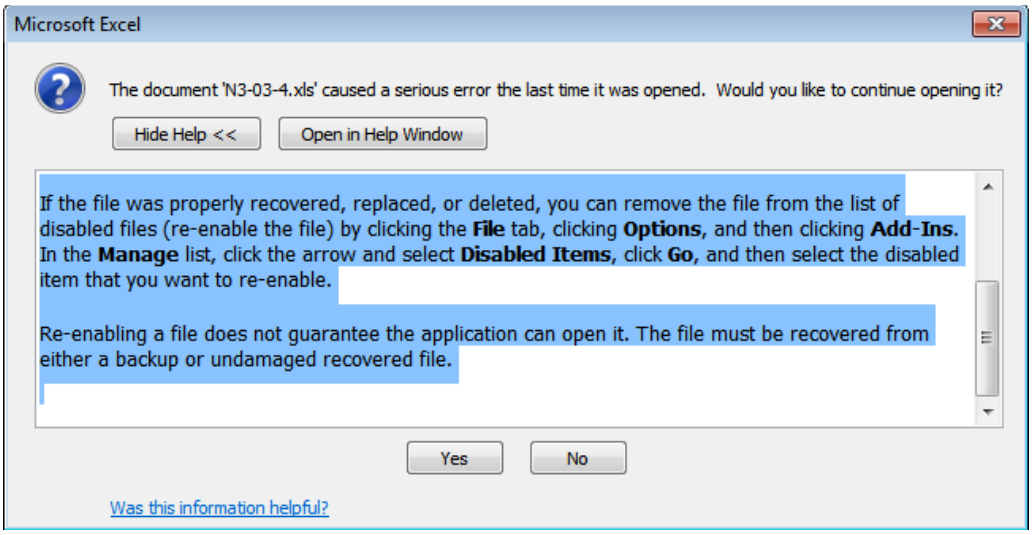

Figure 5.4 Excel error warning

SUGGESTION

It saves labor and time to employ macros; however, there were still issues that needed to be solved. The biggest issue was to ensure smooth running of macros, which determined the efficiency of this method. It would be helpful to develop a similar but more robust program in the future.

CHAPTER 6

RESULTS AND DISCUSSIONS

INTRODUCTION

The MEPDG uses a mechanistic model to predict the pavement response based on design inputs, and applies transfer functions to correlate the pavement response to various distresses over the design life. In the study, three distresses: fatigue cracking, rutting, and IRI were evaluated since sufficient data were available for them from the Test Track. The study was to first examine the MEPDG predictions provided by nationally-calibrated models. Then, the MEPDG predictions were compared with actual Test Track measurement to evaluate whether they reflected the field performance. If the accuracy of predictions was not satisfactory, the local calibration of MEPDG would be applied using the Test Track data from the 2003 research cycle. The calibration was performed by adjusting the calibration coefficients to reduce the bias or standard error between measured and predicted distress data.

Statistics were computed to measure the prediction performance. The standard error shows how much variation or dispersion the data points have from their average. The SSE evaluates how accurate the predictions replicate the measured data. Minimizing the SSE results in maximum model fit.

RESULTS OF CALIBRATION

Fatigue Cracking

Figure 6.1 shows that the nationally-calibrated model predictions appear reasonably consistent with measured values for fatigue cracking.

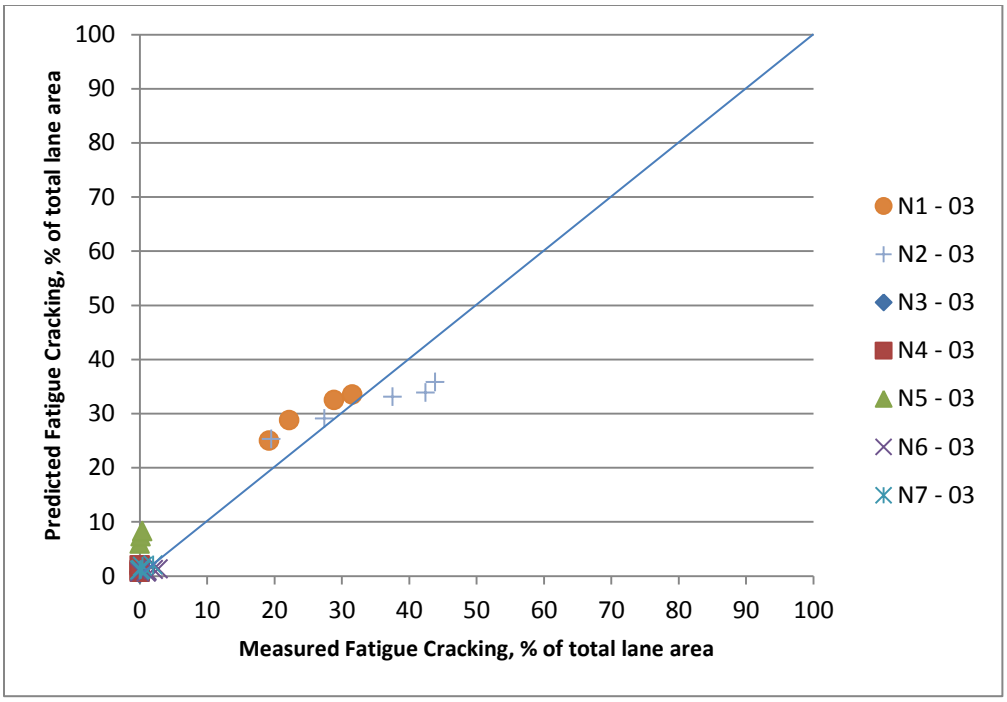

Figure 6.1 Model predictions vs. measured values for fatigue cracking

The statistics of the nationally-calibrated model predictions are shown in Table 6.1. Results for section N8 were not included is because though cracking was observed in this section extensive forensic investigation had determined the cracking resulted from the layer slippage not predicted by the MEPDG (Willis and Timm, 2007).

Table 6.1 Statistical analysis for the 2003 fatigue cracking predictions

	nationally-calibrated model
standard error	2.84%
SSE	452.28
number of data points	28
p-value	0.38

*The p-value is derived from the Student's *t*-test on measured fatigue cracking and nationally-calibrated model predictions.

The local calibration tried 66 sets of calibration coefficients in which each coefficient was adjusted from the MEPDG default. The adjustment was performed on three coefficients individually and simultaneously with a range of +/- 0.2 from defaults in which the SSE did not sharply increase. The optimization process is presented in Figure 6.2. The red line sets a SSE level of 452.28, which is calculated based on nationally-calibrated model predictions. It can be

seen that there was no appropriate calibration coefficients found that could significantly improve the model prediction accuracy.

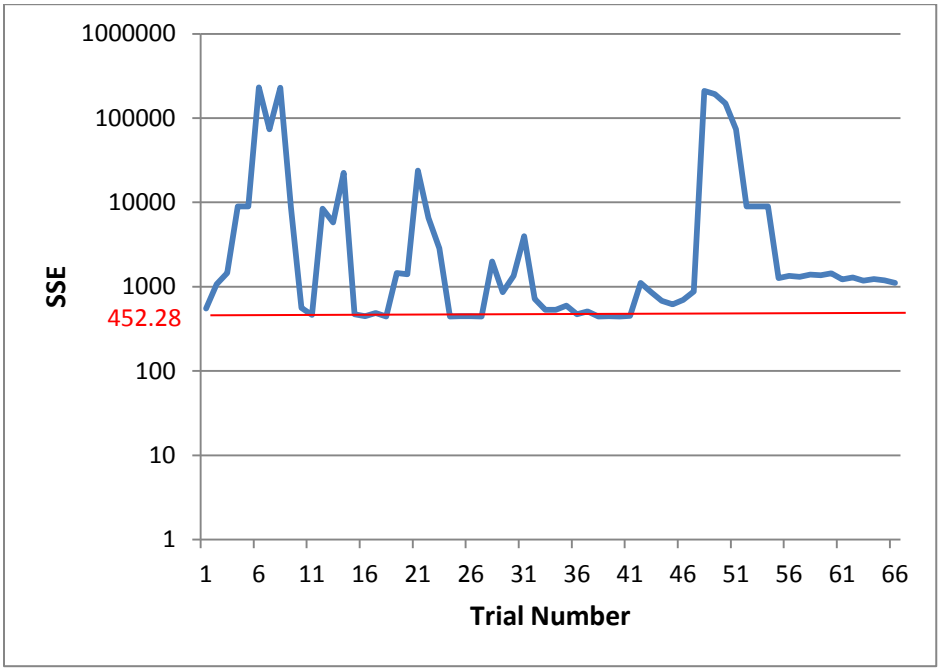

Figure 6.2 Fatigue cracking model prediction optimization

Rutting

Figure 6.3 shows that the nationally-calibrated model over-predicted the rut depths for all the 2003 sections.

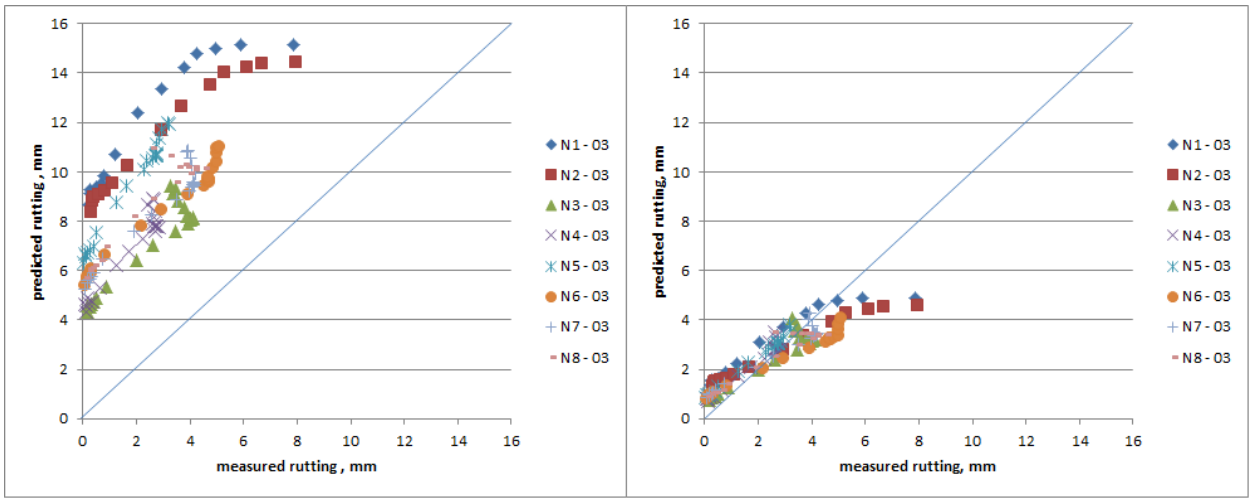

(a) National calibration **(b) Local calibration**

Figure 6.3 Model predictions vs. measured values for rutting

The local calibration using the Test Track data improved the accuracy of the rutting model. The locally-calibrated rutting model predicted much less rutting (Figure 6.3 (b)). Using the locally-calibrated model may allow designers to select a more economical pavement design (i.e., thinner pavement and/or lower cost materials).

From Table 6.2, the standard error was reduced by 55%, and the SSE decreased by a factor of 58 after the local calibration. The Student's *t*-test showed that the MEPDG predictions were no longer statistically different from the measured rut depths after performing the local calibration.

Table 6.2 Statistical analysis for the 2003 rutting predictions

	nationally-calibrated model	locally-calibrated model
standard error	0.20 mm	0.09 mm
SSE	6644.36	114.05
number of data points	157	157
p-value	8.79E-78	0.37

*****The p-value is derived from the Student's *t*-test on measured rut depths and nationally-calibrated/locally-calibrated model predictions.

The local calibration tried 106 sets of calibration coefficients in which each coefficient was varied from the MEPDG default. The adjustment was performed on five coefficients individually and simultaneously. The trial coefficient value was within a range (i.e., between 0.05 and 1.2) in which the SSE did not sharply increase. The optimization process is presented in Figure 6.4. The red line sets a SSE level of 6644.36, which is calculated based on nationally-calibrated model predictions.

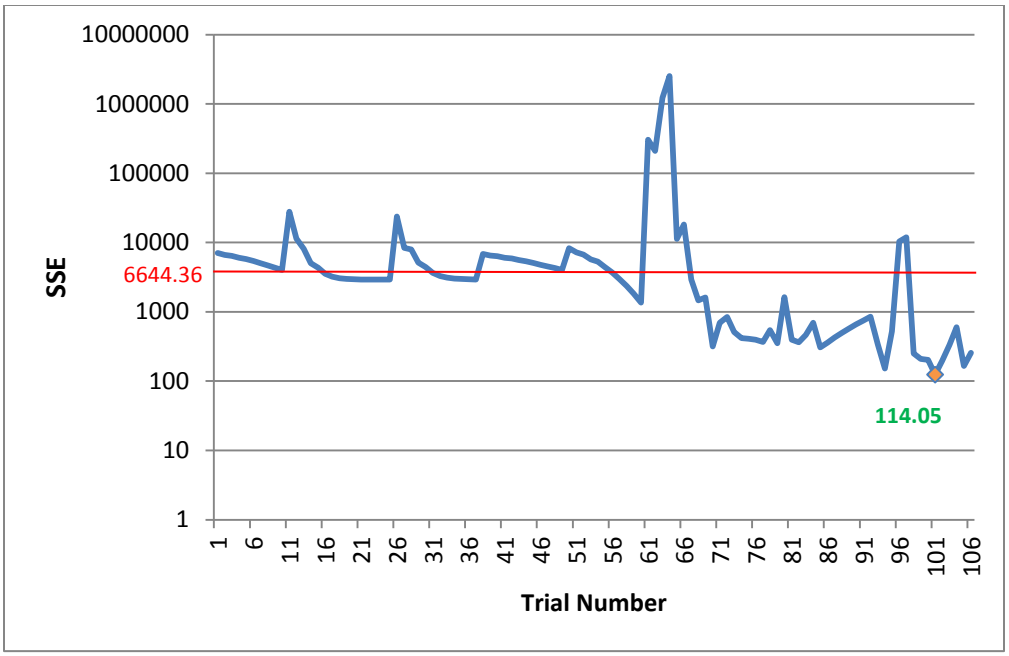

Figure 6.4 Rutting model prediction optimization

It was found that the SSE decreased to be 114.05 when the trial calibration coefficients were $\beta_1 = \beta_2 = \beta_3 = 1$ in Equation (2-13), $\beta_1 = 0.05$ in Equation (2-14) for granular base, and $\beta_1 = 0.05$ in Equation (2-14) for subgrade.

$$\frac{\varepsilon_p}{\varepsilon_r} = \beta_1 * 10^{-3.35412} * T^{1.5606*\beta_2} * N^{0.4791*\beta_3} \quad (2\text{-}13)$$

$$\delta_i = \beta_1 * k_1 * \left(\frac{\varepsilon_p}{\varepsilon_r}\right) * e^{-\left(\frac{\rho}{N}\right)^{\beta}} * \varepsilon_v * h_i \quad (2\text{-}14)$$

IRI

In Figure 6.5, it can be seen that the nationally-calibrated model predictions reasonably matched the measured values. Using the locally-calibrated rutting model also improved the IRI prediction. However, it still can be seen that the data points were mostly below the line of equality after adjusting the calibration coefficients. No additional adjustments could improve the accuracy of IRI predictions. N8 was not included because it was eliminated from the fatigue cracking analysis which strongly affected its IRI predictions.

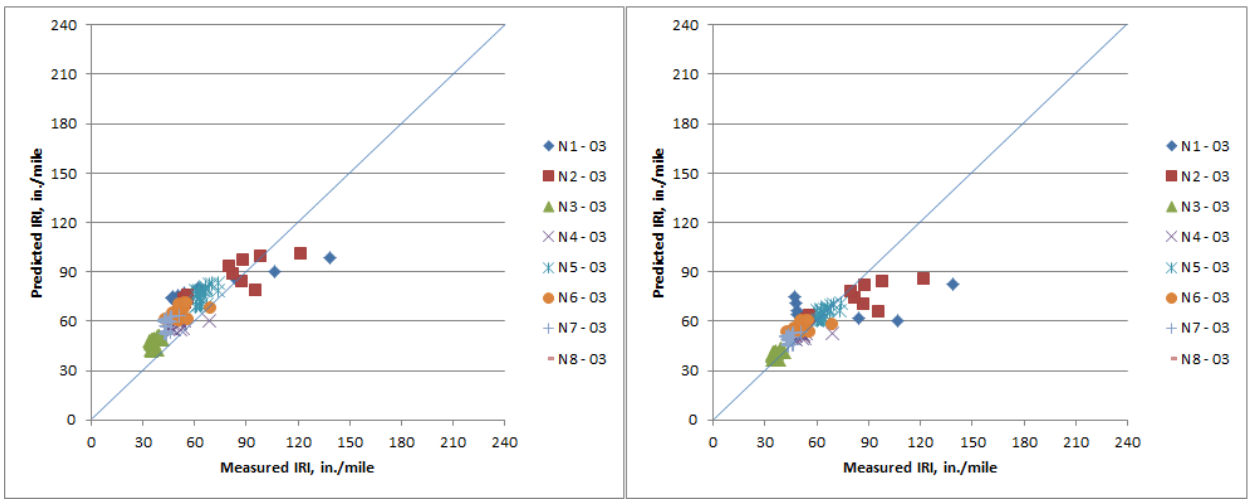

(a) National calibration **(b) Local calibration**

Figure 6.5 Model predictions vs. measured values for IRI

From Table 6.3, the standard error decreased by 17%, and the SSE decreased by 51% after adjusting the rutting model while using the same calibration coefficients for the IRI prediction. In addition, the Student's *t*-test showed that the MEPDG predictions were no longer statistically different from the measured IRI after adjusting the rutting model.

Table 6.3 Statistical analysis for the 2003 IRI predictions

	IRI predictions using nationally-calibrated model	IRI predictions after adjusting the rutting model
standard error	0.99 in./mile	0.82 in./mile
SSE	28706.39	14090.60
number of data points	143	143
p-value	6.65E-11	0.10

*The p-value is derived from the Student's *t*-test on measured IRI and nationally-calibrated/locally-calibrated model predictions.

RESULTS OF VALIDATION

Fatigue Cracking

Since the nationally-calibrated fatigue model was found to reasonably predict performance of the 2003 Test Track sections, the model was then validated using the 2006 sections. In Figure 6.6, it can be seen that these data points scattered over both sides of the

equality line. The nationally-calibrated model poorly predicted the fatigue cracking for the 2006 sections.

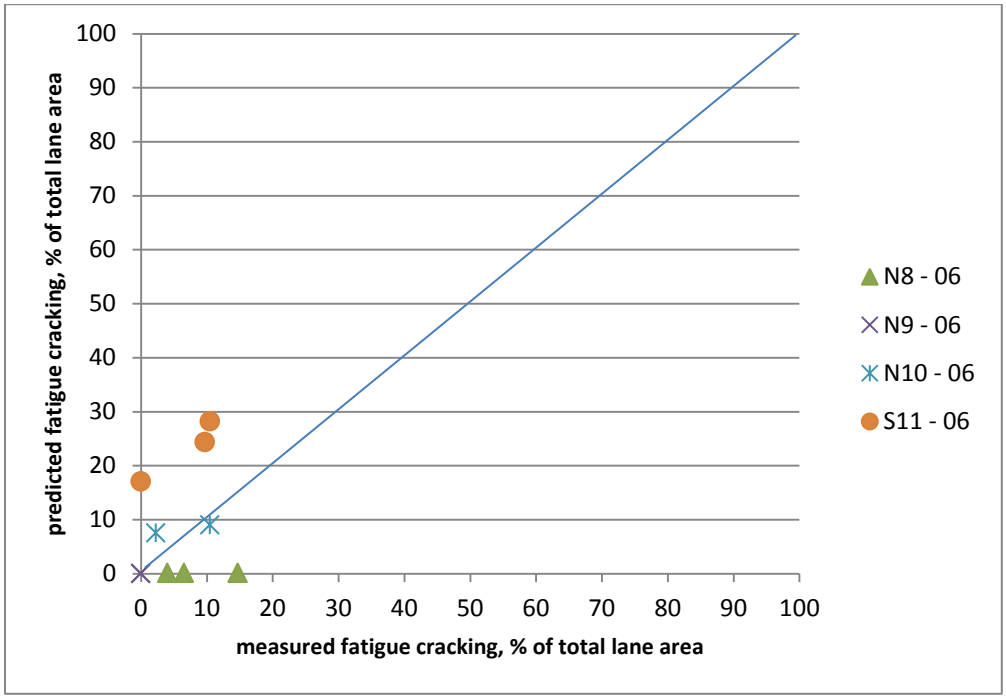

Figure 6.6 Model predictions vs. measured values for fatigue cracking

N1 and N2 in the 2006 research cycle were not included in the validation analysis because the cracking in those sections were identified as top-down cracking. Sections N3 through N7 were left in place from the 2003 research cycle and sustained additional two-year traffic; The MEPDG does not allow users to input two sets of traffic characteristics (i.e., one for the 2003 research and the other for the 2006 research cycle). The statistics of the nationally-calibrated model predictions are shown in Table 6.4.

Table 6.4 Statistical analysis for the 2006 fatigue cracking predictions

	nationally-calibrated model
standard error	3.30%
SSE	1119.56
number of data points	10
p-value	0.23

*The p-value is derived from the Student's *t*-test on measured fatigue cracking and nationally-calibrated model predictions.

Rutting

In Figure 6.7, it can be seen that the nationally-calibrated model over-predicted the rut depths for all Test Track sections. Using the adjusted coefficients from the local calibration based on the 2003 sections, the rutting predictions for most of the 2006 sections were closer to the equality line. However, the rut depths in N1 and N2 were still over-predicted, which implied that the local calibration coefficients were not suitable for these two sections. Only these two sections were built on a thick limerock base over strong subgrade material, which resulted in minor actual rutting. The reason for the prediction inaccuracy was believed to be due to unique material characteristics of the limerock base which differ from the granular based used in the other test sections. It is recommended to initiate section-specific calibration only using N1 and N2 data if higher prediction accuracy was needed.

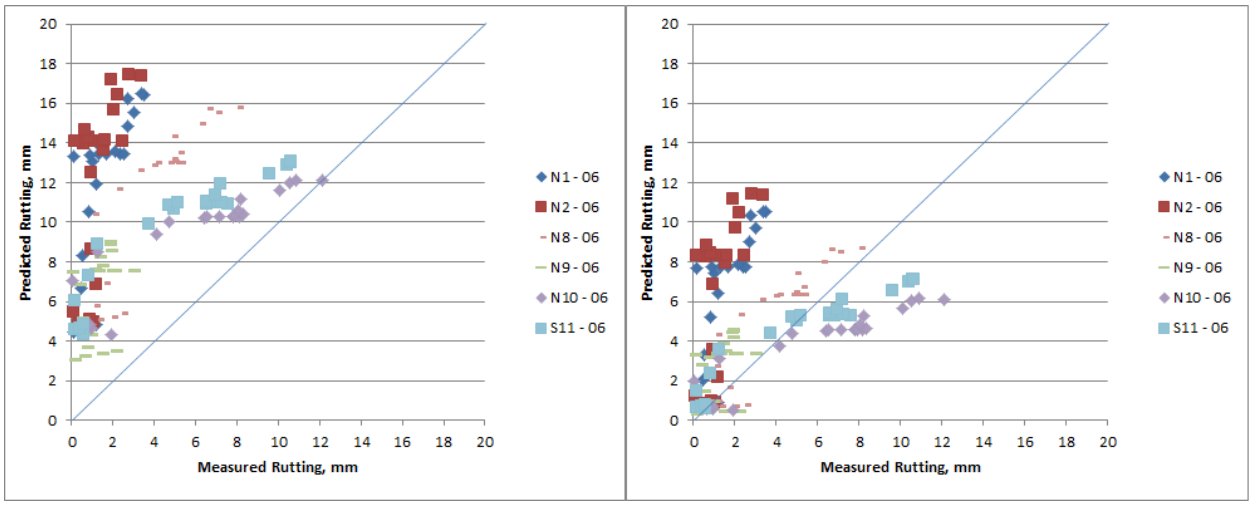

(a) National calibration **(b) Local calibration**

Figure 6.7 Model predictions vs. measured values for rutting

From Table 6.5, the standard error was dropped down by 12%, and the SSE decreased by a factor of 4 after the local calibration. Although the best-fit calibration coefficients improved the accuracy of predictions, the predicted rut depths were still statistically different from the measured values.

Table 6.5 Statistical analysis for the 2006 rutting predictions

	nationally-calibrated model	locally-calibrated model
standard error	1.96 mm	1.73 mm
SSE	8422.68	2020.98
number of data points	136	136
p-value	1.04E-42	4.72E-6

*The p-value is derived from the Student's *t*-test on measured rut depths and nationally-calibrated/locally-calibrated model predictions.

N1 and N2 used limestone base combined with unusually strong subgrade. If they were excluded, the improvement of prediction accuracy was more significant using the locally best-fit calibration coefficients. In Figure 6.8, it can be seen that the predicted vs. measured rutting plots without N1 and N2 are much better. In fact, the best-fit calibration coefficients significantly improved the accuracy of model predictions.

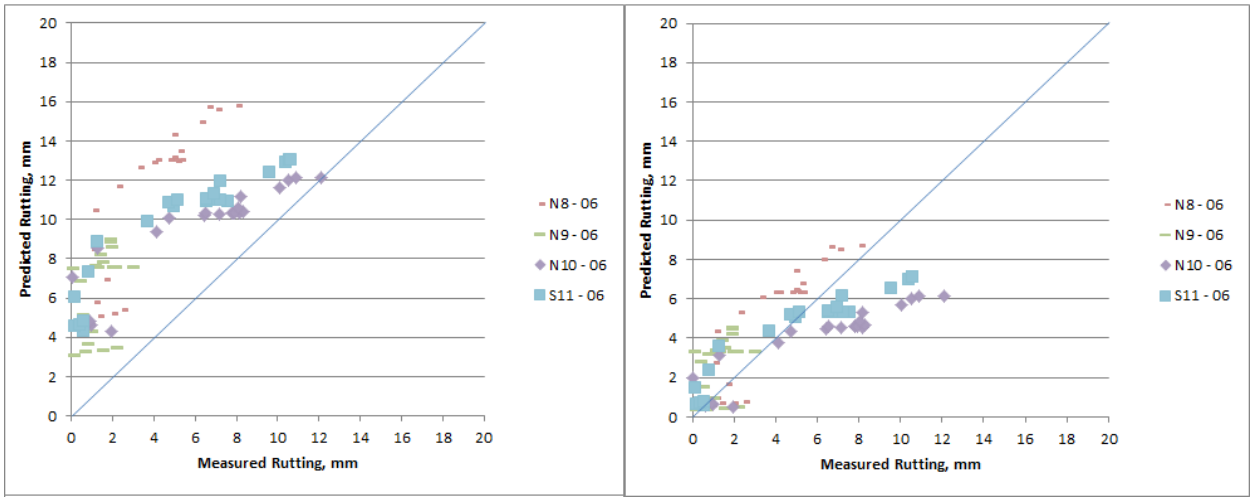

(a) National calibration **(b) Local calibration**

Figure 6.8 Model predictions vs. measured values for rutting (excluding N1 and N2)

From Table 6.6, the standard error decreased by 17%, and the SSE diminished approximately by a factor of 6 after the local calibration. In addition, the Student's *t*-test showed that the MEPDG predictions were no longer statistically different from the measured rut depths after adjusting the rutting model.

Table 6.6 Statistical analysis for the 2006 rutting predictions (excluding N1 and N2)

	nationally-calibrated model	locally-calibrated model
standard error	1.82 mm	1.51 mm
SSE	2864.79	429.73
number of data points	91	91
p-value	1.51E-20	0.42

*****The p-value is derived from the Student's *t*-test on measured rut depths and nationally-calibrated/locally-calibrated model predictions.

IRI

Figure 6.9 shows that the IRI values shifted slightly after adopting the best-fit coefficients of rutting model. The data points of N8 and N10 were distributed with a gentle slope, which suggested the increase of predicted IRI did not progress at the same rate as the measured values. N1and N2 were not included because they were eliminated from the fatigue cracking analysis which strongly affected their IRI predictions.

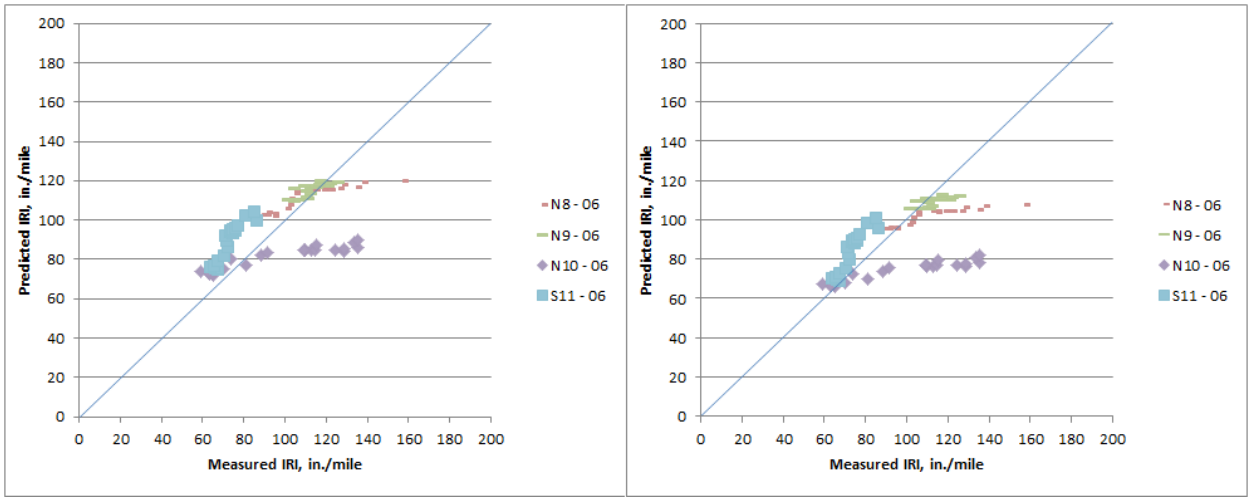

(a) National calibration **(b) Local calibration**

Figure 6.9 Model predictions vs. measured values for IRI

From Table 6.7, the standard error barely changed, and the SSE increased significantly by 29% after calibrating the rutting model. The MEPDG predictions were statistically different from the measured IRI after calibrating the rutting model. It is recommended to perform local calibration on the IRI model using the 2006 sections in the future.

Table 6.7 Statistical analysis for the 2006 IRI predictions

	predictions using nationally-calibrated model	predictions after adjusting the rutting model
standard error	3.99 in./mile	3.98 in./mile
SSE	26653.26	34442.98
number of data points	88	88
p-value	0.47	0.003

*****The p-value is derived from the Student's *t*-test on measured IRI and nationally-calibrated/locally-calibrated model predictions.

SUMMARY

The local calibration of this study was performed using the data from the 2003 research cycle. The nationally-calibrated fatigue cracking model performed fairly well. It was not able to be locally-calibrated for better prediction accuracy. The rutting prediction model in the MEPDG was able to be calibrated to field measured values. By adopting the best-fit values (as Table 6.8 shows), the rutting prediction model could provide reasonable estimation of rut depth development during service life. The IRI prediction model was significantly improved after adopting the local calibration of the rutting model so it did not need to be locally-calibrated.

Table 6.8 Best-fit calibration coefficients for three models in the MEPDG

Calibration coefficients	Local calibration values
Fatigue Cracking	
β_{f1}	1
β_{f2}	1
β_{f3}	1
AC Rutting	
β_{r1}	1
β_{r2}	1
β_{r3}	1
Granular Rutting	
β_{s1}	0.05
Subgrade Rutting	
β_{s1}	0.05
IRI	
C_1	40
C_2	0.4
C_3	0.008
C_4	0.015

The validation was conducted using the data from 2006 research cycle. Five sections left in place from the 2003 research cycle were not used due to their different design scenarios. The validation for the fatigue cracking model was performed on nationally-calibrated model since the fatigue cracking model could not be locally calibrated. The model poorly predicted the fatigue cracking so it is recommended to perform local calibration using the 2006 sections in the future. In terms of the rutting model, the validation indicated that the local calibration did greatly improve the accuracy of rutting prediction. In addition, the IRI model was validated to have no remarkable improvement on the prediction accuracy after the adoption of local calibration for the rutting model.

CHAPTER 7

CONCLUSION AND RECOMMENDATION

This study mainly focuses on calibrating the fatigue cracking, rutting, and IRI models to the Test Track condition. The MEPDG inputs, in terms of traffic, climate, and material properties, were characterized at highest level of details to represent the Test Track design scenario. The eight 2003 sections (i.e., N1 through N8) were investigated for nationally-calibrated model evaluation and local calibration. In the calibration process, 66 sets of calibration coefficients, in which each coefficient was varied from the MEPDG default, were tried for the fatigue cracking model; 106 sets of calibration coefficients were tried for the rutting model. The eleven 2006 sections were investigated for the validation of local calibration results. Four of them were used for the fatigue cracking model, and six of them were used for the rutting model. Statistical analysis was applied to evaluate the model predictability. Based on the study presented in the previous chapters, conclusions and recommendations were drawn as follows:

1. For the 2003 sections, the predicted fatigue cracking from the nationally-calibrated model reasonably matched the measured values. No local calibration coefficients were found that further improved the accuracy of the model.
2. For the 2006 sections, used for validation purposes, the default fatigue cracking model did not provide good predictions that matched the measured values. It is recommended to perform local calibration on the 2006 sections in the future.
3. For the 2003 sections, the nationally-calibrated model significantly over-predicted rut depths. The standard error was 0.20 mm. The best-fit calibration coefficients found were $\beta_1 = \beta_2 = \beta_3 = 1$ in the AC rutting model, $\beta_1 = 0.05$ in the unbound rutting model for granular base, and $\beta_1 = 0.05$ in the unbound rutting model for subgrade, which could

significantly improve the prediction accuracy. Using the best-fit calibration coefficients, the standard error was 0.09 mm.

4. For the 2006 sections, again used for validation purposes, the best-fit calibration coefficients were able to improve rutting model predictions but the predictions still did not match the measured values very well. If N1 and N2 were excluded from dataset for their uncommon material use, the standard error decreased from 1.82 mm to 1.51 mm. It suggested that the best-fit coefficients for the rutting model are a choice for pavement designers.
5. For the 2003 sections, the nationally-calibrated IRI model fairly predicted the trend of measured values. The standard error was 0.99 in./mile. Although no local calibration coefficients were found for the IRI model, the adoption of the rutting calibration coefficients improved the predictions of the IRI model. The standard error decreased to 0.82 in./mile.
6. For the 2006 sections, the adoption of best-fit calibration coefficients for the rutting model was not able to improve the accuracy of the IRI model. The standard error changed from 3.99 in./ mile to 3.98 in./mile. It was recommended to perform local calibration on the IRI model using the 2006 sections in the future.
7. The VB-based macro program significantly reduced the labor intensity in trying different sets of calibration coefficients in the MEPDG. Although the reliability of the program was not completely guaranteed, the program can be recommended for further development in the local calibration studies.
8. The level of improvement on the prediction accuracy tends to be section-specific since the local calibration results depend on the calibration data. The local calibration using

various sections would result in the prediction accuracy improvement over all sections, rather than for one particular section or a group of sections that have similar pavement structures. Therefore, the local calibration of MEPDG could be tried using smaller groups of sections to seek a further enhancement of prediction accuracy for different categories of pavement structures.

9. Owing to the limited amount of sections at the Test Track, the calibration results would not cover the all material use in local design projects in the Southeastern states. Therefore, the calibration coefficients still need to be validated for pavement sections with rare local materials before applying them into pavement design practice.
10. The identification of cracking types is important in the local calibration of fatigue cracking model. The cracking caused by slippage between asphalt layers can be possibly regarded as bottom-up cracking from pavement surface survey. Coring is necessary to identify where the cracks initialized. If the cracking that happened was not fatigue cracking, the sections should not be included in the calibration dataset.
11. The local calibration for the IRI model needs to be performed after the calibration for the fatigue cracking and rutting models. The IRI model provides results based on the fatigue cracking and rutting predictions.

REFERENCES

1. *Equivalent Single Axle Load* 2009, Pavement Interactive, accessed Jul 10th 2013, <http://www.pavementinteractive.org/article/equivalent-single-axle-load/>
2. Yang H. Huang. *Pavement Analysis and Design*, 1st edition, Prentice-Hall, Inc., Englewood Cliffs, New Jersey, 1993.
3. Charles W. Schwartz, and Regis L. Carvalho. *Implementation of NCHRP 1-37A Design Guide, Final Project, Volume 2: Evaluation of Mechanistic-Empirical Design Procedure*, Department of Civil and Environmental Engineering, The University of Maryland, Prepared for Maryland State Highway Administration, Lutherville, MD, February, 2007.
4. A. I. M. Claussen , J. M. Edwards, P. Sommer, and P. Uge. "Asphalt Pavement Design – The Shell Method", Proceedings of the 4th International Conference on the Structural Design of Asphalt Pavements, pp. 39-74, 1977.
5. Shook J. F., F. N. Finn, M. W. Witczak, and C. L. Monismith. "Thickness Design of Asphalt Pavements – The Asphalt Institute Method", Proceedings of the 5th International Conference On the Structural Design of Asphalt Pavements, pp. 17-44, 1982.
6. M. A.Miner, "Cumulative Damage in Fatigue", J. Applied Mechanics, 12, A159-A164, 1945.
7. Qiang Li, Danny X. Xiao, Kelvin C. P. Wang, Kevin D. Hall, and Yanjun Qiu. "Mechanistic-Empirical Pavement Design Guide (MEPDG): a bird's-eye view", Journal of Modern Transportation, Volume 19, Page 114-133, June 2011.
8. "MEPDG Overview & National Perspective", CEMEX, Federal Highway Administration, 88th Annual TRB meeting, January 2009.
9. Tommy E. Nantung. "Implementing the Mechanistic-Empirical Pavement Design Guide for Cost Savings in Indiana", TR News Journal, Number 271, page 34-36, November-December 2010.

10. Jianhua Li, Linda M. Pierce, and Jeff Uhlmeyer. “Calibration of Flexible Pavement in Mechanistic-Empirical Pavement Design Guide for Washington State”, Transportation Research Record: Journal of the Transportation Research Board. No. 2095, Transportation Research Board of the National Academies. Washington, D. C., pp. 73-83, 2009.
11. Naresh R. Muthadi, and Y. Richard Kim. “Local Calibration of Mechanistic-Empirical Pavement Design Guide for Flexible Pavement Design”, Transportation Research Record: Journal of the Transportation Research Board. No. 2087, Transportation Research Board of the National Academies. Washington, D. C., pp. 131-141, 2008.
12. Kyle Heogh, Lev Khazanovich, and Maureen Jensen. “Local Calibration of Mechanistic-Empirical Pavement Design Guide Rutting Model, Minnesota Road Research Project Test Sections”, Transportation Research Record: Journal of the Transportation Research Board. No. 2180, Transportation Research Board of the National Academies. Washington, D. C., pp. 130-141, 2010.
13. David H. Timm, and Angela L. Priest. NCAT Report 06-01, “Material Properties of the 2003 NCAT Test Track Structural Study”, 2006.
14. *Fatigue cracking* 2009, Pavement Interactive, accessed April 17th 2013, <http://www.pavementinteractive.org/article/fatigue-cracking/>
15. *Rutting* 2008, Pavement Interactive, accessed April 17th 2013, <http://www.pavementinteractive.org/article/rutting/>
16. *longitudinal cracking* 2008, Pavement Interactive, accessed April 17th 2013, <http://www.pavementinteractive.org/article/longitudinal-cracking/>
17. *Transverse cracking* 2006, Pavement Interactive, accessed April 17th 2013, <http://www.asphaltwa.com/2010/09/18/transverse-thermal-cracking/>

18. *Roughness* 2007, Pavement Interactive, accessed March 5th 2013, <http://www.pavementinteractive.org/article/roughness/>
19. *Loads*, WSDOT Pavement Guide, accessed March 5th, 2013 from <http://classes.engr.oregonstate.edu/cce/winter2012/ce492/>
20. NCHRP 1-37A Report, *Guide for Mechanistic-Empirical Pavement Design of New and Rehabilitated Pavement Structures*, ARA, Inc., Part 2, Chapter 4, Champaign, IL, 2004.
21. Khaled Ksaibati, and Ryan Erickson, "Evaluation of Low Temperature Cracking in Asphalt Pavement Mixes", the University of Wyoming, October, 1998.
22. Yoder E. J., and M. W. Witczak, "Principles of Pavement Design", John Wiley & Sons, Inc., New York, 1975.
23. Richard D. Barksdale, Jorge Alba, N. Paul Khosla, Ricahrd Kim, Phil C. Lambe, and M.S. Rahman, "Laboratory Determination of Resilient Modulus for Flexible Pavement Design", Georgia Tech Project E20-634, June, 1997.
24. *Elastic Modulus* 2007, Pavement Interactive, accessed April 23th, 2013, < http://www.pavementinteractive.org/article/elastic-modulus/>
25. *Resilient Modulus* 2007, Pavement Interactive, accessed April 23th, 2013, < http://www.pavementinteractive.org/article/resilient-modulus/>
26. M.W. Witczak, K. Kaloush, T. Pellinen, M. El-Basyouny, and H. Von Quintus, NCHRP Report 465, *Simple Performance Test for Superpave Mix Design*. Transportation Research Board, National Research Council, Washington, D.C., 2002.
27. Pavement Distress Survey Manual, Pavement Services Unit, Oregon Department of Transportation, Jun. 2010.

28. Angela L. Priest, and David H. Timm, “Methodology and Calibration of Fatigue Transfer Functions for Mechanistic-Empirical Flexible Pavement Design”, NCAT Report 06-03, December 2006.
29. NCHRP 1-37A Report, *Guide for Mechanistic-Empirical Pavement Design of New and Rehabilitated Pavement Structures*, ARA, Inc., Appendix II-1, Champaign, IL, 2004.
30. Pavement Preservation Manual, Part 2: pavement condition data, Office of Asset Management, Utah Department of Transportation, 2009.
31. AASHTO and TRIP 2009, *Rough Roads Ahead*, e-book, accessed March 5th, 2013 from books.google.com
32. Qiang Li, Danny X. Xiao, Kelvin C.P. Wang, Kevin D. Hall, and Yanjun Qiu, “Mechanistic-empirical pavement design guide: a bird’s-eye view”, Journal of Modern Transportation, Volume 19, June 2, pp. 114-133, January 2011.
33. Nicholas J. Garber, and Lester A. Hoel, *Traffic and Highway Engineering*, 4th edition, Cengage Learning, Toronto, Canada, 2009.
34. Asphalt Institute. *Asphalt Overlays for Highways and Street Rehabilitation, Manual Series No. 17 (MS-17)*, College Park, Maryland, June, 1983.
35. AASHTO Guide for Design of Pavement Structures. American Association of State Highway and Transportation Officials, Washington D.C., 1993.
36. *Asphalt Design Procedure* 2007, accessed March 11th 2013, <https://engineering.purdue.edu/NCSC/documents/presentations/FHWA%20National%20update>
37. AASHTO Interim Guide for Design of Pavements Structures, American Association of State Highway and Transportation Officials, Washington, D.C., 1972.

38. AASHTO Guide for Design of Pavements Structures, American Association of State Highway and Transportation Officials, Washington, D.C., 1986.
39. AASHTO Guide for Design of Pavements Structures, American Association of State Highway and Transportation Officials, Washington, D.C., 1993.
40. FHWA Report, "Seasonal Variations in the Moduli of Unbound Pavement Layers", Chapter 2, July 2006.
41. Cary W. Sharpe, Memorandum, "Distribution of the Recommended Mechanistic-Empirical Pavement Design Guide (NCHRP Project 1-37A)", American Association of State Highway and Transportation Officials, 2004.
42. NCHRP 1-37A Report, *Guide for Mechanistic-Empirical Pavement Design of New and Rehabilitated Pavement Structures*, Part 2, Chapter 3, ARA, Inc., Champaign, IL, 2004.
43. Angela L. Priest, "Calibration of Fatigue Transfer Functions for Mechanistic-Empirical Flexible Pavement Design", Unpublished Master's thesis, Auburn University, 2005.
44. NCHRP 1-37A Report, *Guide for Mechanistic-Empirical Pavement Design of New and Rehabilitated Pavement Structures*, Part 3, Chapter 3, ARA, Inc., Champaign, IL, 2004.
45. Asphalt Institute, *Research and Development of the Asphalt Institute's Thickness Design Manual (MS-1)*, 9th edition, Research Report 82-2, 1982.
46. Jagannath Mallela, Leslie Titus Glover, Michael I. Darter, Harold Von Quintus, Alex Gotlif, Mark Stanley, and Suri Sadasivam, ARA, Inc., *Guidelines for Implementing NCHRP 1-37A M-E Design Procedures in Ohio: Volume 1- Summary of Findings, Implementation Plan, and Next Steps*, Champaign, IL, 2009.
47. Kyle Hoegh, Lev Khazanovich, and Maureen Jensen, "Local Calibration of Mechanistic-Empirical Pavement Design Guide Rutting Model: Minnesota Road Research Project Test

Sections", Transportation Research Record: Journal of the Transportation Research Board. No. 2180, Transportation Research Board of the National Academies. Washington, D. C., pp. 130-141, 2010.

48. Randy West, David Timm, Richard Willis, Buzz Powell, Nam Tran, Don Watson, Maryam Sakhaeifar, Ray Brown, Mary Robbins, Adriana Vargas Nordcbeck, Fabricio Leiva Villacorta, Xiaolong Guo, and Jason Nelson. NCAT Report 12-10, "Phase IV NCAT Pavement Test Track Findings", 2012
49. Angela Priest, Auburn University, "NCAT Test Track Structural Study", accessed March 18th, 2013 <http://www.webpages.uidaho.edu/bayomy/trb/afd60/TRB2005/Committee%20Meeting%20Presentations/NCAT%20Test%20Track.pdf>
50. David H. Timm, and Angela L. Priest, NCAT Report 06-01, "Material Properties of the 2003 NCAT Test Track Structural Study", 2006
51. David H. Timm, NCAT Report 09-01, "Design , Construction, and Instrumentation of the 2006 Test Track Structural Study", 2009
52. R. Buzz Powell, and Bob Rosenthal, "Reference Information Describing the NCAT Fleet", Opelika, 2011
53. Adam J. Taylor, and David H. Timm, NCAT Report 09-06, "Mechanistic Characterization of Resilient Moduli for Unbound Pavement Layer Materials", 2009
54. David H. Timm, Nam Tran, Adam Taylor, Mary M. Robbins, and Buzz Powell, NCAT Report 09-05, "Evaluation of Mixture Performance and Structural Capacity of Pavements Using Shell Thiopave, Phase I: Mix Design, Laboratory Performance Evaluation and Structural Pavement Analysis and Design", 2009

55. Mary R. Robbins, “New Method for Predicting Critical Tensile Strains in an M-E Framework”, Doctoral Dissertation, Auburn University, 2013
56. Kendra Davis (2009), MEPDG Local Calibration, Unpublished raw data.
57. Adam J. Taylor, “Mechanistic Characterization of Resilient Moduli for Unbound Pavement Layer Materials”, Unpublished Master’s thesis, Auburn University, 2008
58. Michael I. Darter, Leslie Titus-Glover, and H. Von Quintus, “Implementation of the Mechanistic-Empirical Pavement Design Guide in Utah: Validation, Calibration, and Development of the UDOT MEPDG User’s Guide”, Applied Research Associates, Inc., October 2009.
59. AASHTO, “Guide for the Local Calibration of the Mechanistic-Empirical Pavement Design Guide”, Publication Code: LCG-1, Washington, DC, 2010
60. Scott A. Schram, and Magdy Abdelrahman, “Integration of Mechanistic-Empirical Pavement Design Guide Distresses with Local Performance Indices”, Transportation Research Record: Journal of the Transportation Research Board. No. 2153, Transportation Research Board of the National Academies. Washington, D. C., pp. 13-23, 2010.
61. Ambarish Banerjee, Jose P. Aguiar-Moya, and Jorge A. Prozzi, “Calibration of Mechanistic-Empirical Pavement Design Guide Permanent Deformation Models – Texas Experience with Long-Term Pavement Performance”, Transportation Research Record: Journal of the Transportation Research Board. No. 2094, Transportation Research Board of the National Academies. Washington, D. C., pp. 12-20, 2009.
62. James R. Willis, and David H. Timm, “A Forensic Investigation of Debonding in a Rich-Bottom Pavement,” Transportation Research Record: Journal of the Transportation Research Board. No. 2040, Washington, D. C., 2007, pp. 107-114.

APPENDIX A

Each asphalt concrete mix was designated with a number. The following tables show the mix number for each lift of the 2003 and 2006 test sections. Also, the E* data for each mix was presented.

Table A-1 Mix number for each lift of the 2003 Test Track sections

Test section	Lift number	Mix number
N1	1	1
N1	2	2
N1	3	2
N2	1	3
N2	2	4
N2	3	4
N3	1	3
N3	2	4
N3	3	4
N3	4	4
N3	5	4
N4	1	1
N4	2	2
N4	3	2
N4	4	2
N4	5	2
N5	1	1
N5	2	2
N5	3	2
N5	4	2
N6	1	3
N6	2	4
N6	3	4
N6	4	4
N7	1	5
N7	2	4
N7	3	4
N7	4	4
N8	1	5
N8	2	4
N8	3	4
N8	4	6

Table A-2 E* data for mixes in the 2003 research cycle (Timm and Priest, 2006)

Mix number	Test temperature (°F)	Test frequency (Hz)	E* (psi)
1	14	0.1	2083358
1	14	0.5	2468142
1	14	1	2629424
1	14	5	2985601
1	14	10	3162982
1	14	25	3344061
1	40	0.1	974980
1	40	0.5	1241885
1	40	1	1362085
1	40	5	1656076
1	40	10	1793318
1	40	25	2000360
1	70	0.1	298959
1	70	0.5	436418
1	70	1	511874
1	70	5	732658
1	70	10	867760
1	70	25	1029622
1	100	0.1	85463
1	100	0.5	124986
1	100	1	147902
1	100	5	245658
1	100	10	310272
1	100	25	380289
1	130	0.1	41408
1	130	0.5	55332
1	130	1	63164
1	130	5	99387
1	130	10	124043
1	130	25	152833
2	14	0.1	2277563
2	14	0.5	2725367
2	14	1	2907715
2	14	5	3304176
2	14	10	3502587
2	14	25	3689759
2	40	0.1	1153195
2	40	0.5	1474779
2	40	1	1623189
2	40	5	1988503
2	40	10	2148479
2	40	25	2404942

Mix number	Test temperature (°F)	Test frequency (Hz)	E* (psi)
2	70	0.1	394829
2	70	0.5	565357
2	70	1	653141
2	70	5	913955
2	70	10	1061821
2	70	25	1243734
2	100	0.1	151383
2	100	0.5	214801
2	100	1	254106
2	100	5	404945
2	100	10	507342
2	100	25	614706
2	130	0.1	65267
2	130	0.5	83832
2	130	1	95036
2	130	5	142898
2	130	10	174009
2	130	25	218137
3	14	0.1	2029222
3	14	0.5	2417379
3	14	1	2581816
3	14	5	2944301
3	14	10	3101703
3	14	25	3271941
3	40	0.1	791507
3	40	0.5	1031399
3	40	1	1139742
3	40	5	1432827
3	40	10	1564304
3	40	25	1723628
3	70	0.1	288879
3	70	0.5	430798
3	70	1	508140
3	70	5	737843
3	70	10	859820
3	70	25	1031689
3	100	0.1	87639
3	100	0.5	123391
3	100	1	146234
3	100	5	235505
3	100	10	295514
3	100	25	382066

Mix number	Test temperature (°F)	Test frequency (Hz)	E* (psi)
3	130	0.1	31256
3	130	0.5	39958
3	130	1	45397
3	130	5	64941
3	130	10	77414
3	130	25	97647
4	14	0.1	2298485
4	14	0.5	2724243
4	14	1	2897164
4	14	5	3289201
4	14	10	3421801
4	14	25	3617276
4	40	0.1	1072481
4	40	0.5	1395625
4	40	1	1543418
4	40	5	1920335
4	40	10	2087564
4	40	25	2327093
4	70	0.1	378875
4	70	0.5	547046
4	70	1	643423
4	70	5	930961
4	70	10	1064722
4	70	25	1310597
4	100	0.1	139490
4	100	0.5	197650
4	100	1	233293
4	100	5	359657
4	100	10	445592
4	100	25	574095
4	130	0.1	63055
4	130	0.5	79553
4	130	1	89815
4	130	5	135103
4	130	10	167845
4	130	25	215345
5	14	0.1	2501030
5	14	0.5	3002969
5	14	1	3219256
5	14	5	3670070
5	14	10	3851331
5	14	25	4038067

Mix number	Test temperature (°F)	Test frequency (Hz)	E* (psi)
5	40	0.1	1271183
5	40	0.5	1639905
5	40	1	1818265
5	40	5	2239708
5	40	10	2427604
5	40	25	2700312
5	70	0.1	378222
5	70	0.5	526886
5	70	1	602668
5	70	5	840348
5	70	10	962434
5	70	25	1150910
5	100	0.1	136843
5	100	0.5	192356
5	100	1	227383
5	100	5	354291
5	100	10	434497
5	100	25	536096
5	130	0.1	54679
5	130	0.5	71504
5	130	1	82128
5	130	5	132746
5	130	10	166975
5	130	25	203415
6	14	0.1	2761276
6	14	0.5	3333933
6	14	1	3219220
6	14	5	3974323
6	14	10	4214904
6	14	25	4448777
6	40	0.1	1157219
6	40	0.5	1588235
6	40	1	1796618
6	40	5	2290544
6	40	10	2514047
6	40	25	2828271
6	70	0.1	366474
6	70	0.5	537292
6	70	1	639000
6	70	5	954565
6	70	10	1119401
6	70	25	1364623

Mix number	Test temperature (°F)	Test frequency (Hz)	E* (psi)
6	100	0.1	127959
6	100	0.5	177671
6	100	1	209543
6	100	5	324123
6	100	10	403205
6	100	25	533630
6	130	0.1	52540
6	130	0.5	66536
6	130	1	75637
6	130	5	116139
6	130	10	142935
6	130	25	180318

Table A-3 Mix number for each lift of the 2006 Test Track sections

Test section	Lift number	Mix number
N1	1	1
N1	2	1
N1	3	2
N2	1	3
N2	2	3
N2	3	2
N8	1	4
N8	2	5
N8	3	6
N8	4	7
N9	1	4
N9	2	5
N9	3	6
N9	4	6
N9	5	7
N10	1	8A
N10	2	8B
N10	3	9
S11	1	28A
S11	2	28B
S11	3	2
S11	4	2

Table A-4 E* data for mixes in the 2006 research cycle

Mix number	Test temperature (°F)	Test frequency (Hz)	E* (psi)
1	15	0.5	2157627
1	15	1	2410856
1	15	2	2693804
1	15	5	3119436
1	15	10	3485547
1	15	20	3894627
1	40	0.5	1046350
1	40	1	1173742
1	40	2	1313558
1	40	5	1501575
1	40	10	1649804
1	40	20	1805284
1	70	0.5	331943
1	70	1	399192
1	70	2	477657
1	70	5	597217
1	70	10	701644
1	70	20	821300
1	100	0.5	101212
1	100	1	123625
1	100	2	157849
1	100	5	214849
1	100	10	268658
1	100	20	334312
1	130	0.5	69097
1	130	1	77207
1	130	2	86268
1	130	5	99899
1	130	10	111624
1	130	20	124724
2	15	0.5	2458627
2	15	1	2750572
2	15	2	3077182
2	15	5	3569202
2	15	10	3993019
2	15	20	4467161

Mix number	Test temperature (°F)	Test frequency (Hz)	E* (psi)
2	40	0.5	1157594
2	40	1	1304856
2	40	2	1459611
2	40	5	1676636
2	40	10	1848167
2	40	20	2021584
2	70	0.5	362401
2	70	1	438207
2	70	2	526632
2	70	5	662194
2	70	10	779674
2	70	20	910982
2	100	0.5	101227
2	100	1	123137
2	100	2	155480
2	100	5	210643
2	100	10	263824
2	100	20	330154
2	130	0.5	70623
2	130	1	79009
2	130	2	88391
2	130	5	102524
2	130	10	114698
2	130	20	128318
3	15	0.5	2164720
3	15	1	2404672
3	15	2	2671222
3	15	5	3069457
3	15	10	3409696
3	15	20	3787650
3	40	0.5	1055004
3	40	1	1178044
3	40	2	1307756
3	40	5	1483590
3	40	10	1622101
3	40	20	1763900
3	70	0.5	349879
3	70	1	417370
3	70	2	494772
3	70	5	613171
3	70	10	715519
3	70	20	829761

Mix number	Test temperature (°F)	Test frequency (Hz)	E* (psi)
3	100	0.5	99167
3	100	1	118974
3	100	2	149824
3	100	5	201119
3	100	10	249852
3	100	20	309317
3	130	0.5	71687
3	130	1	79633
3	130	2	88461
3	130	5	101649
3	130	10	112916
3	130	20	125432
4	15	0.5	2703490
4	15	1	2994983
4	15	2	3317905
4	15	5	3798828
4	15	10	4208421
4	15	20	4662178
4	40	0.5	1184842
4	40	1	1321351
4	40	2	1464910
4	40	5	1663524
4	40	10	1818250
4	40	20	1972919
4	70	0.5	321868
4	70	1	385365
4	70	2	460930
4	70	5	575335
4	70	10	675179
4	70	20	785611
4	100	0.5	97097
4	100	1	119862
4	100	2	152214
4	100	5	205185
4	100	10	256073
4	100	20	317038
4	130	0.5	55862
4	130	1	61886
4	130	2	68558
4	130	5	78495
4	130	10	86959
4	130	20	96335

Mix number	Test temperature (°F)	Test frequency (Hz)	E* (psi)
5	15	0.5	2649429
5	15	1	2932408
5	15	2	3245610
5	15	5	3711559
5	15	10	4107980
5	15	20	4546743
5	40	0.5	1311068
5	40	1	1458970
5	40	2	1610788
5	40	5	1816343
5	40	10	1975921
5	40	20	2135970
5	70	0.5	422966
5	70	1	505348
5	70	2	600746
5	70	5	745893
5	70	10	870516
5	70	20	1007939
5	100	0.5	124707
5	100	1	153417
5	100	2	195620
5	100	5	265165
5	100	10	331194
5	100	20	413611
5	130	0.5	91896
5	130	1	101711
5	130	2	112575
5	130	5	128736
5	130	10	142486
5	130	20	157705
6	15	0.5	2853544
6	15	1	3125467
6	15	2	3423302
6	15	5	3861014
6	15	10	4228941
6	15	20	4631929
6	40	0.5	1525071
6	40	1	1674363
6	40	2	1826363
6	40	5	2023856
6	40	10	2175227
6	40	20	2324616

Mix number	Test temperature (°F)	Test frequency (Hz)	E* (psi)
6	70	0.5	566179
6	70	1	669494
6	70	2	781656
6	70	5	945936
6	70	10	1083093
6	70	20	1229629
6	100	0.5	164473
6	100	1	202618
6	100	2	255218
6	100	5	338421
6	100	10	415678
6	100	20	507729
6	130	0.5	138663
6	130	1	151876
6	130	2	166349
6	130	5	187619
6	130	10	205497
6	130	20	225080
7	15	0.5	1852345
7	15	1	2088949
7	15	2	2355775
7	15	5	2761508
7	15	10	3114241
7	15	20	3512029
7	40	0.5	862249
7	40	1	983597
7	40	2	1112197
7	40	5	1289095
7	40	10	1427703
7	40	20	1565150
7	70	0.5	249030
7	70	1	311686
7	70	2	385075
7	70	5	499075
7	70	10	599924
7	70	20	712618
7	100	0.5	61936
7	100	1	79263
7	100	2	102812
7	100	5	146749
7	100	10	190434
7	100	20	245404

Mix number	Test temperature (°F)	Test frequency (Hz)	E* (psi)
7	130	0.5	50456
7	130	1	56901
7	130	2	64169
7	130	5	75221
7	130	10	84829
7	130	20	95664
8A	15	0.5	2533493
8A	15	1	2807917
8A	15	2	3112066
8A	15	5	3565268
8A	15	10	3951453
8A	15	20	4379469
8A	40	0.5	1158174
8A	40	1	1292866
8A	40	2	1432586
8A	40	5	1622391
8A	40	10	1768444
8A	40	20	1914739
8A	70	0.5	318793
8A	70	1	386332
8A	70	2	466538
8A	70	5	588273
8A	70	10	691588
8A	70	20	809649
8A	100	0.5	92713
8A	100	1	117891
8A	100	2	153005
8A	100	5	212238
8A	100	10	268803
8A	100	20	337889
8A	130	0.5	61988
8A	130	1	68702
8A	130	2	76144
8A	130	5	87233
8A	130	10	96682
8A	130	20	107154
8B	15	0.01	1872962
8B	15	0.1	2673802
8B	15	0.5	3429180
8B	15	1	3817066
8B	15	5	4895428

Mix number	Test temperature (°F)	Test frequency (Hz)	E* (psi)
8B	40	0.01	868486
8B	40	0.1	1325886
8B	40	0.5	1703564
8B	40	1	1872146
8B	40	5	2268873
8B	70	0.01	171773
8B	70	0.1	385317
8B	70	0.5	615540
8B	70	1	732199
8B	70	5	1066414
8B	115	0.01	20494
8B	115	0.1	42032
8B	115	0.5	75492
8B	115	1	98776
8B	115	5	192078
8B	130	0.01	58961
8B	130	0.1	84171
8B	130	0.5	107950
8B	130	1	120161
8B	130	5	154108
9	15	0.5	2399518
9	15	1	2670238
9	15	2	2971501
9	15	5	3422533
9	15	10	3808672
9	15	20	4238377
9	40	0.5	1181658
9	40	1	1322744
9	40	2	1468724
9	40	5	1669420
9	40	10	1824538
9	40	20	1982448
9	70	0.5	371840
9	70	1	449218
9	70	2	539721
9	70	5	675912
9	70	10	792885
9	70	20	923382

Mix number	Test temperature (°F)	Test frequency (Hz)	E* (psi)
9	100	0.5	110254
9	100	1	139298
9	100	2	179593
9	100	5	246419
9	100	10	307842
9	100	20	382392
9	130	0.5	81342
9	130	1	90519
9	130	2	100732
9	130	5	116022
9	130	10	129112
9	130	20	143678
28A	15	0.5	1756400
28A	15	1	1968603
28A	15	2	2206444
28A	15	5	2565513
28A	15	10	2875471
28A	15	20	3222877
28A	40	0.5	835804
28A	40	1	944340
28A	40	2	1058002
28A	40	5	1218220
28A	40	10	1344113
28A	40	20	1472277
28A	70	0.5	259521
28A	70	1	313185
28A	70	2	377436
28A	70	5	476981
28A	70	10	563375
28A	70	20	660985
28A	100	0.5	77489
28A	100	1	94120
28A	100	2	119100
28A	100	5	163573
28A	100	10	205132
28A	100	20	259472
28A	130	0.5	52461
28A	130	1	58799
28A	130	2	65903
28A	130	5	76628
28A	130	10	85886
28A	130	20	96262

Mix number	Test temperature (°F)	Test frequency (Hz)	E* (psi)
28B	15	0.01	1458885
28B	15	0.1	2126002
28B	15	0.5	2766145
28B	15	1	3098177
28B	15	5	4031044
28B	15	10	4514906
28B	40	0.01	1438870
28B	40	0.1	1595850
28B	40	0.5	1977347
28B	40	1	2141433
28B	40	5	1094986
28B	40	10	726107
28B	70	0.01	595186
28B	70	0.1	701402
28B	70	0.5	990559
28B	70	1	1141978
28B	70	5	385317
28B	70	10	171483
28B	130	0.01	59497
28B	130	0.1	86704
28B	130	0.5	112811
28B	130	1	126352
28B	130	5	164397
28B	130	10	184130

It should be noted that the underlined E values were not obtained from the lab test but predicted by using the Equation (3-1) shown earlier.

APPENDIX B

The following table shows the G* data of asphalt binders in the 2003 and 2006 test sections.

Table B-1 G* data of asphalt binders in the 2003 and 2006 test sections

Test section & Year	Layer number	Binder type	Test temp. (°F)	G* (Pa)	Phase angle (δ)
N1, N4 & N5 2003	All	PG 76-22	70	1,881,000	57.98
N1, N4 & N5 2003	All	PG 76-22	100	134,200	60.55
N1, N4 & N5 2003	All	PG 76-22	130	22,420	58.39
N2, N3, & N6 2003	All	PG 67-22	70	2,156,000	55.80
N2, N3, & N6 2003	All	PG 67-22	100	241,800	61.59
N2, N3, & N6 2003	All	PG 67-22	130	26,710	70.67
N7 & N8 2003	1	PG 76-22	70	1,881,000	57.98
N7 & N8 2003	1	PG 76-22	100	134,200	60.55
N7 & N8 2003	1	PG 76-22	130	22,420	58.39
N7 & N8 2003	2, 3 & 4	PG 67-22	70	2,156,000	55.80
N7 & N8 2003	2, 3 & 4	PG 67-22	100	241,800	61.59
N7 & N8 2003	2, 3 & 4	PG 67-22	130	26,710	70.67
N1 2006	1 & 2	PG 67-22	70	2,053,000	55.59
N1 2006	1 & 2	PG 67-22	100	225900	62.21
N1 2006	1 & 2	PG 67-22	130	28460	69.96
N1 & N2 2006	3	PG 67-22	70	2,156,000	55.80
N1 & N2 2006	3	PG 67-22	100	241,800	61.59
N1 & N2 2006	3	PG 67-22	130	26,710	70.67
N2 2006	1 & 2	PG 76-22	70	2,177,000	55.88
N2 2006	1 & 2	PG 76-22	100	267,400	59.63
N2 2006	1 & 2	PG 76-22	130	37,560	65.30
N8 2006 & N9 2006	1 & 2	PG 76-28	70	2,672,000	54.25
N8 2006 & N9 2006	1 & 2	PG 76-28	100	344,800	57.77
N8 2006 & N9 2006	1 & 2	PG 76-28	130	34,410	59.23
N8 2006 & N9 2006	3	PG 64-22	70	2,109,000	56.23
N8 2006 & N9 2006	3	PG 64-22	100	228,700	62.42
N8 2006 & N9 2006	3	PG 64-22	130	29,080	73.34
N8 2006 & N9 2006	4	PG 64-22	70	768,800	57.77
N8 2006 & N9 2006	4	PG 64-22	100	183,600	62.92
N8 2006 & N9 2006	4	PG 64-22	130	25,920	68.94
N10 2006	1 & 2	PG 70-22	70	2,413,000	60.11
N10 2006	1 & 2	PG 70-22	100	223,600	65.73
N10 2006	1 & 2	PG 70-22	130	21,580	70.63
N10 2006	3	PG 64-22	70	2,066,000	56.25
N10 2006	3	PG 64-22	100	220,100	62.21
N10 2006	3	PG 64-22	130	24,310	70.56

Test section & Year	Layer number	Binder type	Test temp. (°F)	G* (Pa)	Phase angle (δ)
S11 2006	1 & 2	PG 76-22	70	1,881,000	57.98
S11 2006	1 & 2	PG 76-22	100	134,200	60.55
S11 2006	1 & 2	PG 76-22	130	22,420	58.39
S11 2006	3 & 4	PG 67-22	70	2,156,000	55.80
S11 2006	3 & 4	PG 67-22	100	241,800	61.59
S11 2006	3 & 4	PG 67-22	130	26,710	70.67

APPENDIX C

The following table shows the as-built volumetric properties of asphalt mixes in the 2003 and 2006 test sections.

Table C-1 As-built volumetric properties for the 2003 and 2006 Test Track sections

Test section & Year	Lift number	Air voids (%)	Unit weight (pcf)	Effective binder content (%)
N1 2003	1	7.2	143.7	13.4
	2	7.2	149.1	9.7
	3	7.0	150.1	9.2
N2 2003	1	7.1	144.2	13.1
	2	6.1	151.8	9.2
	3	5.9	151.2	9.9
N3 2003	1	7.2	144.1	13.1
	2	6.7	150.8	9.1
	3	6.3	150.6	9.8
	4	7.0	149.2	9.7
	5	5.4	150.7	10.7
N4 2003	1	6.6	145.4	13.0
	2	7.1	149.0	9.7
	3	6.8	149.3	9.9
	4	7.2	148.1	10.5
	5	7.3	148.7	9.8
N5 2003	1	6.7	145.2	13.0
	2	7.1	149.0	9.7
	3	7.2	148.7	9.9
	4	6.8	148.7	10.5
N6 2003	1	6.3	145.0	13.6
	2	5.9	151.3	9.9
	3	6.6	149.3	10.2
	4	4.0	153.2	11.1
N7 2003	1	6.9	141.6	13.7
	2	5.7	151.6	9.9
	3	6.7	149.0	10.2
	4	5.0	151.6	11.0
N8 2003	1	6.9	141.6	13.8
	2	7.0	149.5	9.8
	3	7.0	148.6	10.2
	4	6.7	148.9	10.9
N1 2006	1	5.4	147.5	10.4
	2	7.8	143.1	10.6
	3	7.9	147.5	9.7

Test section & Year	Lift number	Air voids (%)	Unit weight (pcf)	Effective binder content (%)
N2 2006	1	5.0	148.1	10.3
	2	5.8	145.5	11.3
	3	5.1	152.0	10.1
N8 2006	1	8.2	137.3	10.9
	2	6.4	145.8	7.8
	3	7.1	145.1	7.1
	4	2.8	147.0	11.2
N9 2006	1	7.0	139.1	11.1
	2	7.1	144.7	7.7
	3	4.9	148.5	7.5
	4	6.1	146.9	6.9
	5	5.6	142.8	10.7
N10 2006	1	8.7	139.9	10.8
	2	7.5	143.9	8.8
	3	6.7	144.7	9.6
S11 2006	1	6.8	143.3	14.2
	2	5.8	150.4	10.9
	3	7.4	148.4	10.0
	4	8.2	147.3	9.8